Laboratoire des Systèmes Photoniques

Thèse

présentée pour obtenir le grade de

Docteur de l'Université Louis Pasteur Strasbourg I

Discipline : Sciences Pour l'Ingénieur - Photonique

par Sylvain Lecler

Etude de la diffusion de la lumière par des particules sub-microniques

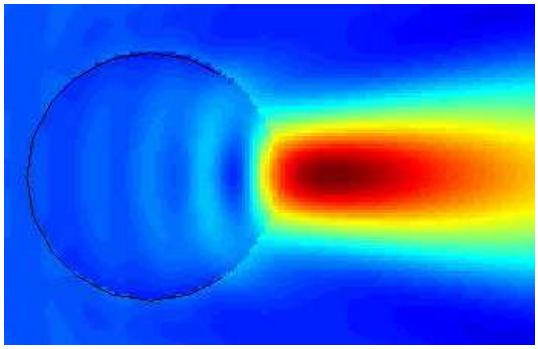

Soutenue publiquement le 18 novembre 2005

Membres du jury

Directeur de thèse :	M.Patrick Meyrueis, Professeur, ULP (Strasbourg)
Rapporteur interne :	Charles Hirlimann, Directeur de Recherche, ULP (Strasbourg)
Rapporteur externe :	Frédérique De Fornel, Directrice de recherche, UB (Dijon)
Rapporteur externe :	Pinar Mengüc, Professor, Univ. of Kentucky (Lexington USA)
Examinateur :	Yoshitate Takakura, HDR, ULP (Strasbourg)

Laboratoire des Systèmes photoniques
Boulevard Sébastien BRANT
BP 10413
F- 67 412 Illkirch Cedex - France

http://lsp.u-strasbg.fr
Phone : +33(0)3 90 24 46 14
Fax : +33(0)3 90 24 46 19

UNIVERSITÉ LOUIS PASTEUR STRASBOURG

Laboratoire des Systèmes Photoniques

Thesis

to obtain the

Natural Philosophy Degree of Louis Pasteur University - Strasbourg I

by Sylvain Lecler

Light scattering by sub-micrometric particles

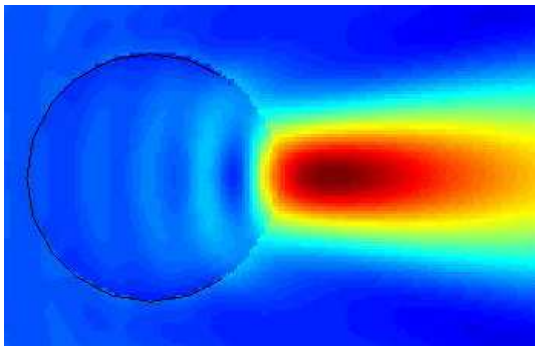

Public presentation the 18^{th} November 2005

Jury members

Thesis supervisor :	M.Patrick Meyrueis, Professor, ULP (Strasbourg)
Internal examinator:	Charles Hirlimann, Research Director, ULP (Strasbourg)
External examinator:	Frédérique De Fornel, Research Director, UB (Dijon)
External examinator:	Pinar Mengüc, Professor, Univ. of Kentucky (Lexington, USA)
Scientific adviser :	Yoshitate Takakura, HDR, ULP (Strasbourg)

Photonics Systems Laboratory
Boulevard Sébastien BRANT
BP 10413
F-67 412 Illkirch Cedex - France

http://lsp.u-strasbg.fr
Phone : +33(0)3 90 24 46 14
Fax : +33(0)3 90 24 46 19

Contents

Acknowledgments

I would like to thank the following people:

Yoshitate Takakura for having accepted to spend time following my scientific work through and for the scientific method he has tried to teach me.

Patrick Meyrueis for having made my PhD work possible and for the material that his laboratory has trustfully placed at my disposal.

Pinar Mengüc, Frédérique de Fornel, Charles Hirlimann for having accepted to be in my jury of thesis and to consider my work.

Patrice Twardowski for the long and interesting discussions we had.

Jean-Claude Worms for having made me aware of the ICAPS project.

The PhD students of the laboratory for having helped me with the process that we have tried to initiate in the laboratory and for their liking.

Alexis Bony for always being in a good mood and for putting up with being with me in the same office.

Vinvent Francois and Sarah T. for having helped me to proofread this thesis.

Thierry Engel and Joel Fontaine for the teaching that they permitted me to do in the INSA of Strasbourg.

My parents for their support and for having made my university education possible.

Keywords

Light scattering, T-matrix, multipole method, spherical vectorial functions, near-field, sub-wavelength focusing, electromagnetic couplings, Mie, spheres, aggregate of spheres, photonic jet.

Abstract

The objective of this work has been to contribute to the physical understanding of interactions of visible light with sub-micrometric spherical particles, in particular in the near field. Two different phenomena have been studied, the possibility to concentrate light in a photonic jet and the electromagnetic couplings between two close particles. The Lorenz-Mie theory and the T-matrix algorithm, which is an extension to simulate rigorously light interaction with several spheres, have been used for simulations. In the two cases, the Maxwell equations have been analytically solved.

First, we have observed the possibility with spherical dielectric particles to highly concentrate energy under the diffraction limit and to reach the diffraction limit in the near field. We have shown that the laws of these focusing are different from the geometrical optics. This near field focusing occurs when the radius size can be compared to the wavelength but also for larger spheres. When the focus point is just on the surface of the sphere or a few wavelengths behind, the width (FWHM) of the beam can be smaller than the wavelength, the beam has a low divergence and the energy is highly concentrated. Such a focused beam is called a photonic jet. We have shown its existence for spherical particles and described its main physical properties according to the optical properties of the sphere. Several possible applications have been presented.

This energy concentration in the near field has raised the question of possible electromagnetic couplings between particles inside an aggregate of dielectric spheres. To study these electromagnetic couplings, we have simulated couples of micrometric particles. The study has been performed for two dielectric and two perfectly conductive spheres for several orientations. Our objective has been to propose physical interpretations of the possible electromagnetic couplings between two close particles.

For a couple of particles, which would be orthogonal to the incident plane wave vector, a comparison with circular Young slits has been made. In single scattering, the scattered intensity in the far field can be described as interferences and diffraction. We have extended this comparison to multiple scattering regimes and we have shown that interactions due to multiple scattering mainly change the ratio of the incident wave that interacts with the particles.

We have also considered a couple of particles parallel to the incident wave vector. In multiple scattering and in backward direction, we have pointed out a shadow effect for perfectly conductive spheres that makes the interference intensity decreases. In opposition, a Perot-Fabry effect (cavity resonances) has been observed for a couple of dielectric spheres. This effect makes the interference intensity increases and can be used in future applications.

Résumé

L'objectif de ce travail a été de contribuer à la compréhension physique de l'interaction de la lumière visible avec des particules sub-microniques, en particulier en champ proche. Deux phénomènes particuliers ont été étudiés, la possibilité de concentrer la lumière en un jet photonique et les couplages électromagnétiques entre particules proches. La théorie de Lorenz-Mie et l'algorithme de la T-matrice, qui est une extension pour simuler rigoureusement l'interaction de la lumière avec plusieurs sphères, ont été utilisés pour les simulations. Dans les deux cas, les équations de Maxwell ont été résolues analytiquement.

En premier lieu, nous avons observé la possibilité qu'avaient des sphères diélectriques de focaliser jusqu'à la limite de diffraction et de fortement concentrer l'énergie en champ proche. Cette focalisation en champ proche a lieu quand le rayon de la sphère a une taille comparable avec la longueur d'onde, mais aussi pour des sphères de taille plus grande. Quand le point focal est juste sur la surface de la sphère ou à quelques longueurs d'onde devant, la largeur (FWHM) du faisceau peut être plus petite que la longueur d'onde, le faisceau est faiblement divergent et l'énergie peut être fortement concentrée. Un tel faisceau focalisé a été appelé un jet photonique. Nous avons montré son existence pour des particules sphériques et avons décrit ses principales propriétés en fonction des propriétés optiques de la sphère. Plusieurs applications possibles ont été présentées.

Cette concentration d'énergie en champ proche a posé la question des couplages électromagnétiques qui peuvent intervenir entre particules au coeur d'un agrégat de sphères diélectriques. Pour étudier ces couplages, nous avons simulé des couples de particules. L'étude a été réalisée avec des couples de sphères diélectriques et des couples de sphères conductrices parfaites et ceci pour plusieurs orientations. Notre but a été de proposer une interprétation physique des phénomènes de couplages qui peuvent avoir lieu entre deux particules proches.

Pour un couple de particules qui serait orthogonal au vecteur d'onde de l'onde plane incidente, une comparaison avec des trous d'Young a été faite. En diffusion simple, l'intensité diffusée en champ lointain peut être décrite en terme d'interférences et de diffraction. Nous avons étendu cette comparaison aux cas où il y a diffusion multiple et nous avons montré que les interactions dues à la diffusion multiple influaient essentiellement sur la fraction de l'onde incidente qui interagissait avec les particules.

Nous avons également considéré le cas où le couple de particules serait parallèle au vecteur d'onde de l'onde plane incidente. En diffusion multiple et dans la direction de rétro diffusion, nous avons mis en évidence un phénomène d'ombrage dans le cas de sphères conductrices parfaites, qui fait décroître l'intensité des interférences observées. A l'inverse, un effet de type Fabry-Perot (résonances d'une cavité) a été observé pour un couple de particules diélectriques, effet qui fait augmenter l'intensité des interférences observées et qui pourra être utilisés pour des applications futures.

Figure 1: Jacques Harthong.

I would like to dedicate this thesis to Jacques Harthong, who honored me by accepting to be in the jury of thesis, but whose life was cut short.

You are sorely missed.

See his web site : http://moire4.u-strasbg.fr

"Peut-être vous demandez-vous pourquoi cette" *These*"... est en anglais. ...La vraie raison est simple : ...l'anglais est la seule langue qui peut être comprise aussi bien par un Allemand, un Italien, un Néerlandais, un Espagnol, un Anglais, un Suédois, ou un Français. La langue utilisée ici n'est d'ailleurs pas vraiment l'anglais, ni l'américain; c'est tout simplement le Basic English, la langue internationale."
Extrait de la page d'accueil du site web de Jacques Harthong.

What could have been translated in English:
Perhaps you ask yourself why this *thesis*... is in English. The reason is easy to understand: ... English is the only language that can be understood by a German, an Italian, a Dutchman, a Spaniard, a British, a Swedish or a French. However, the used language is not really the English, nor American, it is only the Basic English, the international language.
(Inspired from the first page of the website of Jacques Harthong).

Unfortunately some spelling mistakes are still in this thesis. Pardon me...

Foreword : PhD work and scientific work

I did not do a PhD just to have a new degree, that was not an opportunity, but something substantial I had wanted to do for a long time. A PhD has been one of the possibility to have time to observe and try to understand the reality with rational arguments. Therefore among all the scientific domains, mine was necessarily physics. *Physics* not in opposition to *biology* or *chemistry*, but as *Physis*, the word used by Aristote to describe the nature. Because I am very surprised by the accuracy of science but I am more surprised by nature itself.

In scientific work as a thesis, there is a technical aspect: making programs, formulae demonstrations, plotting curves, but all these indispensable steps are not scientific results, there are tools to find meaning. A real result is what we call the physical understanding of a phenomenon, probably not the true explanation of a phenomenon but something that makes sense.

Mathematics are one of the tools that physicists use. They often consider that physics has its reasons that mathematics ignore. One of the things that I have learned during my PhD, is that a good (experimental or theoretical) physicist does not have to be a specialist in mathematics but has to apply the same strictness as in mathematic. What we call an approximation, can be inspired by physical intuitions but must be mathematically controlled. What we call an experimental error is necessary but must be rigorously determined.

Another thing that I have learned during my PhD is that independent of our results or knowledge, independent of the apparently power of science, one of the main qualities of a scientist must be his humility. This quality is necessary to learn, to ask oneself questions, to observe and to be able to progress. Paradoxically teaching can be a good school for humility, with this condition, to be open to all questions.

At the beginning of my PhD work, I hoped to progress more rapidly. I did not know that understanding needs more time than doing. I would have liked to plan my work, but I was not aware that in science, it is the unexpected results that have more interest than the other ones. Actually, during my PhD work, I probably asked myself more questions than I found answers, but I have tried to explain what I have come to understand.

Sylvain Lecler

September 2005

List of Figures

List of Tables

Résumé long en français

Etude de la diffusion de la lumière par des particules sub-microniques

Thèse soutenue par Sylvain Lecler en novembre 2005 - LSP - Strasbourg I - France
French abstract of 10 pages

Introduction

La lumière et plus généralement les ondes électromagnétiques sont un moyen privilégié pour sonder et observer le monde qui nous entoure. Cependant pour que le scientifique puisse extraire à partir de ses mesures optiques une information objective sur le milieu qu'il étudie, il est nécessaire qu'il connaisse les lois d'interaction de la lumière avec la matière. Au cours de l'histoire, afin d'en déterminer les lois, ces interactions ont été divisées en sous-familles dont les principales sont la réfraction, la diffraction et la diffusion [3]. Cette dernière, la diffusion, est sans aucun doute la plus générale car elle englobe les deux autres. C'est elle qui en faisant des objets des sources secondaires, les rend perceptibles par notre oeil. Quand un faisceau lumineux interagit avec une surface rugeuse ou un milieu hétérogène, sa puissance va être redistribuée dans toutes les directions de l'espace. C'est cette redistribution de l'intensité dans toutes les directions qui semble le mieux caractériser la diffusion lumineuse. Dans la lumière diffusée, on distinguera la diffusion spéculaire, qui correspond à la fraction de lumière réfléchie au sens de la formule de Snell-Descartes et la partie liée aux formes des objets rencontrés et qui correspond à la diffraction.

Les premières études de la diffusion lumineuse ont été faites dans le cadre de l'observation astronomique [3]. En effet le flux lumineux qui vient des étoiles jusque dans nos télescopes a subi une atténuation due à la lumière diffusée dans les nuages de poussières qu'il a rencontré sur sont parcours. La diffusion apparaît donc là comme un défaut que les astronomes ont voulu estimer. Mais les physiciens se sont très vites rendu compte que cette diffusion n'avait pas seulement atténué le faisceau de lumière mais avait changé ses propriétés, entre autre de polarisation. A partir de là, la diffusion n'était plus vue comme un défaut. L'étude des propriétés de la lumière collectée allait devenir un moyen de déduire les propriétés des nuages interstellaires traversés : propriétés de densité du gaz, de taille et de forme des particules [4, 5, 6], mais à la condition d'avoir de bons modèles.

Les premiers modèles développés (fin XIX et début XX), et qui sont encore très utilisés, sont la diffusion de Rayleigh [7] et la théorie de Lorenz-Mie [8, 9]. La diffusion de Rayleigh concerne la diffusion de la lumière par des particules très petites comparées à la longueur d'onde. La théorie de Lorenz-Mie décrit, elle, la diffusion de la lumière par une particule sphérique de taille quelconque. Ces deux modèles sont très performants mais possèdent deux limites importantes. D'abord ils ne rendent pas compte des propriétés de diffusion de particules n'ayant pas une symétrie sphérique, ensuite ils ne peuvent être utilisés que dans le cas où les particules sont suffisamment espacées entre elles pour que leurs interactions puissent être négligées. C'est à dire que ce sont des modèles adaptés à l'étude de la diffusion de milieux peu denses. On parle de diffusion simple.

Cependant, de nouveaux besoins ont vu le jour concernant la diffusion de la lumière par des particules non forcément sphériques et dans des milieux plus denses. Comme exemples peuvent être citées l'étude du rayonnement thermique dans des milieux denses en combustion [10, 11] et l'interaction de la lumière avec des matières biologiques [12]. Dans ces cas là, on parle de diffusion multiple. Une particule ne diffuse pas seulement l'onde incidente, mais également le champ diffusé par les autres particules. De nouveaux modèles et algorithmes ont été développés d'abord pour tenir compte de la forme des particules diffusantes, ensuite pour prendre en considération leurs interactions. Les deux grandes familles d'algorithme [13] sont d'une part les algorithmes basés sur l'expression des équations différentielles dans un espace discrétisé et d'autre part les algorithmes modales qui décrivent avec le théorème intégral le lien entre les fonctions d'une base sur laquelle les champs électromagnétiques sont décomposés.

Là encore, ces algorithmes ont une limite. S'ils permettent de décrire la diffusion de la lumière par des agrégats de particules complexes, ils ne permettent pas toujours d'identifier les phénomènes physiques élémentaires qui ont lieu. C'est dans ce cadre que c'est placé mon travail de thèse. Notre but a été d'amener des éléments de compréhension concernant les couplages électromagnétiques entre particules proches et en particulier de sonder ce qu'il se passait en champ proche. Ceci afin de mieux comprendre la diffusion par des milieux complexes et de permettre une meilleure exploitation de la lumière pour sonder le réel. Nous nous sommes restreints au cas de particules sphériques, diélectriques ou parfaitement conductrices et ayant une taille de l'ordre de grandeur de la longueur d'onde. Les algorithmes rigoureux que nous avons utilisés sont la théorie de Mie et l'algorithme de la T-matrice.

Les premiers résultats que nous revendiquons concernent l'interprétation physique du couplage entre particules en fonction de leurs natures, de leurs orientations et de la distance qui les sépare [14]. Le deuxième résultat important concerne la mise en évidence et l'étude d'une concentration d'intensité en champ proche que l'on nomme jet photonique [15]. Quand les conditions sont réunies, ce faisceau focalisé se manifeste à la surface de particule diélectrique et permet d'atteindre la limite de diffraction. Ce faisceau est intense, peu large et peu divergence, c'est ce qui fait son intérêt.

Propriétés et étude de la diffusion lumineuse

Quand la lumière interagit avec un agrégat de particules, la lumière diffusée dépend de nombreux paramètres [3, 13]: la taille des particules comparées à la longueur d'onde, leurs propriétés optiques (absorption, indice de réfraction, conductivité), leur forme, l'orientation de l'agrégat par rapport à l'onde incidente, la densité en particules de l'agrégat, la nature plus ou moins homogène et isotrope de la répartition et de l'orientation des particules dans l'agrégat, la forme de l'agrégat, etc.

Si l'agrégat est beaucoup plus petit que la longueur d'onde, on pourra utiliser la diffusion de Rayleigh [7, 3]. Dans ce cas l'intensité de lumière diffusée est inversement proportionnelle à la λ^4 (λ est la longueur d'onde de la lumière incidente). La lumière diffusée a la même polarisation que l'onde incidente et si l'onde incidente est linéairement polarisée le diagramme de diffusion sera similaire au diagramme d'émission d'un dipôle oscillant. Quand l'agrégat est plus volumineux, on peut dans de nombreux cas l'assimiler à une sphère et utiliser la théorie de Mie.

Dans la théorie de Mie [9, 8], on décompose les ondes incidentes, diffusées et le champ à l'intérieur de la sphère sur la base des fonctions vectorielles sphériques. Ces fonctions sont les solutions de l'équation de propagation vectorielle exprimée en coordonnées sphériques. En appliquant la continuité des composantes tangentielles du champ à la surface des particules on trouve les lois qui décrivent le lien entre les coefficients de décomposition de l'onde incidente et ceux de l'onde diffusée et interne à la sphère. Le nombre d'ordre à prendre en compte dans cette décomposition des champs, dépend de la taille en unité de longueur d'onde de l'agrégat de particules. Si la particule est très petite comparée à la longueur d'onde, on retombe sur la diffusion de Rayleigh. Seul le premier ordre est excité. Plus la particule est grande comparée à la longueur d'onde plus le nombre de modes excités sera grand. Pour certaines longueurs d'onde et pour une taille de particule donnée, des résonances peuvent apparaître. En diffusion de Mie plusieurs lobes de diffusion peuvent être observés dont le nombre, la taille et l'intensité dépendent les propriétés de la particule. Si l'onde incidente est linéairement polarisée, l'onde diffusée pourra, elle, avoir une polarisation linéaire, circulaire ou elliptique selon la direction d'observation.

La figure 2 représente la section efficace normalisée d'une particule sphérique d'indice 1.52 en fonction de son rayon en unité de longueur d'onde. Par définition le produit de la section efficace normalisée par la section géométrique de la particule (πR^2) et par le flux incident, donne le flux total diffusé. Quand la particule est très petite ($R < 0.2\lambda$), la courbe est croissante en puissance de 4, il s'agit de la diffusion de Rayleigh. Quand la particule est plus grande, on voit apparaître des résonances et une courbe décrivant le flux total diffusé qui devient plus complexe. C'est la diffusion de Mie.

Cependant quand l'agrégat de particules ne peut pas être ramené à une simple particule sphérique, que la forme des particules et leurs interactions doivent être prises en compte (diffusion multiple), d'autres modèles sont utilisés [13]. Les modèles basés sur

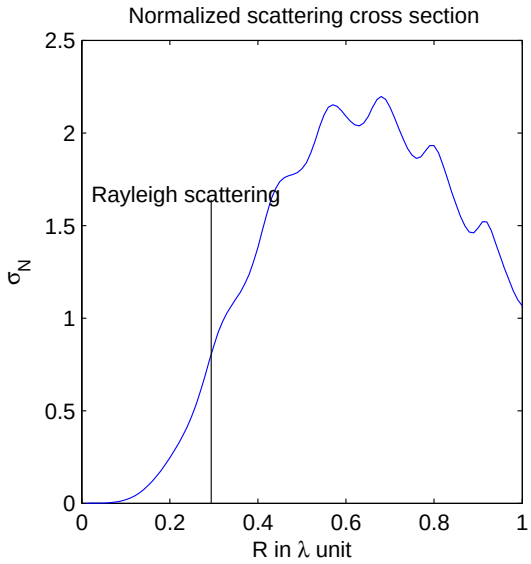

Figure 2: Section efficace normalisée d'une sphère de rayon R et d'indice de réfraction $n_2 = 1.52$. Onde incidente plane linéairement polarisée.

les éléments finis ou les différences finies comme la FDTD [16] résolvent les équations de Maxwell dans un espace discrétisé. Ce sont des méthodes génériques mais qui nécessitent de grande capacité de calcul et beaucoup de place mémoire. La DDA [17] est une autre méthode qui décrit la particule comme une matrice de dipôles en interaction et qui considère le flux diffusé comme la somme des contributions de tous ces dipôles. Enfin les méthodes modales [13] sont basés sur une décomposition des champs sur une base de fonctions orthogonales. L'application des théorèmes intégral [18] permet de retrouver les liens entre les coefficients de décomposition des champs. L'algorithme de la T-matrice, que j'ai codé pendant la thèse, fait partie de cette catégorie de méthode. Il constitue un outil idéal car rapide et rigoureux pour permettre l'étude des couplages entre particules.

L'algorithme de la T-matrice

L'algorithme de la T-matrice [19, 13, 20] est considéré comme une extension de la théorie de Mie au cas d'un agrégat de particules sphériques. C'est une méthode modale. La base des fonctions sur lesquelles les champs sont décomposés est la même que celle de la théorie de Mie. Il s'agit de la base des fonctions vectorielles sphériques. La T-matrice est la matrice qui lie les coefficients de décomposition de l'onde diffusée aux coefficients de décomposition de l'onde incidente.

Pour calculer cette T-matrice, le champ en un point quelconque, hors de l'agrégat est exprimé comme une somme de l'onde incidente et (l'intégrale) des composantes tangentielles du champ à la surface des particules multipliées par la fonction de Green qui contient un terme de déphasage. Une formulation légèrement différente permet

d'avoir l'expression du champ aux points situés à l'intérieur de l'agrégat. Ces deux équations permettent d'établir le lien entre l'onde incidente et l'onde diffusée à condition d'être capable de calculer les intégrales décrites. Le champ étant décomposé sur une base de fonctions adaptée aux coordonnées sphériques, les termes intégrales sont faciles à calculer quand le repère est placé au centre de la sphère sur laquelle est réalisée l'intégration. Comme il y a plusieurs sphères et un seul repère, le théorème de translation addition est utilisé. Il permet d'exprimer les fonctions données dans un repère sphérique comme une combinaison linéaire des mêmes fonctions données dans un autre repère sphérique.

Toutes ces formules étant connues sous leurs formes littérales les coefficients de la T-matrice peuvent être calculés analytiquement, ce qui fait de cette méthode, une des méthodes les plus rapides et précises. L'étude des temps de calcul a été faite. Deux approximations sont faites dans le calcul. Les champs sont décomposés sur une base tronquée, c'est à dire sur un nombre fini de fonctions. Une inversion de matrice, nécessaire dans le processus de calcul, est réalisée numériquement. Ces deux approximations ont une conséquence s'est de limiter la taille maximale de l'agrégat simulé. Les agrégats simulés pourront atteindre une centaine de longueurs d'onde de diamètre, ce qui fait de cette méthode une des méthodes capable de simuler les agrégats les plus gros [13].

Nous avons codé notre propre algorithme sous Matlab afin d'en avoir une bonne maîtrise (interface figure 3). Notre travail s'est basé sur la publication de Peterson et Strö̈m [20]. Une fois calculé le champ diffusé, plusieurs autres programmes ont été codés pour exploiter les résultats obtenus. Parmi les grandeurs physiques que nous avons calculées, on peut trouver, les composantes du champ électromagnétique, le vecteur de Poynting, le diagramme de diffusion 2 et 3D, les éléments de Stokes décrivant les états de polarisation, les axes de polarisation, ainsi que les sections efficaces de diffusion, d'extinction et de rétrodiffusion. L'ensemble constituant l'outil de base pour notre étude.

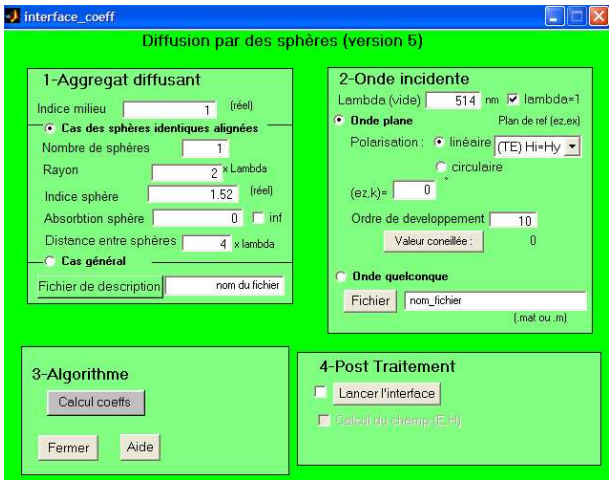

Figure 3: Interface permettant de décrire l'agrégat et l'onde incidente pour ensuite calculer le champ diffusé.

Couplages électromagnétiques entre particules

Notre but était de pouvoir identifier et interpréter les phénomènes physiques élémentaires qui surviennent quand il y a des couplages électromagnétiques entre des particules. C'est pour cette raison que nous nous sommes restreints à l'étude d'un système à deux particules identiques. L'étude a été réalisée avec des particules similaires, pour plusieurs tailles, avec deux orientations des particules et deux polarisations incidentes différentes et cela pour des particules diélectriques et parfaitement conductrices [21, 14]. L'étude a été réalisée avec l'algorithme rigoureux de la T-matrice.

Pour savoir si nous étions en diffusion simple ou multiple, c'est à dire pour savoir s'il y avait interaction où pas entre les particules, nous avons étudié la rétrodiffusion du couple de particules en fonction de la distance qui les séparait (figure 4a). Nous avons comparé le résultat avec ce que l'on aurait eu en sommant les champs (modèle cohérent) rétrodiffusés par chaque particule seule. Nous avons évidement tenu compte du déphasage qui pouvait venir de leurs positions différentes. Quand la distance qui sépare les particules est grande comparée au rayon des particules, l'intensité rétrodiffusée est équivalente à la somme (cohérente) des champs rétrodiffusés par les deux particules. Par contre quand les particules sont proches l'une de l'autre, par exemple quand leurs centres sont séparés de quelques rayons, il apparaît une différence. C'est ce cas, où il y a interaction, que nous avons voulu étudier afin de donner une interprétation physique de l'interaction. Comme nous l'avons constaté l'interprétation physique est différente selon l'orientation des particules et la nature des particules.

Nous avons d'abord considéré le cas où l'onde incidente se propage dans le plan normal à l'axe portant les deux sphères. Nous avons comparé le diagramme de diffusion vers l'avant et vers l'arrière du couple de sphères avec la figure de diffraction créée par deux ouvertures circulaires ayant le même rayon que les sphères et étant séparées par la même distance qui sépare les deux sphères (Trous d'Young [8]). L'avantage de cette comparaison est qu'elle permet une interprétation physique du diagramme de diffusion. Quand les sphères sont suffisamment éloignées l'une de l'autre pour qu'il n'y ait pas d'interaction, les deux courbes (intensités en fonction de l'angle) correspondent bien (figure 4b). Le maximum d'intensité correspond à la fraction du flux incident qui a interagit avec les particules (à la section efficace autrement dit). La distance entre deux maxima consécutifs est lié au phénomène d'interférence entre les ondes diffusées par chaque particule, c'est à dire dans notre cas à la distance inter-billes. Enfin l'enveloppe globale représente le terme de diffraction, c'est à dire la géométrie et la taille des structures vues par l'onde. Dans le cas sans interaction, la diffraction est liée à la section géométrique d'une particule.

Qu'est ce que le couplage entre particules va changer ? Pour répondre à cette question, nous avons refait la comparaison entre le diagramme de diffusion et la diffraction par des trous d'Young, mais dans le cas où nous avions identifier qu'il y avait interaction. Notre conclusion est la même pour les particules diélectriques et parfaitement conductrices. Le phénomène d'interférence reste à peu près identique au cas sans in-

teraction. La taille et la géométrie de la structure vue par l'onde reste similaire à la section géométrique d'une particule. Le paramètre qui change le plus est celui de la section efficace du couple de particules, c'est à dire la fraction de l'onde incidente qui interagit avec les particules. Selon la distance qui sépare les particules, elle peut être plus grande ou plus faible.

Nous nous sommes également posé la question de l'interprétation du couplage dans

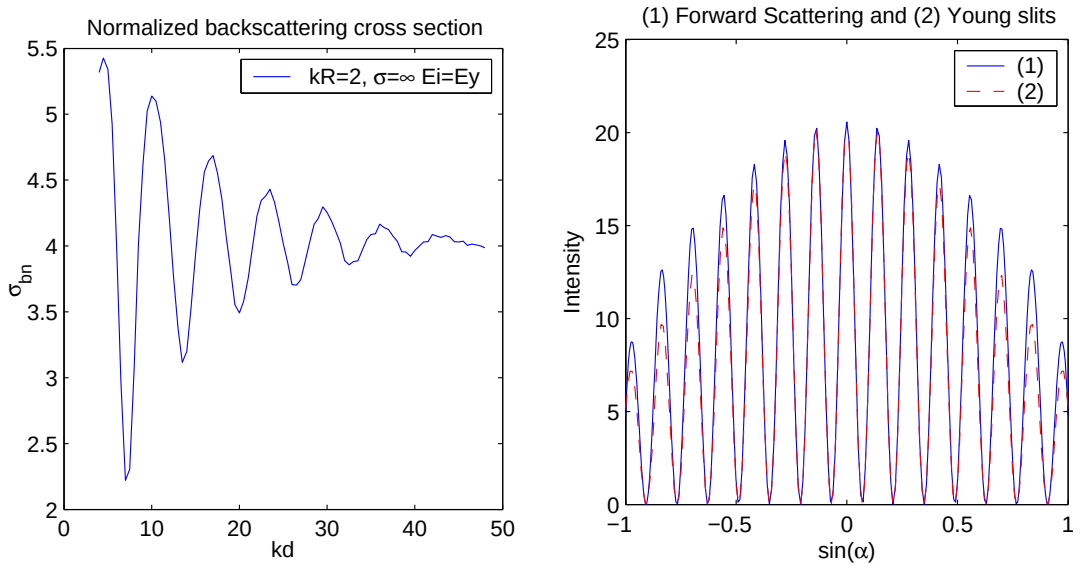

(a) (b)

Figure 4: (a) Section efficace de rétrodiffusion (b) Comparaison entre la diffraction par des trous d'Young ($--$) et la lumière diffusée ($-$). Système diffusant : 2 sphères, rayon a: $ka = 2$, conductivité $\sigma_2 = \infty$, distance entre le centre des 2 sphères d: $kd = 45$. Le vecteur d'onde $\vec{k}$ et le champ électrique, linéairement polarisé, sont orthogonaux à l'axe des 2 particules.

le cas où les deux sphères sont dans l'axe du vecteur d'onde incident. Dans ce cas l'interprétation physique n'est pas la même selon que la particule est diélectrique ou parfaitement conductrice. Pour les sphères parfaitement conductrices, un effet d'ombrage se manifeste qui fait décroître la section efficace des deux sphères quand elles se rapprochent (figure 5(a)). A l'inverse quand les deux sphères sont diélectriques, la section efficace des deux sphères aura tendance à augmenter quand elles se rapprochent (figure 5(a)). Dans ce cas, il y a un effet similaire à un Fabry-Perot [8], l'espace entre les deux particules se conduit comme une cavité avec des maxima de transmission.

Cette étude montre bien les couplages électromagnétiques qui apparaissent entre des particules illuminées quand celles-ci se rapprochent. Nous avons interprété physiquement comment se manifeste ce couplage, mais pour mieux comprendre sa cause, nous avons étudié la répartition d'intensité en champ proche, c'est à dire autour d'une particule.

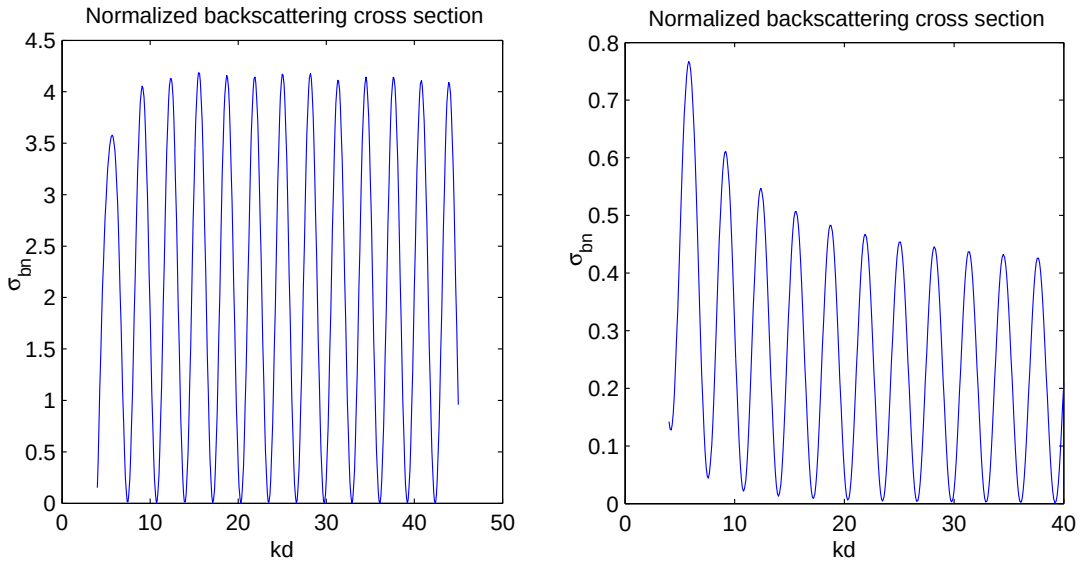

(a) Sphères parfaitement conductrices (b) Sphères diélectriques $n_2 = 1.5$

Figure 5: Section efficace de rétrodiffusion en fonction de la distance d entre les sphères. Rayon a: $ka = 2$. Ici les deux sphères sont dans l'axe du vecteur d'onde incident $\vec{k}$.

Le jet photonique

En général, lorsqu'on étudie l'interaction de la lumière avec des particules de taille comparable à la longueur d'onde, on ne considère que le champ diffusé et l'observation est faite en champ lointain [3]. Pour mieux comprendre la cause des couplages entre particules, nous avons étudié la répartition d'intensité autour d'une particule diélectrique en champ proche [15]. Dans ce cas, dans la théorie de Mie, le champ hors de la particule est la somme du champ diffusé et du champ incident. Ce que nous avons calculé et qui corrobore les simulations de Taflove effectuées par FDTD sur des cylindres diélectriques [22], est qu'il pouvait y avoir une très forte concentration d'intensité en champ proche (figure 6). Cette forte concentration d'intensité est appelée un jet photonique. Nous avons voulu mieux comprendre ses propriétés et son origine.

Nos simulations montrent qu'une sphère diélectrique de quelques longueurs d'onde, selon son indice de réfraction peut concentrer (focaliser) l'intensité dans la sphère (fort indice de réfraction) ou hors de la sphère (faible indice). Si on appelle point focal le lieu sur l'axe optique où l'intensité est maximale, alors ce point focal n'obéit pas aux lois habituelles de l'optique géométrique. Pour une sphère de taille donnée, nous avons montré que le maximum d'intensité était atteint quand le point focal tombait juste à la surface de la sphère. Si la sphère ne fait que quelque longueur d'onde, nous avons montré qu'il fallait utiliser un matériau ayant un indice de réfraction de l'ordre de 1.6. Si la particule est plus large, l'indice nécessaire tendra vers 2.

La deuxième observation importante était que ce jet photonique pouvait atteindre la limite de diffraction, c'est à dire atteindre une largeur totale à mi hauteur d'une

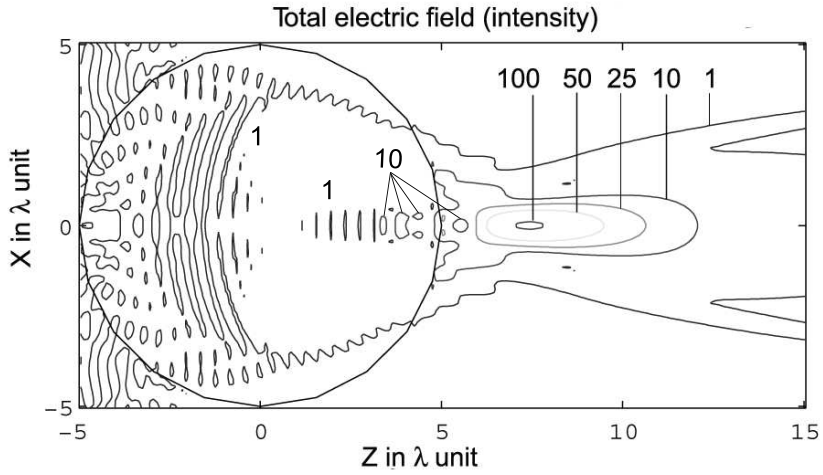

Figure 6: Intensité du champ électrique autour d'une sphère de rayon $R = 5\lambda$ et d'indice $n_2 = 1.3$. La largeur totale à mi-hauteur du faisceau est inférieure à λ. Le calcul a été fait avec un ordre $L_{max} = 45$ et pour une onde incidente plane linéairement polarisée $Hi = H_y$ and $k_i = k_z$.

demi-longueur d'onde. Nous avons alors recherché dans quel cas la largeur du faisceau focalisé allait garder une largeur inférieure à la longueur d'onde sur la plus longue distance de propagation possible. Pour avoir un tel phénomène, nous avons montré qu'il fallait focaliser, non plus juste à la surface de la particule, mais quelques longueurs d'onde derrière (figure 6). Indépendamment de la taille de la particule, la longueur maximale de propagation en dessous de la longueur d'onde est atteinte pour un indice de réfraction de l'ordre de 1.3.

Nous nous sommes également intéressé à la nature électromagnétique d'un jet photonique. Nous avons montré que sa polarisation (en champ proche) était la même que celle de l'onde incidente et cela malgré que le champ dans une direction quelconque proche de la particule n'est plus rigoureusement transverse. En effet, en champ proche, la composante radiale du champ électrique n'est pas nulle dans toutes les directions.

Enfin nous avons voulu savoir pour quelle taille de particules le phénomène du jet photonique pouvait avoir lieu. Il n'a pas lieu dans le régime de Rayleigh ($kR < \lambda$). Dans ce cas, quand la particule est trop petite comparée à la longueur d'onde, les maxima d'intensité ne sont plus sur l'axe optique mais de part et d'autre de la particule [23]. Si nous avons trouvé une taille minimale, en revanche nous n'avons pas trouvé de taille maximale. Un jet photonique avec les mêmes propriétés que celles décrites ci-dessus semble pouvoir être réalisé avec des particules de grandes tailles ($R >> 20\lambda$). Ce qui semble montrer que l'apparition d'un jet photonique ne serait pas due à la taille de la particule mais bien à la proximité du point focal avec la surface de la particule.

Pour résumer, dès qu'une particule diélectrique a un rayon supérieur ou de l'ordre de la longueur d'onde, il est possible en choisissant un indice de réfraction n_2 qui per-

mette de focaliser juste à sa surface ($1.6 < n_2 < 2$) ou bien juste derrière la sphère, d'avoir un jet photonique, c'est à dire un faisceau focalisé, avec une largeur inférieure à la longueur d'onde, avec une très forte intensité et une faible divergence. Cela permet mieux de comprendre pourquoi deux particules proches peuvent se comporter comme une petite cavité avec un effet Fabry-Perot. Mais le jet photonique seul pourrait aussi être utilisé dans de nombreuses applications comme nous allons le voir.

Conclusion

Afin d'étudier les couplages électromagnétiques en diffusion multiple et pour en obtenir une interprétation physique nous avons codé deux algorithmes rigoureux de résolution des équations de Maxwell: la théorie de Mie et l'algorithme de la T-matrice.

Grâce à l'algorithme de la T-matrice nous avons pu mettre en évidence et interpréter physiquement le couplage entre deux particules qui survient quand elles sont très proches [14]. Nous avons montré que quand les particules sont orthogonales à la direction de propagation, le couplage se traduisait majoritairement par un changement de la fraction de l'onde incidente qui était diffusée. Les phénomènes de diffraction et d'interférence étaient très faiblement affectés par l'interaction. Nous avons également étudié le cas où les particules sont alignées dans la direction de propagation de l'onde incidente. Un phénomène d'ombrage, se traduisant par une baisse de la section efficace de diffusion est observé si les particules sont parfaitement conductrices. A l'inverse un phénomène similaire aux pics de transmission d'une cavité Fabry-Perot est observé sous la forme d'une augmentation de la section efficace de diffusion lors de l'interaction de deux particules diélectriques.

Une étude complémentaire de l'intensité en champ proche autour d'une particule diélectrique a permis de mettre en évidence la possibilité qu'elle avait de fortement concentrer l'intensité. Ceci en plus de permettre une meilleure compréhension des couplages entre particules proches, constitue un phénomène intéressant en soi. Ce faisceau focalisé, appelé jet photonique, survient quand le point de focalisation est juste sur ou juste derrière la surface de la sphère. Il atteint une très grande intensité, peut rester avec une largeur inférieure à la longueur d'onde sur plusieurs longueurs d'onde de propagation et a une faible divergence [15].

Ce jet photonique pourrait avoir plusieurs applications intéressantes :

- amélioration de l'usinage laser [23],
- amplification de phénomènes non linéaires optiques,
- augmentation des capacités des mémoires optiques (CD),
- détection de nano-particules [24],
- amélioration de la résolution en microcopie [25], SNOM par exemple.

L'exploration de ces pistes semble prometteuse. La mise en évidence expérimentale d'un jet photonique reste également un défi intéressant. Indépendamment de cela l'amélioration des algorithmes d'étude de la diffusion multiple sera une étape nécessaire pour simuler des agrégats plus gros, plus réalistes et pour permettre de mieux comprendre les couplages électromagnétiques dans les milieux hétérogènes.

Chapter 1

Introduction

1.1 Introduction

In the Bible, if God created light the first day, that was probably to observe his creation. Actually, light may be one of the best means of observing reality. Light is able to go through a medium, to have various interactions according to the shape and the properties of the matter. Often these interactions do not affect the observed object. The information propagates fast and ends up in our eyes or sensors. However our small brain must know the laws of interaction of light with matter to deduct information about this light. In order to know that we see an object before us, we must (unconsciously) know that the surface of the object scatters light and behaves as secondary sources. We must know the law of refraction and reflection of the propagating light, etc. The physicist must understand the same kind of knowledge about light to be able to extract objective data from the reality. That is the reason for explaining the interest for studying interaction between light and matter. In this work, we focus our attention on the description of one of these interactions: light scattering. I will explain this choice more in depth below.

Since the first laws of Lord Rayleigh in 1871 which deal with light scattering of particles with a size small compared with the wavelength, significant improvement has been made for a better description of this phenomenon [3, 26]. We can cite, for example, the Mie theory in 1908 [9, 27, 28], and before the work of Lorenz [29, 30], which describes rigorously light scattering by spherical particles. However, most of these developments only deal with single scattering. That is, when each particle is supposed to scatter only the incident light independently of the other particles. This hypothesis is true when the distance between particles is large compared to the wavelength. When light is scattered by a dense cloud of particles, multiple scattering must be taken into account. Each particle scatters the incident light but also the light scattered by the other particles. The study of these electromagnetic interactions between the particles is more difficult to describe and often needs the use of a numerical resolution of Maxwell equation.

Several specific algorithms have been developed these two last decades (see section 2.6) to describe such multiple scattering interactions. The need to understand multiple

scattering that occurs in many new applications can probably explain the increase of interest for this subject.

Yet another great change can explain the increase of light scattering interest. For a long time, light scattering has been considered a cause of loss of information and power during propagation. For example, the light scattered by cosmic particles explains a part of the decrease of light collected by astrophysicists telescopes, what is called the extinction phenomenon [3]. Scattering can be considered too, as a reason for decrease of polarization degree of a beam propagating in a medium. However it is now understood that the optical properties of the scattered field can be used to learn information on the media. The intensity scattered according to the direction (scattering phase function) and the degree of linear polarization of the scattered field can be used to find the density, the shape, the optical properties of particles or aggregates of particles. Scattering phenomena are no longer a drawback but become a non-destructive means to investigate matter.

The need to understand multiple scattering effects and to solve inverse problems to obtain information about media, can probably explain the increased interest for light scattering. As a result many new numerical methods have been developed to improve the understanding of light scattering. Because of the size of particles, which can be compared to the wavelength, these methods are based on the rigorous Maxwell's equations. Differential methods as Finite Element Method (FEM) [31][32] or Finite Difference Time Domain Method (FDTD) [33, 16, 34] have been used in 2D. New methods based on a physical description of matter have been developed such as the Discrete Dipole Approximation (DDA) [35, 36]. These methods allow the study of 3D problems, although only for small particles or aggregates. Actually only the integral methods, such as the T-matrix algorithm [37], have shown to be capable of modelling light scattered by large irregular particles or aggregates.

In this context, the main objective of this PhD work is to contribute to bring complementary physical explanations of some basic phenomena that occur in visible light scattering for sub-micrometric particles, in particular in the near field region. The work is theoretical but has been carried out by considering experimental conditions. In single scattering, we have analyzed the possibility with dielectric spheres to focus light until the diffraction limit and to obtain a high spatial concentration of energy in the near field, what is called a photonic jet. This possibility can have applications in microscopy or in laser processing, but it also illustrates the high electromagnetic coupling that can appear inside an aggregate of particles. That is the reason why we have also studied in the far field the electromagnetic coupling between a couple of close particles. Our objectives were not only to study the influence of several optical parameters but to give physical interpretations of these effects. In particular the transition between single and multiple scattering has been described as interferences, diffraction and energy coupling. Such a knowledge may have applications for aggregate characterization by light scattering. To carry out these theoretical studies, a T-matrix algorithm has been coded and will be described in this report.

Before introducing our work, we would like to summarize the main historical steps in the understanding of volume light scattering and corresponding applications.

1.2 Light scattering: short history and background

This section deals with the main steps in the understanding and applications of light scattering in order to situate our work in a more general context.

- XIXth century : the birth of electromagnetism
Several observations and famous experiments in the XVIIIth century led to the apparition of two different domains, the electrostatic and the magnetostatic. They respectively describe strength created by charges and magnets on other charges and magnets. Because of new experiments such as the experiment of Oersted, these two domains have been brought together by Maxwell [38] at the end of the XIXth century to create the electromagnetism. The main historical contributions in electromagnetism are summarized in appendix A.1. The understanding of light scattering was mainly to be carried out in the XXth century.

- 1871 The Rayleigh scattering
Lord Rayleigh (figure 1.1) is one of the first to rigorously describe light scattering by particles smaller than wavelength [7, 1]. By using symmetries and a dimensional study, he deduced that the scattered intensity of such a particle is inversely proportional to λ^4, where λ is the wavelength of light (see section 2.2). Thus he explained that the small water drops in the sky scatter more blue light than red, that is the reason why the sky is blue (scattered light) in the day and red (direct light) immediately before and after the sunset.

Figure 1.1: Lord Rayleigh: J.W. Strutt 1842-1919 Cambridge [1]

- Physical colors
Colors are often a consequence of absorption properties of material. However colors can

also be a consequence of physical phenomena, for example the "prism effect". Scattering is another example of physical colors [39]. We have yet pointed that the scattered intensity in the Rayleigh case depends on the wavelength and that it explains why the sky is blue. The white color of ice and paper can also be explained by multiple scattering. Their components (crystal and chalk) are smaller than the visible wavelengths, thus all the colors are scattered and create together a white appearance. The color of some butterflies (figure 1.2) can also be explained by scattering [2] and the color of some glasses are produced by including nano-size metallic objects in the glass.

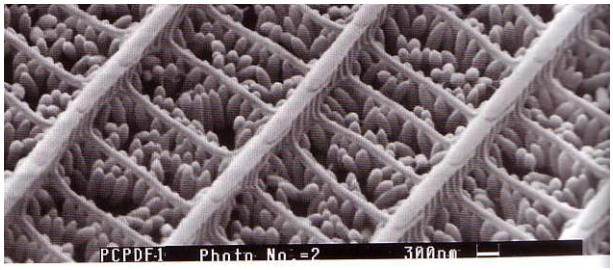

Figure 1.2: Microscope view of the scattering structure on the wing of a butterfly called *pieris brasicae*[2].

- 1891 Lorenz and 1908 the Mie scattering
Gustave Mie (1868-1957) used the analogy with sound to solve the propagation equation of electromagnetic waves in a dielectric sphere [8, 9, 27, 28](see section 2.3). A similar work had been made before by Lorenz [29, 30]. The Mie theory makes the calculation of light scattering possible for spheres larger than the wavelength. This theory is also called the Lorenz-Mie theory.

- Atmospheric applications
During half a century, all scattering problems were described as the sum of light scattered by spheres. The effective shape of a particle and the electromagnetic interaction between particles were considered as negligible [3]. The main family of applications were the atmospheric ones. The effects (extinction, polarization change) of aerosols, cloud or haze scattering about atmospheric optics [40] as radar and satellite communications were studied. Light scattering was also used to observe atmosphere for the meteorology and pollutant quantification.

- 1966 Waterman: arbitrary shape particles
The conceptual contribution of Waterman [19] is very important because it lead the way to the future methods. By using an integral formulation and the vectorial Green function, he described light scattering by a particle with an arbitrary shape (will be discussed in chapter 3). The Green function describes an electromagnetic impulse source. The integral formulation is the vectorial analogue of the Huygens-Fresnel integral in scalar theory. This new theory is considered as the birth of the T-matrix algorithm and is also called the Extended Boundary Condition Method (EBCM). At the beginning, this formulation was applied for spheroidal particles in order to be able to carry out

analytical calculations. Recently because of advance of computers this method has been applied for more arbitrary shapes (discus in section 2.6).

- 1973 Peterson and Ström: scattering by an aggregate of particles
The contribution of Peterson and Ström is the second great contribution in light scattering description related to this work. The integral formulation of Waterman is extended for the scattering of several particles [20]. Thus dependent (that is with phase effects) and multiple scattering can be rigorously taken into account. Other algorithms have been developed to simplify computing by using assumption (see section 2.6). More recently **Mishchenko** has contributed to the development of the T-matrix algorithm and of its use in several domains [37, 13].

- Astrophysical observations and particle characterization
Light scattering is of a great interest in astrophysics. Initially what has been understood is that light scattering was a reason for the decrease of the incident flux in our telescope. This *extinction* of light is due to absorption and light scattering by the interstellar particles. Auguste Comte in the XIX^{th} century considered the studies of astrophysical object impossible because of their distance and cited them as examples of the limits of science [41]. Electromagnetism has contradicted his point of view.

The scattering phenomena change the properties of the transmitted light. More recently physicists have understood that the study of these properties (scattering phase function, polarization) was a means to study these interstellar particles (size, shape, density, etc.). Among the particles of interest are the stellar particles, the comets (surface and tail), the regolith (dust on the planet surfaces).

In order to have a better understanding the interaction of light with matter in microgravity, to describe planetary formations and to understand the light scattering properties in function of the scattering aggregates, several projects have been carried out. PROGRA2 [4, 5][Web1] and the ICAPS (Interaction in Cosmic and Atmospheric Particle Systems) project [6], where some experiments will be carried out in the International Space Station (ISS), are two of these projects.

- Dense media and biological applications
Because of the possibility to describe more realistic scattering phenomena, light scattering is now used in new domains such as oceanography, colloidal chemistry, biophysics, among others.

One of the more recent aims is to describe light scattering by dense media of particles or propagation of light in dense media of particles (powder, dust, heterogenic media). In this case, electromagnetic couplings between particles occur, there is multiple scattering. Such descriptions of scattering by dense media often use radiative transfer (see section 2.6) and need the calculation of the scattering phase function in the material. To be computed, this last function may need assumption. In particular the propagation of near infrared light in biological tissues [12] (they are slightly ab-

sorbed) is a new cheap studied means, that could be used to make 3D reconstructions of organs (optical tomography)[42].

1.3 Necessity of understanding light-matter interactions

As we have seen in the previous part, light scattering can be used for particles characterizations. For example, polarization response are linked to the shape of scatterers. A comparison between polarization response of spherical and spheroidal particles is presented in reference [43] and illustrates this possibility.

However, we must underline the limitation of such an inverse problem. The properties of the light scattered by an aggregate depend on a large number of parameters:

- shape and dispersion of shape of particles,
- size and dispersion of size of particles,
- density, that is the number of particles per volume unit,
- structure of aggregates (fluffy, fractal, dense, etc.),
- optical properties of particles (permittivity, absorption, isotropy),
- quality of particle surfaces (roughness, buffing, etc.).

An inversion problem is possible if only some of the parameters are unknown and only if the dispersion of the characteristic of particles is low. The particle description obtained by inversion may have significant errors. Different kinds of scatterers can also give the same scattering phase function or polarization properties. That is the reason why for a given optical response there is not necessarily only one solution to an inversion problem. These inversion algorithms use numerical methods, whose limitations do not permit sufficient modelling compared with the complexity of reality. Therefore the better understanding of scattering that we would like to reach in this work, can also have interest to develop better inversion algorithms.

To understand the interaction between matter and light, we need:

- new more accurate scattering measurements,
- a better characterization of the scattered particles (microscopy),
- development of more powerful algorithms (able to describe interactions between larger aggregates or media),
- a better physical comprehension of the phenomena.

The objective of this work is to contribute to this last point, in particular by understanding what happens in the near field region, just around the particle. What is the intensity map around a single dielectric particle? What are the electromagnetic couplings between particles close compared to the wavelength?

1.4 Objective and outline of the dissertation

In this dissertation, first the fundamentals of light scattering phenomena will be outlined. After that, different methods used to model light scattering by particles will be discussed. Then, in chapter 3, we will describe the electromagnetic approach that we have used to model the interaction of visible light with close sub-micrometric particles. In the context of this work only a small number of particles, and particles with a size smaller or comparable with a few wavelengths will be considered. The wavelengths are assumed to be in the visible light. Most of the considered particles will be dielectric and without absorption. The case of perfectly conductive sphere, or of dielectric sphere with absorption, will only be studied in few cases. The physical measurable values will also be described.

Our studies have been carried out with a T-matrix algorithm and the Lorenz-Mie theory that have been programmed during the thesis with Matlab (programs will be accessible in Internet). The principles and limitations of this algorithm will also be presented in chapter 3. Then two main sets of results will be presented. The first result described in chapter 4 (and published in [15]) is the possibility with a simple sphere, that scatters in the far field, to focus in the near field in a point smaller than the wavelength and to highly concentrate energy the near field. This focused beam in the near field has been called a photonic jet. This new observation can open the way to applications but also points out the particular phenomena that can occur inside an aggregate of particles. The second main result, described in chapter 5 (and presented in [14]): is about a proposed physical interpretation of the electromagnetic coupling between two spheres. If a single dielectric sphere is able to concentrate energy in the near field, importance of electromagnetic couplings between close particles can be understood. The chapter 6 will summarize our main results and outline the future problems and potential research directions.

Chapter 2

Light scattering

After giving a general definition of what light scattering is, here we will discuss the fundamentals equations and properties induced with light scattering phenomena. Scattering regimes will be described depending on size and refractive index, for single particle and aggregates. Then a-state-of-the-art in measurement techniques and rigorous electromagnetic solvers for light scattering, will be presented. The transition from single to multiple scattering will also be discussed. More detailed technical aspect will be left to the next chapter.

Light scattering is the general concept to point out light interaction with matter. First we must distinguish several particular cases that are also included in light scattering:

- We discuss **refraction and reflection** when the boundaries between materials are plane or with smooth variation on a large scale compared to the wavelength. The material must be homogeneous and able to be described by the macroscopic concept of refractive index. In this case the Snell-Descartes laws (geometric optics) and reflective coefficient of Fresnel can be used to describe light path.

- We discuss **diffraction**, when we consider the optical effect of a spatial change in the optical property of a material, if this change has a size of the same order of the wavelength and if this change has a regular shape or is periodically repeated. In this case the electric field must be considered as a wave: Fourier optics, gratings etc. [44, 45, 46].

- We discuss **scattering** when we consider small, irregular spatial variations of the optical properties of the matter (permittivity, shape). When these variations cannot be easily described (random media, roughness, inhomogeneities, etc.). As represented in figure 2.1 the three previous regimes are included in light scattering phenomena.

- We discuss **quantum optic** when we must take into account the quantification of the energy exchanges that occur during light material interactions. That is when

the incident flux contains only few photons. (Laser is not necessary considered quantum optics).

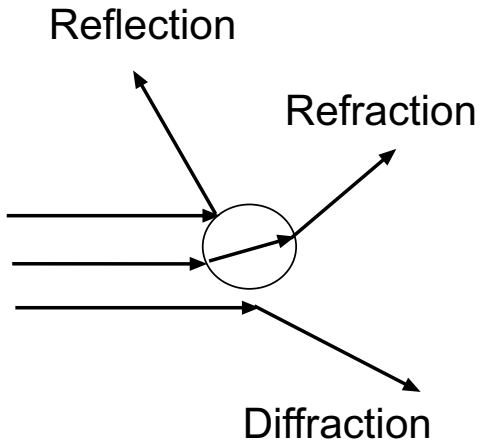

Figure 2.1: Refraction, reflection and diffraction in scattering phenomena.

Diffraction is included in light scattering phenomena, however the difference between scattering and diffraction is not always clear. For example the interaction between light and one spherical particle or aligned spherical particle may simply be considered as diffraction, whereas the interaction of light with randomly positioned spheres is light scattering. In the case of random spheres, if there is independent and single scattering, the laws will be very similar to the case of light scattering by one particle. The only difference will be the use of a function describing the density of particles. In these two cases (random and regular structures) the Lorenz-Mie theory can be used to describe the phenomenon, what illustrates similarities between diffraction and scattering in some cases.

In this work, the considered medium are random with irregular change of optical properties. This change is assumed to be small compared to the wavelength but large enough compared to molecular size. The flux are assumed to be enough to neglect quantum effects. It is why we consider the word "scattering" as being more appropriate for the approach discuss here.

Usually surface and volume scattering are separately studied. Surface scattering deals with surface quality and roughness [47, 48], whereas volume scattering describe the light scattering by particles or inhomogeneities [13]. A lot of works have already been report on surface scattering [47, 48], but in this thesis we will deal only with volume scattering.

2.1 Single and independent scattering

We must also distinguish dependent and independent scattering, that is when phase effects can occur or not:

Independent scattering: if the scattering particles are far from each other and if the incident wave is slightly coherent, no phase effect will appear (no interference between the wave scattered by each particle). The global scattered intensity is the sum of the intensities scattered by each particle.
As approximative criterium, it can be considered that independent scattering occurs when the distance between particles is larger than 3 times de radius of one particle (for few wavelengths radius particles) [3, 21].
Light scattering by the clouds (Drops of $1mm$, density : $1drop/cm^3$) is an example.
Another case can justify independent scattering when the incident field is coherent. There is independent scattering with a coherent incident wave, if the speed of motion v of particles are larger compared to the integration time t of the quadratic sensor ($\lambda/v > t$ with λ the wavelength); for example, a gas of particles [7].

Dependent scattering: if the scattering particles are close together, scattered waves interfere [3]. The global scattered intensity must be computed as the mean square of the electric field. Dependent scattering can also partially occur for an incoherent incident wave. This is the case in the opposition effect (in backscattering, see section 2.4).

The scattering laws, as the electromagnetic ones, do not depend on the size of the particle but of the ratio a/λ where a is the characteristic size of the particle and λ the wavelength. That is the reason why one talks about the **size parameter** $x = ka = 2\pi a/\lambda$ (k is the wave vector). We will use these notations in the following. We first consider particles that scatter independently of the other particles. Depending on the refractive index and of the size parameter of these particles, different approximations can be made. Each of these approximations correspond to a particular family of scattering. These families are represented in figure 2.2.

For single independent scattering, we distinguish [3]:
Rayleigh scattering (1871): the particle is very small compared to the wavelength ($a << \lambda$). This case will be studied section 2.2.
Rayleigh-Gans scattering (1925): it is an extension of Rayleigh scattering for larger particle but with a small refractive index, a small absorption and a parameter size ka such as $|n-1| << 1$ and $ka|n-1| << 1$. This case will not be studied but is very similar to Rayleigh scattering.
Anomalous diffraction: the particle is bigger than the wavelength but the refractive index is small $|n-1| << 1$. Reflection and diffraction are low. The particle only introduces a phase shift $2(n-1)ka$, what will create interferences.
Geometrical optics: for very large particle $a >> \lambda$, ($ka > 300$). Ray tracing can be used to study this case.

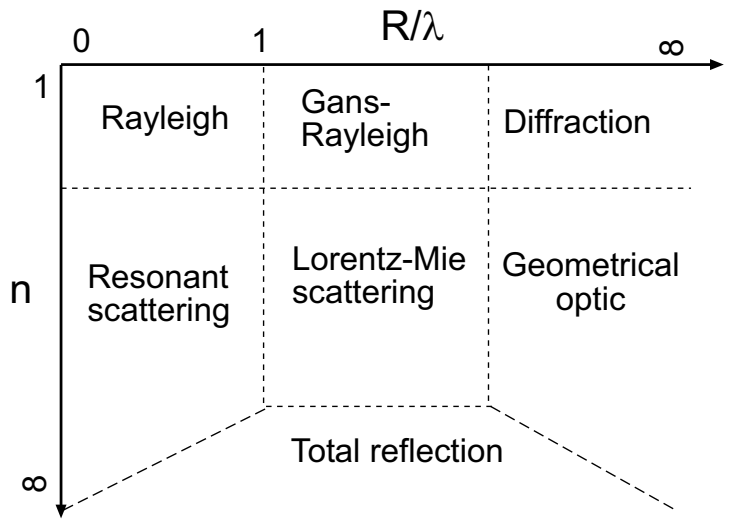

Figure 2.2: Several different scattering regimes as functions of R and n [3].

2.2 Rayleigh scattering

The Rayleigh scattering is historically the first quantitative description of light scattering phenomena. Its success came from its ability to justify why the sky appears blue. This model assumes single scattering and incoherent sum of intensities in the far field. We will discuss Rayleigh scattering below for the cases of polarized and unpolarized incident field.

Basic characteristics [3]
Consider particles with radius a, which is small compared with the wavelength ($a << \lambda$) and a density of particles not too large. In this case, the linear polarized light is scattered with a scattering phase function (describing the scattered intensity according to the direction) which appears like in figure 2.3 (dimpled-ellipsoid). There is no local intensity maximum. No light is scattered in the axis of the incident electric field vector, but light is scattered in all the other directions. When particles are larger the scattering phase function is modified: local intensity maxima appear in several directions, with angle-widths which are more narrow. The forward scattering increases (figure 2.4 a and b).

In Rayleigh scattering the scattered field has the same polarization than the incident wave. In figure 2.6c, for an linear polarized incident wave, we can see that the degree of polarization is equal to 1 in all directions and that $S3 \simeq 0$, consequently the polarization of the scattered field is linear in all direction. The orientation of the electric field is represented in figure 2.6b. However if the incident wave is unpolarized, the light will be scattered in all directions, the light will stay unpolarized in forward and backward directions but will be linearly polarized in the orthogonal plane of propagation. This can explain the partially polarization of a clear sky light [7].

Now if we put a small particle in an unitary incident plane wave, we would like to know what is the ratio of the incident flux that is scattered? To find the answer, we study the normalized scattered cross section. The scattered cross section multiplied by the incident flux yields the total scattered power by the particle (definition). This cross section can be normalized by dividing by πa^2 (see section also 3.7). Figure 2.5 shows that the part of flux that will be scattered does not depend only on the effective section πa^2 of the particle (if it was the case the normalized cross section would be equal to 1) but falls when the radius of the particle decreases.

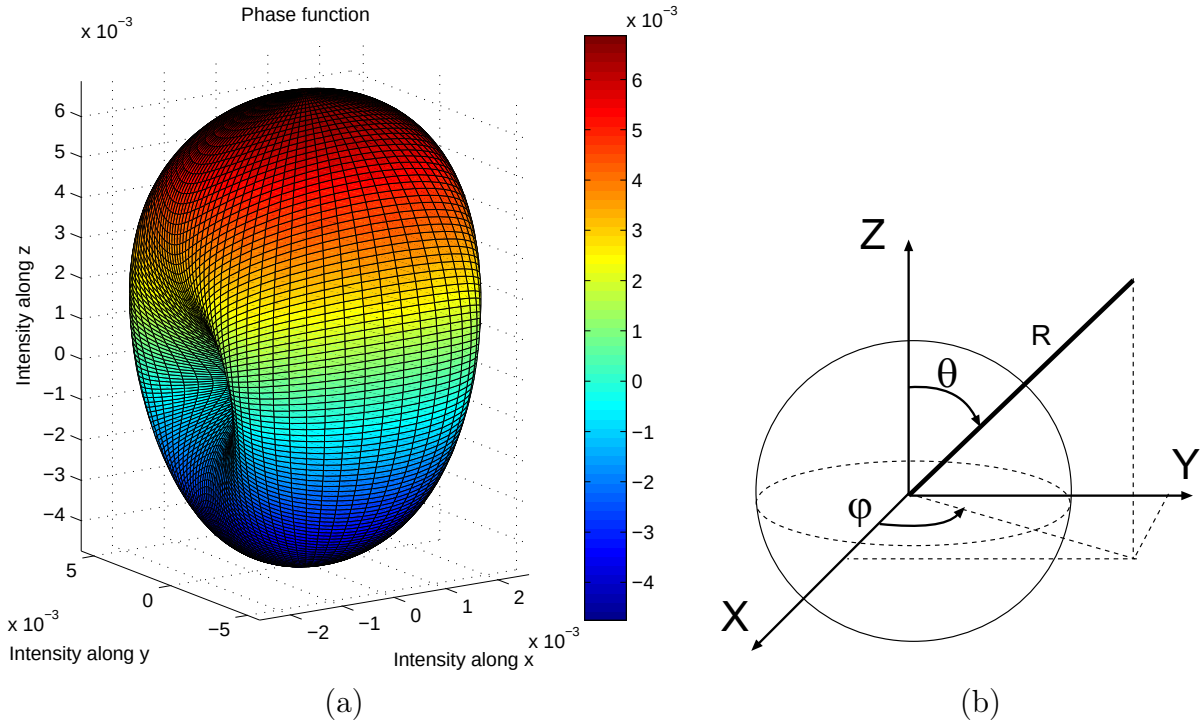

(a) (b)

Figure 2.3: (a) $I(\theta, \varphi)$ for one sphere $a = 0.1\lambda$, $n = 1.52$, $H_i = H_y$, $k = k_z$ (angles in degree). (b) Spherical coordinates.

Qualitative demonstration

To understand the phenomenon of light scattering by small particles, we will first use the same qualitative reasoning given by Lord Rayleigh in 1871 [7].

One assumed that because of the particles motions, no phase effect (interferences) are taken into account (Note: it is not true in the forward and backward direction, see the *opposition effect* in section 2.4). Therefore the total scattered intensity is the sum of the intensity scattered by each particle. Because of the very small size of particles compared to the wavelength, the shape of the particle is assumed not to have influence (it is not always true [49]), the particle is assumed isotropic and homogeneous. That is the reason why the particle behaves as punctual disturbance, from which the scattered waves disperse outward.

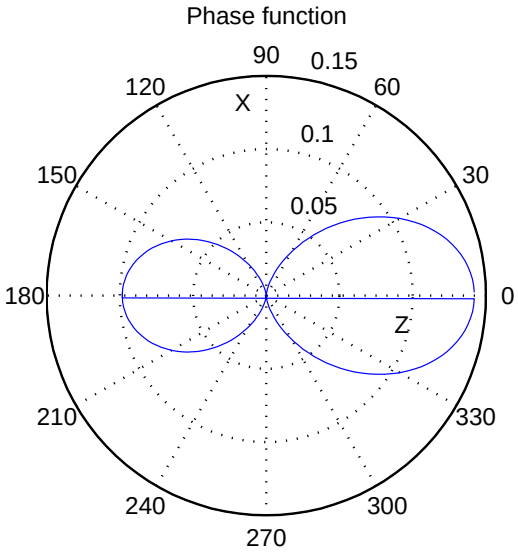

(a) $a = 0.1\lambda$

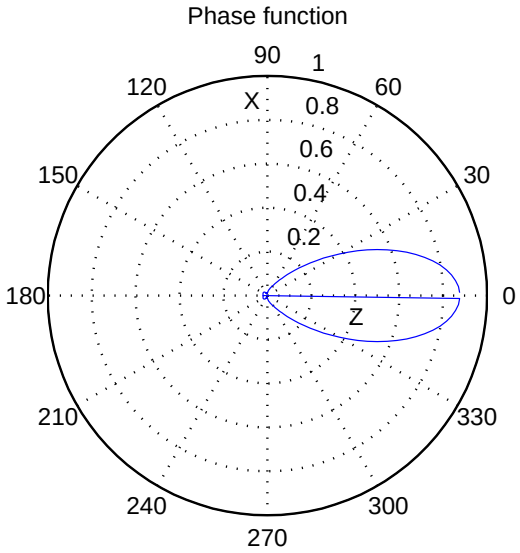

(b) $a = 0.5\lambda$

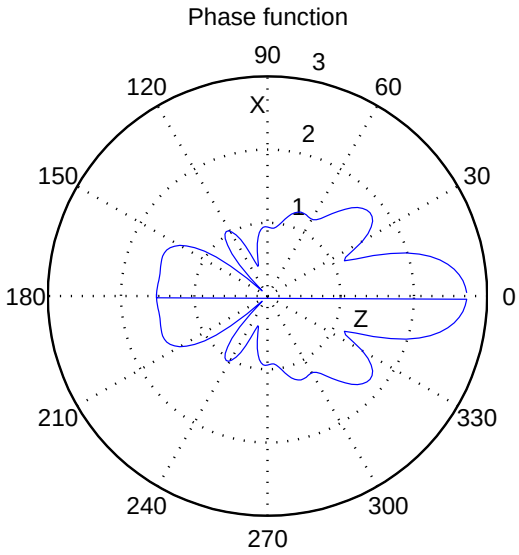

(c) $a = \lambda$ (log scale)

Figure 2.4: $I(\theta, \varphi = 0)/(k^2 C_{sca})$ for a sphere with $n = 1.52$, $H_i = H_y$, $k = k_z$ and 3 different radii a. $\varphi = 0$ corresponds to the forward scattering. $C_{sca}$is a normalization constant.

If a linear polarized wave is considered, we can find the polarization state of the scattered wave by using a geometrical method (see figure 2.6a). The scattered field at a distance r far from the particle will be in the transverse plane (plane orthogonal to the propagation direction $\vec{k}_s$). Rayleigh explains that this vector will also be in the plane containing the particle, the observation point and the incident electric field (vector). The intersection of the two planes gives the orientation of the electric field. We also

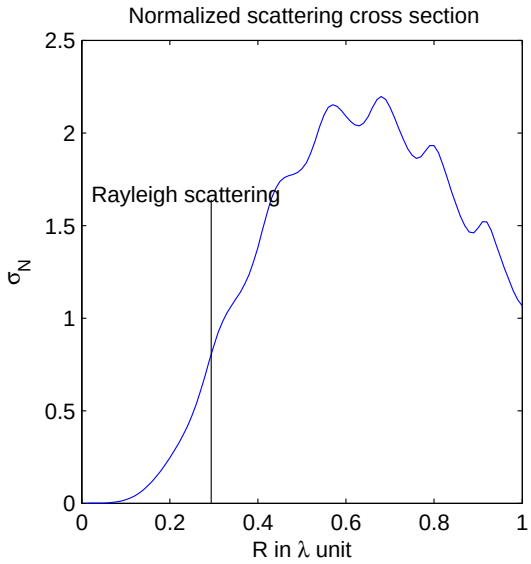

Figure 2.5: Normalized scattering cross section of a sphere of radius R and $n = 1.52$, $H_i = H_y$, $k = k_z$.

deduce that no field will be scattered in the $\vec{E_i}$ axis.

Rayleigh used a dimensional study to find the law describing the total scattered intensity. The electric field amplitude may depend directly on the incident field amplitude E_i, directly on the volume of the particle V (and not of its surface), indirectly of the distance r between observation and particle, and also depends on the wavelength λ. The light velocity in free space cannot appear because it would be the only term with a time dimension. Other dimensionless terms can appear (as the refractive index) but we can not find their influences with this method. If we want an homogeneous equation:

$$E^s \alpha \frac{E^i V}{r\lambda^2} \text{ and } I^s \alpha \frac{I^i V^2}{r^2 \lambda^4}$$

The $1/\lambda^4$ dependence is obvious from this relationship. Rayleigh went on to demonstrate with a mathematical analogy to mechanics, which was usual at his time.

Theoretical models

Several rigorous methods allow to derive the Rayleigh's law:
- by using the potential vector [8],
- by considering only the first order of the Lorenz-Mie theory $\vec{E}^s(\vec{r}) = a_1 \vec{\Psi}_1(\vec{r})$ (see appendix B.4),
- by analogy with a dipole of polarizability α [3].

In this last case the scattering cross section is [3]:

$$C_{sca} = \frac{8}{3}\pi k^4 |\alpha|^2$$

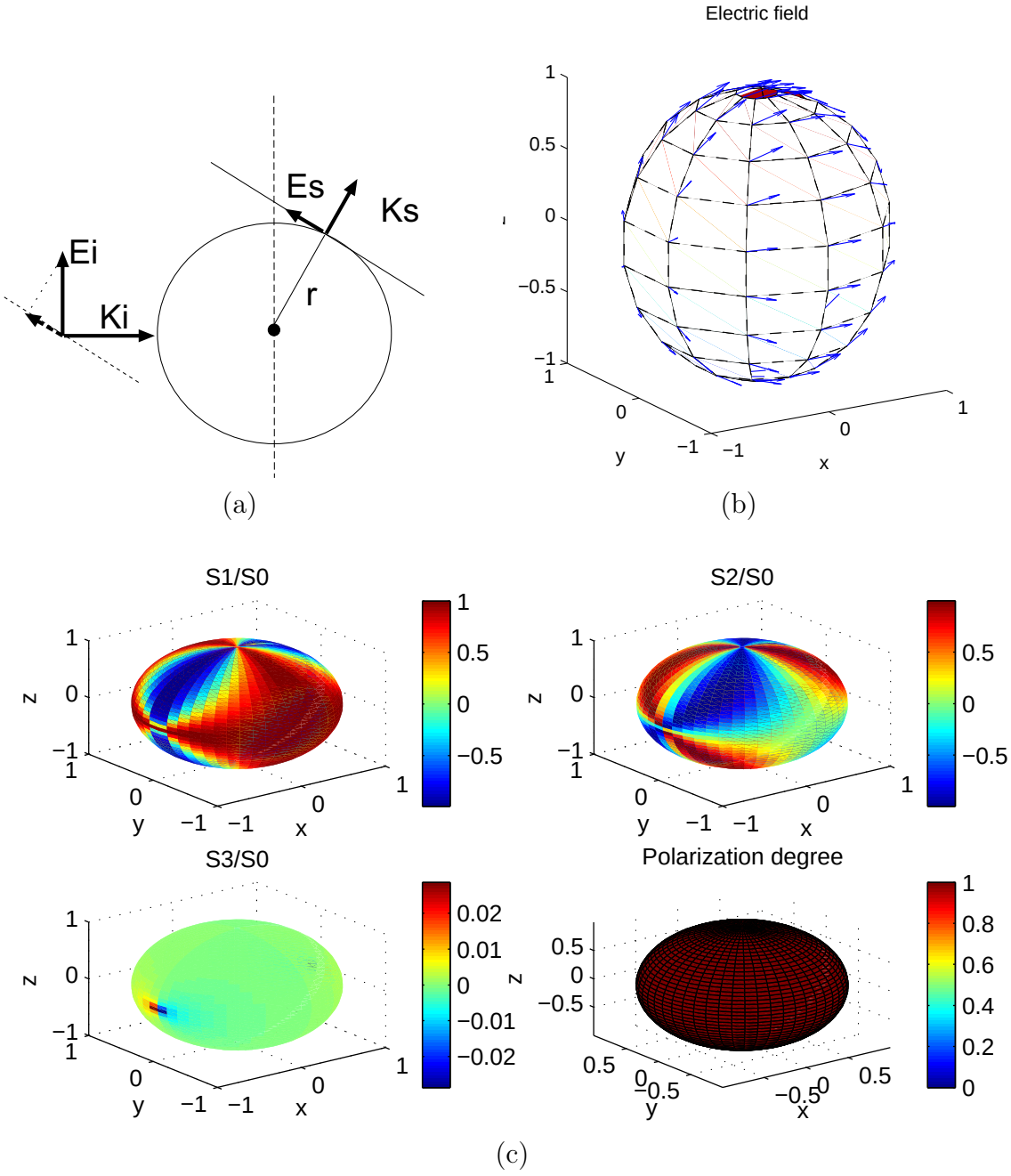

Figure 2.6: (a) Geometrical description of Rayleigh scattering. (b) Scattered electric field vector. (c) Stokes parameters. $a = 0.1\lambda$, $n_2 = 1.52$, $H_i = H_y$, $k = k_z$.

and the scattering diagram [3]:

$$I(\theta) = \frac{1 + \cos^2\theta}{2r^2} k^4 |\alpha|^2 I_0$$

These two values are in $\frac{1}{\lambda^4}$.
The polarizability when the particle is spherical with a radius R is:

$$\alpha = \frac{n^2-1}{n^2+2}R^3$$

When the radius of the particle increases, the intensity of forward scattering grows but with a smaller angle of scattering and other directions of scattering appear (figure 2.4c), the forward scattering is dominated by the Fraunhoffer diffraction. If particles are spherical, their scattering can be described by the Lorenz-Mie Theory.

2.3 The Lorenz-Mie theory: a summary

Lorenz-Mie theory is exact analytical solution of Maxwell equations for spherical particles. Demonstration was made by Gustav Mie in 1908 [9, 27, 28] and had been studied before by Lorenz in 1891 [29, 30]. The demonstration is detailed in section 3.2. A Mie code can be download for example in [Web2], yet we have written a program for our work in order to have a better understanding of it.

The Helmholtz equation (2.1) can be expressed in spherical coordinates (r, θ, φ). These coordinates are represented in figure 2.3(b).

$$\Delta\vec{E} + k^2n^2\vec{E} = 0 \tag{2.1}$$

As it will be shown in section 3.2, solution of this equation can be described by the Spherical Vectorial Functions (SVF) noted $\vec{\Psi}_n(r, \theta, \varphi)$. Because of the superposition principle, the total electromagnetic field out of the sphere can be described as the sum of the incident field $\vec{E^i}$ and the scattered field $\vec{E^s}$. $\vec{E^w}$ is the field inside the particle. Each of these fields can be decomposed in spherical vectorial functions (2.2) with respective components a_n^i, a_n^s and a_n^w.

$$E^\alpha = \sum_n a_n^\alpha \Re e[\psi_n] \text{ with } \alpha = (i, w)$$
$$E^s = \sum_n a_n^s \psi_n \tag{2.2}$$

The a^i components are known. Because of the linearity of Maxwell equations, there is a linear relation between a^i and a^s that can be described with a matrix product. The T-matrix is the matrix T such as $a^s = Ta^i$. This matrix can be found by applying the boundary conditions on the tangential components of the electric and magnetic field [20, 37] (For perfectly conductive spheres, the tangential component of the magnetic field is not continuous but the discontinuity is known and can be described by surface currents). In the case of a single sphere the T-matrix is diagonal because the SVF, which constitute the basis of expansion, are the eigenmodes. In the Lorenz-Mie theory, the scattered field is analytically calculated.

Mie scattering can be used for spherical particles. This kind of particles, with size

that can be compared with the wavelength of visible light, are relatively usual in nature. It can be applied for dependent (sum of the amplitudes) or independent (sum of the intensities) scattering, but considers only single scattering, that is, each particle scatters only the incident wave.

In Mie scattering, the scattering phase function has local maxima in several specific scattering directions. The main scattering direction is the forward direction (with a narrow forward scattering angle). The lower secondary maxima at other angles (see figure 2.4) can be used to find the properties of the scatterer. The laws describing the total scattered intensity as a function of the incident wavelength and particles properties areF more complex than for Rayleigh scattering. The $1/\lambda^4$ dependence of the total scattered intensity in the Rayleigh case is not true in the general case for the Lorenz-Mie theory. These laws depend on the radius, the refractive index and the absorption of the particle. This complexity is due to resonances can occur with the cavity modes inside the sphere.
For a linear incident wave, the polarization of the scattered wave is not necessarily linear as in the Rayleigh case. It will depend on the direction and will be elliptic in the general case (see our computing of $S3$ in figure 2.7). For a long time, scatterers

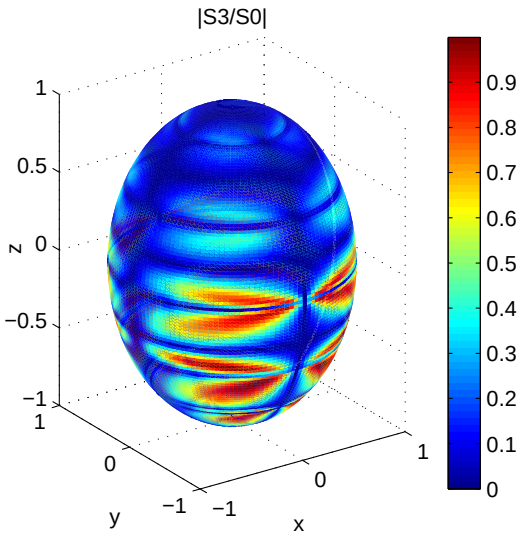

Figure 2.7: Parameter S_3 of Stokes for a sphere of radius $a = 1\lambda$, index $n = 1.52$ and for an linear polarized incident wave $H_i = H_y$, $k = k_z$. Black: circular polarization, white: linear polarization, gray: elliptic polarization.

have been considered as approximately spherical particles. But some phenomena can not be described by light scattering of spherical particles:

- halos and arc observed for atmospheric ice crystals light scattering. [50, 51],
- induced polarization by oriented grains [52],
- depolarization effect in radar scattering by Cirrus Crystals.

Note that the Lorenz-Mie theory describes only single scattering.

2.4 Multiple scattering and aggregates

We must now consider the case of multiple and dependent scattering and first clearly distinguish single and multiple scattering. Then we will give some examples where multiple scattering occurs and some observations about light scattering by real particles.

Single scattering occurs if the density of particles is low or if particles are far from others compared to the wavelength. Each particle only scatters the incident light. Light scattered by N particles is N times the light scattered by one particle.

Multiple scattering occurs if the density of particles is high or if the particles are close to each other compared to the wavelength. Each particle does not only scatters the incident light but the light scattered by the others too. Resonances between particles can affect the scattered light profiles.
For example, in clouds only 10% of the scattered light is due to single scattering, the rest is due to multiple scattering. Several criteria can be used to identify multiple scattering process. There is multiple scattering when an increase in the number of particles induces not the same increase of the scattered intensity. Multiple scattering can also be identify when the extinction increases faster than the number of particles. Multiple scattering also often causes a decrease in the polarization degree.

When there is single scattering, the scattering diagram (or scattering phase function) of each individual scatterer is calculated and the global scattering is found by adding the effect of each scatterer. In multiple scattering, the method must take into account the interaction between particles, that is called electromagnetic coupling.

Multiple volume scattering can mainly be considered in three cases:
-dense media of particles,
-aggregate of particles,
-description of a non-spherical particle by an aggregate of subwavelength particles.

Dense media of particles
The study of dense media of particles is difficult because of the great number of particles, of their difference of shape and orientation, and because of the large scale of electromagnetic coupling. In theoretical simulations, because of algorithm limitations, multiple scattering is only considered along several wavelengths. The dense media of particles are often described as a group of aggregates, but these descriptions are not always accurate.
Macroscopic media are often made of a great number of anisotropic particles with random orientations. If this random orientation is described by an uniform law, that is if all orientations are equally probable, scattering properties are independent of the incident polarization and have an axis symmetry, they depend only on the **phase angle**, that is the angle between the incident and the scattered direction. To simulate such media, Mishchenko [53, 13] has proposed to average the scattered light on the various orientations of the particle by using the Euler's angles (figure 2.8).

In some easier cases, when particles are smaller than the wavelength, the scatter-

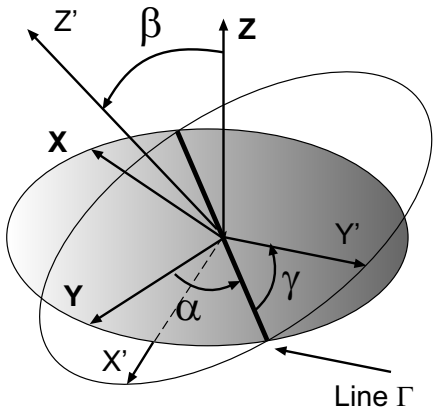

Figure 2.8: The Euler angles allow to describe the orientation of a particle. α is in the (O, x, y) plane and describe the line Γ. z' is orthogonal to Γ and makes an angle β with z. γ is the angle between Γ and y' in the plane orthogonal to z'.

ing medium can be described by an effective complex index (Maxwell-Garnett formula [8] p.634).

Aggregate of particles case
In many practical cases, the scatterer is an aggregate of particles. Multiple scattering occurs inside aggregates but not between aggregates. Several natural phenomena can cause such an aggregation. Cluster-Cluster Aggregation (CCA) and Cluster-Particle Aggregation (CPA) are often distinguished [54]. These two process create several kind of aggregates, with different densities. In some papers [55, 54], these aggregates are described as fractal structures with fractal dimensions, inspired by the work of Mandelbrot (example of dimensions d: $Masse = R^d$ or $Rayon = N^d$ with N the number of particles).

Non-spherical particle case
In the previous case the scatterers were real aggregates, but an aggregate of particles small compared to the wavelength can be used to describe a non-spherical particle. That is the method used in the DDA algorithm. Other algorithms have been coded to generate automatically the shape of non-spherical particles as random gaussian-sphere generated by the code of K. Muinonen [51]. In this thesis, we will consider only spherical particles and aggregates of spherical particles. However the T-matrix algorithm that we have used can be adapted to non-spherical particles.

Observations and comments
Some other scattering effects have been observed on real particles or aggregates:
-the particle absorption increases backscattering and decreases forward scattering,
-roughness on particles' surfaces decreases forward scattering and increases lateral scattering,
-in forward and backward directions the phase effect can not be neglected. A consequence may be the **opposition effect** [56] and the **negative polarization** [57] observed in backscattering.

The opposition effect is a non-linear increase of backscattering intensity when the number of particles increases. The first controlled experimental observation of this phenomenon has been carried out by Kuga and Ishimaru in 1984 [56]. The negative polarization is a small linear polarization observed in backscattering [57] for an unpolarized incident wave. The *negative* expression only describes the orientation of this linear polarization in opposition to the positive polarization that can be measured for $\alpha = 90$ and which is orthogonal to the negative one. In general, this branch of negative polarization for small phase angles may appear for dense aggregates (with multiple scattering) with high absorption and a size parameter bigger than 1 [49]. The more the refractive index of particles is high, the more we would have a chance to observe negative polarization. The typical curves of these two phenomena are represented in figure 2.9, they are still badly understood. We will not study these phenomena.

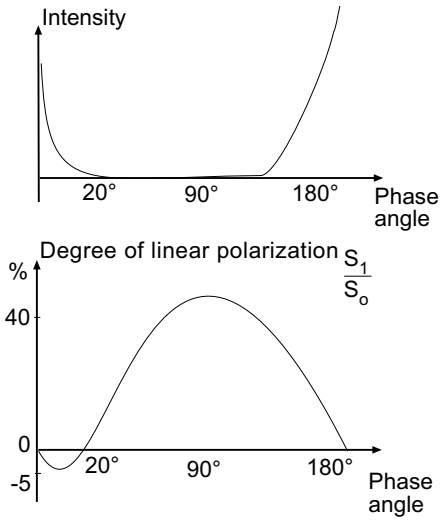

Figure 2.9: Typical curves of intensity and linear polarization degree illustrating negative polarization and opposition effect.

Light scattering by such an aggregate can be studied experimentally or with numerical calculation.

2.5 Measurements

In this section, we present a rapid overview of measurement techniques used to observed light scattering and the possible problems.

A great number of measurement techniques have been reported in the atmosphere and in astronomy:

- a negative polarization was observed in backscattering of light by the surface of the Moon by Lyot in 1924 [58] and recently by Shkuratov in 1992 [59, 49],
- light scattering by asteroids, such as comets, has been measured [60] (brightness and linear polarization degree),
- light scattering by dust (regoliths) of planets or satellites such as Titan [61] or Mars [62] has been carried out, respectively by the space probe Huygens and the space probe Pathfinder,
- interstellar dusts have been studied [63, 64].

In all these cases, the incident light is unpolarized and originates from stars. The scattered light is partially linearly polarized around the orthogonal plane (phase angle $\alpha = 90^o$) and unpolarized in the other directions. A negative polarization can appear in backscattering. Light scattering makes the observed intensity by telescopes decrease, but is also used to identify the structure of scatterers (regoliths, dusts, solar ejections, etc.)[5]. For example, such an information is useful to understand planet formations. Most of the observations were made by satellites. Some new experiments are planned in the International Space Station (ISS) and the details are given in [6].

Experimental Difficulties
Some physical properties of the scatterers and of the scattered light cannot be easily measured. Some measurements are not easy to carry out. That can contribute to explain the difficulty to correlate observations and numerical simulations.
For example, an integration sphere is necessary to measure the total scattering cross section, that is why physicists prefer to measure backscattering or extinction (forward) cross section. Backscattering measurements are not easy because they are to be performed in the same direction of the incident wave. For this purpose beam separators can be used [57].
In experiments, assumptions concerning particles motion is made. The motion of particles can yield a Doppler effect. This can also justify incoherence of light. The immobility can also be assumed; however the verification of these variations is always difficult.
Another difficulty is finding the absorption coefficient of dielectric material. Some low absorption coefficients of material can create high absorption in aggregate because of multiple scattering. This interaction increases the *mean path* in the material and thus the absorbed light. The absorption cross section of an aggregate can be measured, but its link with the absorption of the material is difficult to find.

Another important question is to find statistical information about random media. When it is possible, microscope image analysis is used to find size dispersion, shape, etc. However these data are imperfect. The fabrication of controlled samples of which properties would be known has been tried [65].
In order to carry out comparisons with numerical simulations, the knowledge of the total scattered power or of the incident flux would be useful. Unfortunately these two values are often unknown in experimental measurements. For example, if the scattering of solar light is studied, an integration sphere will be impossible to use and the total scattered power will be unknown.

Microwave analogue experiments
The micro wave analogies are another kind of experiment that have interest [66]. In the electromagnetic theory, spatial dimensions only depend on the ratio of size divided by the wavelength. Thus by using microwave, known macroscopic particles or aggregates can be used to carry out studies. With microwave, electric field can be directly measured. But this method has some limitations. Firstly the optical properties of material for microwave are rarely the same as for visible light. Moreover, in microwave, far field meas urements become difficult (the far field area depends on the wavelength and on the particle size) and precautions must be taken (sensor size, position, etc.).

Even though there are many measurement techniques which have been carried out, it is still difficult to correlate measurements with numerical simulations. There is also significant limitation on simulations such as the difficulties to simulate large aggregates. The next section will describe the numerical simulation methods commonly used in the literature.

2.6 Electromagnetic solvers: libraries and comments

Several algorithms are used to simulate scattering media and are summarized in table 2.1 and in figure 2.11. Figure 2.11 is a non-exhaustive classification of algorithm used to study light scattering. We propose for this classification to ask the following five questions for each algorithm:

1. How does the algorithm take into account the time components? Does it compute the time evolution or calculate the stationary case?

2. How is the physical space described? By sampling or by using an expansion of field on a basis of functions?

3. How are the material properties described? With discrete values, with continuous functions or with a physical system (dipoles for example)?

4. How are the physical equations introduced? By the Maxwell equations (with finite elements or with finite differences), by the Helmholtz propagation equation or by the integral formulation?

5. How are the boundaries considered? With surface currents, with the continuity of the tangential components of the electromagnetic field?

This method of classification we propose is not perfect. However this classification makes it possible to have a global overview of algorithms that are used to study light scattering.

In our case, scatterers are close together. So we cannot only consider the scattered intensity but we must calculate the electromagnetic field. Moreover we do not have to study each scatterer alone but we must take into account interactions between scatterers (multiple and dependent scattering). The methods able to simulate such systems are outlined below:

- **Separation of Variables Method (SVM).** If particle shapes are well-defined, adapted coordinates are searched in order to find analytical solutions of the Helmholtz equation. These analytical solutions are used as an expansion basis for the electromagnetic field. The relation between incident and scattered field is found by applying boundary conditions. This approach was followed for sphere by Mie [9] (see section 3.2), for concentric core-mantle spheres by Aden and Kerker [67], for concentric multilayered spheres [68] and homogeneous isotropic infinite cylinders [69] by Wait, for infinite isotropic elliptical cylinders by Kim and Yed [70], and for homogeneous isotropic spheroids by Asano and Sato [71].

- **Finite Difference Time Domain (FDTD)** [33, 16, 34] is a numerical method, which uses finite difference in space and time to solve the differential equations of Maxwell (Yee formulae [33]). This method makes it possible to have the evolution in time of the electromagnetic field in space by iterative computing among the initial value of the field. Space and time are discretized ($\Delta x \simeq \lambda/20,\ \Delta t = c/(2\Delta x)$ in $2D$). The discretization lattice of space is cartesian like. It is often difficult to find a suitable lattice adapted to the geometry of complex problems. Another difficulty is the choice of numerical boundary conditions that calculate the field close to the computed zone to simulate infinite free space around. These boundary conditions, called Absorbing Boundaries Conditions (ABC) can create non physical reflections. The usual numerical boundaries conditions are the Mur [72] conditions or the Perfectly Matched Layer of Berenger (PML) [73]. The main drawback of FDTD in our case is the time of calculation, and especially because we do not search the evolution in time but only the stationary state. Simulations are often limited to 2D systems because of the large amount of memory needed. Because of the same problem of memory needed, only the field around the studied object is calculated, but integral methods can be used after to calculate far-field [14b].

- **Finite Element Method (FEM)** [31][32]. In this approach, space is also discretized but with a triangular lattice. The Helmholtz's equation (and not the

Maxwell equations as in FDTD) is expressed in all points as a linear system, which must be solved. The stationary solution are directly found. This system can be described with sparse matrix and is solved by using optimization methods as Conjugate Gradient Method or Gaussian Elimination [32]. The main drawback of this method is the memory needed for the calculation.

- **Point Matching Method (PMM)** [74]. In this approach, the incident field, the scattered field and the field inside the sphere are expanded on the spherical vectorial functions. To calculate the expansion coefficients, boundary conditions are applied by applying the mean square method at as many discrete points on the surface of the particles as is necessary. The method is accurate if the particle is not too large and displays symmetry. This method lets us know the field inside the particle.

- **Method of Moments (MoM)** [75]. This method is also called the **Volume Integral Equation Method** and is based on a volume integral (2.3).

$$\vec{E^t}(\vec{r}) = \vec{E^i}(\vec{r}) + k^2 \int_V d^3\vec{r'}[I + \frac{1}{k^2}\nabla\nabla]\frac{\exp(ik(\vec{r} - \vec{r'}))}{4\pi(\vec{r} - \vec{r'})}[n^2 - 1]\vec{E}(\vec{r'}) \qquad (2.3)$$

(I and $\nabla\nabla$ are described section 4.1). The total electric field $\vec{E^t}$ at the position $\vec{r}$ is given as the sum of the incident field $\vec{E^i}$ and an integral on the volume of the particle. The Green function is used: $exp(ik(\vec{r} - \vec{r'}))/(4\pi(\vec{r} - \vec{r'}))$.
The scattered field is calculated in two steps:
1-the scatterer is discretized in small cubes around the size $\lambda/20$. This integral is expressed for each cube and interactions can be described as a matrix equation. An optimization method makes it possible to solve this equation and to find the field inside the aggregate,
2-the field outside the aggregate is calculated by using the integral and the field computed in the previous step.
Each volume of the scatterer can be considered a secondary source. This method makes it possible to simulate inhomogeneous, anisotropic or active media.

- **Discrete Dipole Approximation (DDA)** [17, 35, 36]. This method is another version of the Method of Moment. One version can be download in [Web5]. The volume of the particles is described with an array of discrete dipoles. The N dipoles scatter the incident light and the light scattered by the N-1 others. When the polarizability (oscillating polarization) of dipoles are known, these interactions can be written as a linear equation. Two methods are currently used to calculate the polarizability of each dipole: the Lattice Dispersion Relation (LDR)[54] and the a1-term method, which uses the first expansion coefficient of the Lorenz-Mie theory as polarizability.

- **Radiative Transfer** [13, 10, 11]. This method has the originality of describing directly quadratic values (intensities). Its equation gives the variation of luminance at a point along an optical path as function of the luminance at this point and of the luminance around (2.4). With this method the luminance in space can be found but the knowledge of the scattering phase function of each point is needed. This equation is equivalent to an energy balance in a small volume (figure 2.10):

$$\frac{dL(\tau,\vec{\mu})}{d\tau} = -\beta_o L(\tau,\vec{\mu}) + KL(\tau,\vec{\mu}) + \int_{4\pi} L(\tau,\vec{\mu'})M(\tau,\vec{\mu},\vec{\mu'})d\vec{\mu'} \qquad (2.4)$$

$\vec{\mu}$ is an unit vector describing the direction of propagation.
τ is the optical thickness along the direction $\vec{\mu}$. τ is homogeneous with a refractive index. For example if we consider a gradient of optical index along the z-axis, $\tau = \tau_o e^{-\alpha z}$.
$L(\tau,\vec{\mu})$ is the luminance at the *position* τ in the direction $\vec{\mu}$. Its unit is $Wm^{-2}sr^{-1}$.
β_o is the extinction coefficient (sum of absorption and scattering coefficients).
K is an eventual gain if the medium is active such as the gain due to Plank's blackbody emission.
$M(\tau,\vec{\mu},\vec{\mu'})$ is the scattering phase function

This equation can be vectorial if we replace the luminance L by the Stokes

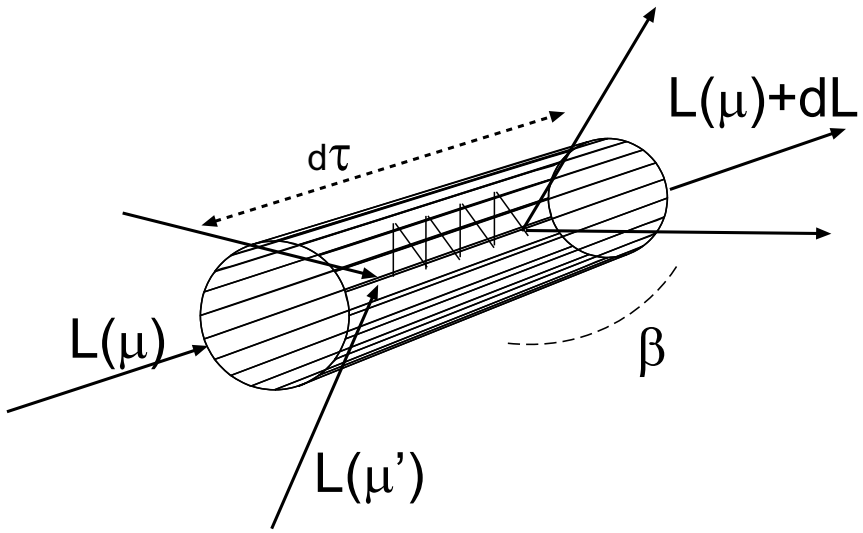

Figure 2.10: Energy balance in a small volume of a scattering medium used in radiative transfer method. L is the luminance, τ the optical thickness, β the extinction coefficient, μ the angular direction.

parameters and the scattering scattering phase function M by the phase matrix (or Mueller Matrix). However the difficulty will often be to find this phase matrix, that is the reason why this method is only applied for particular cases such as atmospheric scattering or with approximations. Another limitation is that this

method only considers far field luminance: The phase matrix is applied to the Stokes parameters, that is in a region where the electromagnetic field is transverse. Close to the scatterers it is not always the case (see discussion in part 4.6).

- **T-matrix method** [37]. In this family of methods the electromagnetic field is decomposed on a basis of functions adapted to the geometry of the scatterer. The T-matrix is a matrix, which links the components of decomposition of the incident wave on this basis to those of the scattered wave. Such a matrix exists because of the linearity of the problem. As explained in section 3.4, we use this method for studying of electromagnetic couplings between particles. There are several methods to calculate this T-matrix:
  - the Discrete Dipole Approximation (DDA),
  - the FDTD is used to calculate the stationary states. The result is decomposed on the chosen orthogonal basis,
  - the Point Matching Method (PMM),
  - in independent scattering, by experimental measurements of the scattered intensity and projection on the orthogonal basis,
  - **the Extended Boundary Condition Method (EBCM)**: this integral method using the Green function will be developed in section 3.4. EBCM and T-matrix are often assimilated.

  Several names are used to describe T-matrix algorithm or algorithms very similar to it:
  - Extended Boundary Condition Method [13]
  - Multipole expansion method [76]
  - KKR Method (for photonic crystals) [77, 78, 79]
  - Multi-Level Fast Multipole Algorithm (MLFMA) [80]

We must also cite other approximative methods:

Equi-Phase Sphere method (EPS): in this method [81] a homogeneous non-spherical particle is replaced by a sphere with the same refractive index and with a diameter corresponding to the longer path that light may make in the non-spherical particle. The equivalent sphere depends on the incident wave direction of propagation.

Monte-Carlo Ray tracing: This method [82] adapted to particles larger than the wavelength is based on a Monte-Carlo algorithm. Random optical rays are traced by applying Fresnel and refractive laws. Phase of each ray is computed. The angular density of rays makes possible to approximate the scattering phase function.

Table 2.1: Comparison of rigorous algorithms for electromagnetic problems. $x = ka$ is the size parameter. The computing time is given as a proportion of the parameter size, in some case different algorithm can be used.

Method	Size	Computing time	Advantages	Disadvantages
SVM	x<40	x^3 or x^4	fast and accurate for simple geometries	badly scaled if kR, n or absorption are too important
FDTD	x<10	x^4 in 2D	easy to code, computing for several λ	needed memory, computing time, bad accuracy, 2D
FEM	x<10	x^4 or x^7 in 2D	simple principles, adaptability	similar to FDTD
PMM	x<1	x^7	field inside particles computed	not accurate for large particle, long time of computing
MoM	x<1	x^7 or x^9	known field inside the scatterer	long computing time, only for small particles
DDA	x<1	x^7 or x^9	similar to MoM	similar to MoM
T-matrix	x<100	x^3 or x^4	fast and accurate	hard to code

2.7 Comments on the choice of the T-matrix approach

There are several reasons for our choice of the T-matrix algorithm for the numerical calculations. They are enumerated below:

- T-matriw approach allows multiple scattering modelling,
- it is a very fast algorithm,
- it can be adapted to very different configurations and geometries,
- it can be used to model large aggregates ($ka = 100$) and multiples of particles (up to 100).
- it allows the study of polarization effects,
- corresponding numerical errors are low, because the main part of the solution is analytically calculated.

The T-matrix algorithms have other advantages, as

- they can be adapted to non-spherical particles,
- they allow averaging on all orientations of particles,
- they allow the calculation of the Mueller matrix elements.

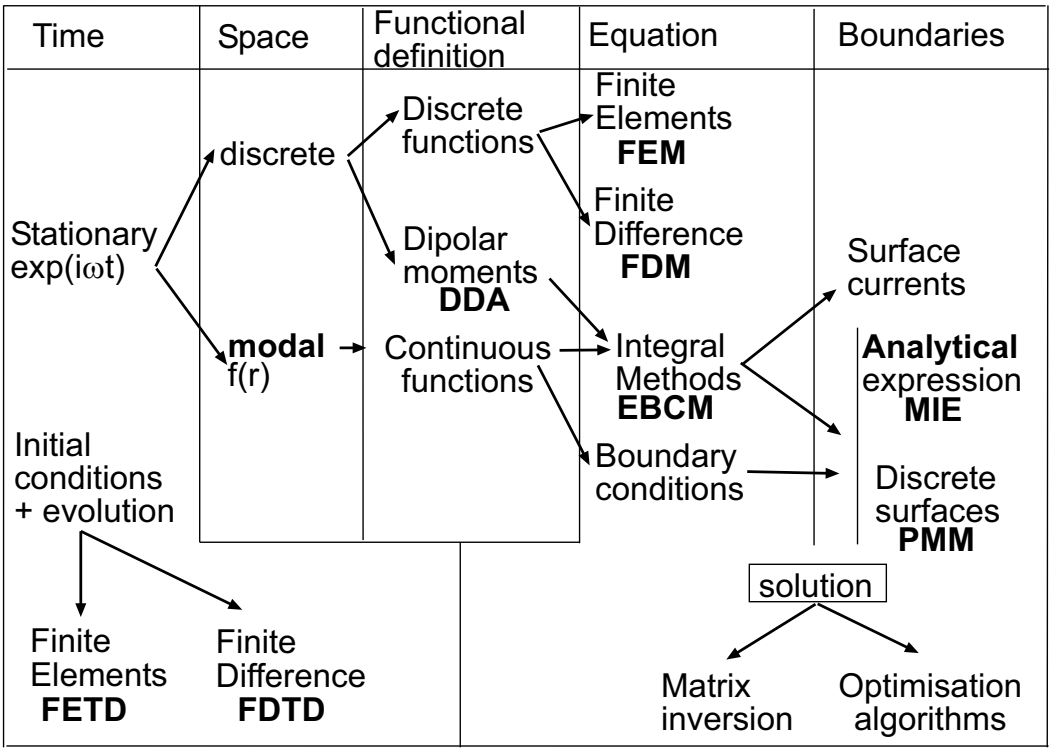

Figure 2.11: Non-exhaustive classification of rigorous algorithms used to study light scattering.

Yet, like all algorithms, the T-matrix has its intrinsic limitations:

- Its first drawback is its theoretical complexity and the difficulties to program it. Mishchenko provides a free code on his website [Web6]; however, in this study we have preferred to use our own code.
- Analytical solution of Maxwell's equations for an aggregate of spheres would need the incident and the scattered field to be expanded on an infinite basis of spherical vectorial functions. In order to carry out the numerical calculations only a finite number of these functions is used. This simplification may cause small discrepancies (see section 3.5).
- Numerical errors can occur in the necessary matrix inversion. If too many orders are used in the field expansion, the matrix to invert can be badly conditioned.
- The computed results are difficult to validate. The validation can be carried out by comparing with measurements or with other algorithm simulations. Some physical properties, like energy conservation or symmetries, can be verified.

To calculate the T-matrix algorithm with the EBCM method, as it will be described in the 3.4 section, there are several necessary conditions:

- the particle geometry has to allow the decomposition in a discrete orthogonal basis,
- the scatterer has to be made of an isotropic material which response has to be linear regarding the electromagnetic field,
- a point inside each scatterer must exist such as if this point is chosen as the origin of a spherical coordinate system, the surface of the scatterer could be described as a continuous function $r(\theta,\varphi)$,
- the surface of scatterers must be continuous and piecewise smooth.

Chapter conclusion

In this chapter we have outlined the physical details of Rayleigh scattering and Lorenz-Mie theory. We have also shown that for more complex aggregates other algorithms are needed and that the physical properties of the scattered field was different. Newsletters which deal with light scattering by particles can be found in [Web3] and [Web4]. The next chapter will describe the electromagnetic approach that we have adopted for the discussion involved in this thesis work. The Lorenz-Mie theory, that has been used in this work to study the light in the near field area of a single particle will be presented, but also the T-matrix algorithm used to study in the far field the consequences of electromagnetic couplings between close particles.

Chapter 3

Light scattering by spheres via T-matrix approach

In this chapter, we describe the rigorous electromagnetic approach which we have used to study light scattering by spheres. We begin with the Lorenz-Mie theory that describes interaction of light with a single sphere and go on with the T-matrix algorithm that generalizes this interaction to several spheres. The Lorenz-Mie theory allows us to study what happens in the near field around a single dielectric particle, whereas the T-matrix permit to study in the far field the consequences of electromagnetic couplings between close particles. The origins of these algorithms are rigorously explained. Some complementary calculations are provided in Appendices B,C,D. Then, some useful physical values are defined and their meanings are discussed.

3.1 Description of the problem

We use the Lorenz-Mie theory to outline the absorption and scattering of electromagnetic waves by a spherical particle. There, we consider a sphere (figure 3.1) with a radius a, which is comparable to the wavelength of the incident electromagnetic wave. More precisely, we consider a size range limited by $0.1\lambda \leq a \leq 6\lambda$. Note that even though absorption has been modelled in the program, it has not been studied. There is no absorption in the surrounding medium. The case of a perfectly conductive sphere has been taken into consideration. Only low refractive indexes n_2 for the sphere have been considered $1 < n_2 < 3$. Spheres are assumed to be passive, non-magnetic, isotropic and homogeneous. No surface roughness is considered. Spheres must be able to be very close together (compare to the wavelength) but not to overlap. Therefore electromagnetic interactions between spheres must be taken into account.

The system of Maxwell's equations is considered linear. Therefore harmonic functions (functions whose evolution in time is $e^{i\omega t}$) will be conserved. All incident wave can be expanded on harmonic functions, the associated scattered wave will be the sum of the scattering of each harmonic wave. That is the reason why we will only consider monochromatic stationary states (the harmonic functions). The temporal dependence is assumed to be $e^{-i\omega t}$. Note that some other books use other sign convention; see for

example [3].

We want to find the electromagnetic field not only in the far field but also in the near field. The near field is considered to be just around the particle or the aggregate. It will not always be possible to find the field inside the aggregate (the reasons will be discussed in section 3.5).
The far field is computed as an asymptotic expansion and corresponds to a transverse wave. All harmonic transverse wave can be considered the superposition of two orthogonal independent linear polarized waves [8]. Therefore, the scattering of a harmonic function in the far field can be described by the S-matrix:

$$\begin{pmatrix} E_{\parallel} \\ E_{\perp} \end{pmatrix} = \begin{pmatrix} S_1(\theta,\phi) & S_2(\theta,\phi) \\ S_3(\theta,\phi) & S_4(\theta,\phi) \end{pmatrix} \frac{e^{i(kr-\omega t)}}{ikr} \begin{pmatrix} E_{\parallel o} \\ E_{\perp o} \end{pmatrix} \tag{3.1}$$

where $E_{\parallel}$ and $E_{\perp}$ are the two orthogonal linear polarized waves and the index o indicates the incident field. This matrix S is also called the amplitude matrix.

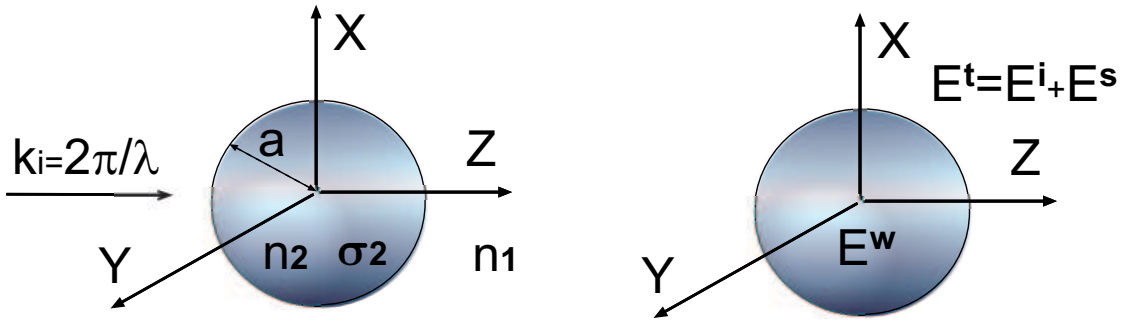

(a) (b)

Figure 3.1: (a) Description of the sphere of radius a, refractive index n_2, conductivity σ_2. (b) Electromagnetic fields.

3.2 Scattering by a single sphere : the Lorenz-Mie theory

To explain the principles of the detailed light scattering approach, we will firstly consider the most simple case, the scattering by a single dielectric sphere. The Lorenz-Mie theory explains these interactions accurately [8][3]. This demonstration with more details is in appendix B. A Mie code can be download for example in [Web2]; however a custom-made programm developed is used in the present study.

Let a sphere with a refractive index n_2 and a conductivity σ_2 to be placed in a non-conductive environment with a refractive index n_1. Let a be its radius (figure 3.1(a)). An electromagnetic plane wave with wavelength λ is to be incident on the sphere.

The Maxwell equations, in a homogeneous isotropic medium with complex refractive n and permeability $\mu = \mu_o$, without charge and current, at the temporal pulsation ω, are written as:

$$\vec{\nabla}.\vec{E} = 0 \tag{3.2}$$
$$\vec{\nabla}.\vec{H} = 0 \tag{3.3}$$
$$\vec{\nabla} \times \vec{E} = ik\vec{H} \tag{3.4}$$
$$\vec{\nabla} \times \vec{H} = -in^2k\vec{E} \tag{3.5}$$

where $\vec{E}$ is the electric field, $\vec{H}$ the magnetic field and, if c is the light speed in free space, $k = \frac{\omega}{c}$. If ϵ is the relative permittivity of the medium and σ is conductivity so $n^2 = \epsilon - \frac{4\pi i\sigma}{\omega}$. Here, the notations used allow to have electric and magnetic fields with same order of amplitude, which decreases numerical error in computation: $\vec{E} = c\epsilon_0\vec{E_{SI}}$ and $\vec{H} = \vec{H_{SI}}$ (appendix A.2).

Solutions of Helmholtz equation in spherical coordinates

$$\forall\ \vec{E}\ \ \vec{\nabla} \times (\vec{\nabla}\times)\vec{E} = -\Delta\vec{E} + \vec{\nabla}(\vec{\nabla}.\vec{E}) \tag{3.6}$$

By applying the Maxwell equation in the two media, $\vec{\nabla}.\vec{E} = 0$ and $\vec{\nabla}\times(\vec{\nabla}\times)\vec{E} = k^2n^2\vec{E}$, we find the vector wave equation for the electric field $\vec{E}$:

$$\Delta\vec{E} + k^2n^2\vec{E} = 0 \tag{3.7}$$

To find the solutions of this vectorial equation we use the scalar wave equation. It is able to demonstrate that if Φ_o and Φ_e are two independent solutions of the scalar wave equation ($\Delta\Phi + k^2n^2\Phi = 0$), the solutions $\vec{E}$ of the vector wave equation, are [3]:

$$\vec{E_1} = \vec{\psi}_{1e} + i\vec{\psi}_{2o} \tag{3.8}$$
$$\vec{E_2} = \vec{\psi}_{1o} + i\vec{\psi}_{2e} \tag{3.9}$$

with

$$\vec{\psi}_1 = (nk)^{-1}\vec{\nabla} \times (nk\vec{r}\Phi) \tag{3.10}$$
$$\vec{\psi}_2 = (nk)^{-1}\vec{\nabla} \times (\vec{\psi}_1) \tag{3.11}$$

This allows us to consider only the **scalar** propagation equation, whose expression in spherical coordinates (r, θ, φ) is (see appendix B):

$$\left[\frac{1}{r^2}\frac{\partial}{\partial r}(r^2\frac{\partial\Phi}{\partial r}) + \frac{1}{r^2}\left(\frac{1}{\sin\theta}\frac{\partial}{\partial\theta}(\sin\theta\frac{\partial\Phi}{\partial\theta}) + \frac{1}{\sin^2\theta}\frac{\partial^2\Phi}{\partial\varphi^2}\right)\right] + k^2n^2\Phi = 0 \tag{3.12}$$

if we search the solution with the form $\Phi(r, \theta, \varphi) = R(r)T(\theta)W(\varphi)$, by dividing (3.12) by Φ and multiplying by r^2, we obtain the three following equations where α and β are

integration constants :

$$\frac{\partial}{\partial r}(r^2\frac{\partial R(r)}{\partial r}) + (k^2n^2r^2 - \alpha)R(r) = 0 \tag{3.13}$$

$$\frac{1}{\sin\theta}\frac{\partial}{\partial\theta}(\sin\theta\frac{\partial T(\theta)}{\partial\theta}) + \left(\alpha - \frac{\beta(\alpha)}{\sin^2\theta}\right)T(\theta) = 0 \tag{3.14}$$

$$\frac{\partial^2 W(\varphi)}{\partial\varphi^2} + \beta(\alpha)W(\varphi) = 0 \tag{3.15}$$

• The solution of (3.15) is $W(\varphi) = a_e\cos(\sqrt{\beta}\varphi) + a_o\sin(\sqrt{\beta}\varphi)$. The variation in φ has to be 2π periodic; therefore, β must be equal to m^2 with m an integer. Thus $W(\varphi) = a_e\cos(\sqrt{\beta}\varphi) + a_o\sin(\sqrt{\beta}\varphi)$
• The equation (3.14) is the spherical harmonics equation. If $\alpha = l(l+1)$, we have :

$$T(\theta) = P_l^{(m)}(\cos\theta)$$

where $P_l^{(m)}$ is the Legendre polynomials of l order and m kind with $0 \leq m \leq l$ (in some books, $W(\varphi)$ is written $e^{im\varphi}$, in this case $-l \leq m \leq l$).
• The solution of equation (3.13) are the Ricatti-Bessel functions or spherical Bessel functions $R(r) = \sqrt{\frac{\pi}{2kr}}\left[c_l J_{l+1/2}(kr) + d_l N_{l+1/2}(kr)\right]$ where J_l and N_l are, respectively, the first order Bessel function of first and second kind. N_l is also called the Neumann function. The $r^{-1/2}$ coefficient and the $l+1/2$ index, are require to have a $1/r$ radial evolution in the far field and to assure energy conservation for a spherical geometry (the J_l Bessel functions were defined for cylindrical geometry).

To summarize, the solution of (3.12) are :

$$\Phi_e = \sum_{l=0}^{\infty}\sum_{m=0}^{l}(a_e)_m\sqrt{\frac{\pi}{2kr}}\left[c_l J_{l+1/2}(kr) + d_l N_{l+1/2}(kr)\right]P_l^{(m)}(\cos\theta)\cos(m\varphi) \tag{3.16}$$

$$\Phi_o = \sum_{l=0}^{\infty}\sum_{m=0}^{l}(a_o)_m\sqrt{\frac{\pi}{2kr}}\left[c_l J_{l+1/2}(kr) + d_l N_{l+1/2}(kr)\right]P_l^{(m)}(\cos\theta)\sin(m\varphi) \tag{3.17}$$

$N_{l+1/2}$ is divergent when $r \to 0$ (non physical result), that is the reason why we must have $d_l = 0$ for the waves define in $r = 0$ (inside the sphere) and use the spherical Bessel function $j_l^{(1)}(kr) = \sqrt{\frac{\pi}{2kr}}J_{l+1/2}$ inside the sphere.
For the other waves (outside the sphere), we will use the spherical Hankel functions $h_l^{(1)}(kr) = \sqrt{\frac{\pi}{2kr}}\left[J_{l+1/2}^{(1)}(kr) - iN_{l+1/2}^{(1)}(kr)\right]$, (e.g. $c_l = 1$ and $d_l = -i$. Other choices could be done). The constant a_e and a_o in (3.16) and (3.17) must now be written $(a_e)_{lm}$ and $(a_o)_{lm}$.

Electromagnetic fields
From Φ_e and Φ_o we can now calculate $\vec{\psi}_{1e}$, $\vec{\psi}_{2e}$, $\vec{\psi}_{1o}$ and $\vec{\psi}_{2o}$ using (3.10)(3.11), with $\gamma = \sqrt{\frac{2(2l+1)(l-m)!}{4\pi l(l+1)(l+m)!}}$ a normalization constant, with f' and f'' for the first and second derivative of f, and with $z_l^{(1)} = j_l^{(1)}$ or $h_l^{(1)}$(respectively, inside and outside the sphere),

as:

$$\vec{\psi}_{1e} = \gamma \begin{cases} 0 \\ -(a_{1e})_{lm}/\sin\theta \left[P_l^{(m)}(\cos\theta) m \sin(m\Phi) z_l^{(1)}(kr)\right] \\ (a_{1e})_{lm} \sin\theta P_l^{(m)'}(\cos\theta) \cos(m\Phi) z_l^{(1)}(kr) \end{cases} \tag{3.18}$$

$$\vec{\psi}_{1o} = \gamma \begin{cases} 0 \\ (a_{1o})_{lm}/\sin\theta \left[P_l^{(m)}(\cos\theta) m \cos(m\varphi) z_l^{(1)}(kr)\right] \\ (a_{1o})_{lm} \sin\theta P_l^{(m)'}(\cos\theta) \sin(m\varphi) z_l^{(1)}(kr) \end{cases} \tag{3.19}$$

$$\vec{\psi}_{2e} = \gamma \begin{cases} (a_{2e})_{lm} \cos(m\varphi)/(knr) z_l^{(1)}(kr) \left[\frac{m^2}{\sin^2\theta} P_l^{(m)}(\cos\theta) + 2\cos\theta P_l^{(m)'}(\cos\theta) - \sin^2\theta P_l^{(m)''}\right] \\ -(a_{2e})_{lm} \sin\theta P_l^{(m)'}(\cos\theta) \cos(m\varphi) \left[\frac{z_l^{(1)}(kr)}{knr} + z_l^{(1)'}(kr)\right] \\ -(a_{2e})_{lm}/\sin\theta P_l^{(m)}(\cos\theta) m \sin(m\varphi) \left[\frac{z_l^{(1)}(kr)}{knr} + z_l^{(1)'}(kr)\right] \end{cases} \tag{3.20}$$

$$\vec{\psi}_{2o} = \gamma \begin{cases} (a_{2o})_{lm} \sin(m\varphi)/(knr) z_l^{(1)}(kr) \left[\frac{m^2}{\sin^2\theta} P_l^{(m)}(\cos\theta) + 2\cos(\theta) P_l^{(m)'}(\cos\theta) - \sin^2\theta P_l^{(m)''}\right] \\ -(a_{2o})_{lm} \sin\theta P_l^{(m)'}(\cos\theta) \sin(m\varphi) \left[\frac{z_l^{(1)}(kr)}{knr} + z_l^{(1)'}(kr)\right] \\ (a_{2o})_{lm}/\sin\theta P_l^{(m)}(\cos\theta) m \cos(m\varphi) \left[\frac{z_l^{(1)}(kr)}{knr} + z_l^{(1)'}(kr)\right] \end{cases} \tag{3.21}$$

Equation (3.8) gives $\vec{E}_1 = \vec{\psi}_{1e} + i\vec{\psi}_{2o}$
To find the magnetic field $\vec{H}$ we must use equation (3.4) (see calculation appendix D.4):

$$\vec{H} = -ik^{-1}\vec{\nabla} \times \vec{E}$$

with respect to (3.8) :

$$\vec{H}_1 = -ik^{-1}\vec{\nabla} \times (\vec{\psi}_{1e} + i\vec{\psi}_{2o})$$
$$\vec{H}_1 = -ik^{-1}(\vec{\nabla} \times \vec{\psi}_{1e} + i\vec{\nabla} \times \vec{\psi}_{2o})$$

$$\vec{H}_1 = n(i\vec{\psi}_{2e} - \vec{\psi}_{1o}) \tag{3.22}$$

The same can be done with $\vec{E}_2$ and $\vec{H}_2$.
Above, we have found the solutions of the vector wave equation in spherical coordinates. These functions are called the **Spherical Vectorial Functions** (SVF), or the vector spherical harmonics, or the spherical multipole fields [76], or the whispering gallery mode. The SVF can be noted $\vec{\Psi}_{\tau\sigma lm}$ with $\tau \in \{1, 2\}$, $\sigma \in \{o, e\}$ and $0 \leq m \leq l$. We also write $\vec{\Psi}_n$ with n for $\tau\sigma lm$.

A condensed expression of the SVF is:

$$\vec{\Psi}_{\tau\sigma mn}(\vec{r}) = \gamma^{1/2}(k^{-1}\vec{\nabla}\times)^{\tau}\left[k\vec{r}Y_{\sigma mn}(\theta,\varphi)h_l^{(1)}(kr)\right] \tag{3.23}$$

with $Y_{emn}(\theta,\varphi) = P_l^{(m)}(\cos\theta)\cos m\varphi$ and $Y_{omn}(\theta,\varphi) = P_l^{(m)}(\cos\theta)\sin m\varphi$.

The Boundary conditions

Next, we must find the constants $(a_{1e})_{lm}$, $(a_{2e})_{lm}$, $(a_{1o})_{lm}$ and $(a_{2o})_{lm}$ by applying the boundary conditions.

Let $\vec{E^i}$ be the incident wave in all space, $\vec{E^s}$ be the scattered wave outside the sphere and $\vec{E^w}$ inside the sphere. $\vec{E^t} = \vec{E^i} + \vec{E^s}$ is the total electric field outside the sphere (see figure 3.1).

We must assure the continuity of the tangential component of field (E_θ, E_φ, H_θ, H_φ) at the boundary of the sphere ($r = a$): equations (3.8) and (3.22) are written for $r = a$ where $((a_e)^i_{lm}, (a_o)^i_{lm})$, $((a_e)^s_{lm}, (a_o)^s_{lm})$, $((a_e)^w_{lm}, (a_o)^w_{lm})$ are respectively the coefficients in equations (3.16) and (3.17) for the incident wave, the scattered wave and the wave inside the sphere. The sum of the tangential component of the scattered and incident fields must be equal to the tangential component of the field inside the particle at $r = a$. The only differences between these fields are their expansion coefficients and the kind of Bessel functions. That is why coupling coefficients do not depend of m.

This yields for the scattered coefficients:

$$(a_e)^s_{lm} = -(a_e)^i_{lm}\frac{n_2^2 j_l(\rho_2)\left(j_l(\rho_1)+\rho_1 j_l'(\rho_1)\right) - n_1^2 j_l(\rho_1)\left(j_l(\rho_2)+\rho_2 j_l'(\rho_2)\right)}{n_2^2 j_l(\rho_2)\left(h_l(\rho_1)+\rho_1 h_l'(\rho_1)\right) - n_1^2 h_l(\rho_1)\left(j_l(\rho_2)+\rho_2 j_l'(\rho_2)\right)} \tag{3.24}$$

$$(a_o)^s_{lm} = -(a_o)^i_{lm}\frac{j_l(\rho_1)\left(j_l(\rho_2)+\rho_2 j_l'(\rho_2)\right) - j_l(\rho_2)\left(j_l(\rho_1)+\rho_1 j_l'(\rho_1)\right)}{h_l(\rho_1)\left(j_l(\rho_2)+\rho_2 j_l'(\rho_2)\right) - j_l(\rho_2)\left(h_l(\rho_1)+\rho_1 h_l'(\rho_1)\right)} \tag{3.25}$$

with $\rho_1 = n_1 ka$ and $\rho_2 = n_2 ka$.

These formulae can be simplified for perfectly conducting spheres ($E^w = 0$):

$$(a_e)^s_{lm} = -(a_e)^i_{lm}\frac{j_l(\rho_1)+\rho_1 j_l'(\rho_1)}{h_l(\rho_1)+\rho_1 h_l'(\rho_1)} \tag{3.26}$$

$$(a_o)^s_{lm} = -(a_o)^i_{lm}\frac{j_l(\rho_1)}{h_l(\rho_1)} \tag{3.27}$$

For dielectric sphere the expansion coefficients of the field inside the dielectric sphere are:

$$(a_e)^w_{lm} = -(a_e)^i_{lm}\frac{n_2 n_1 h_l(\rho_1)\left(j_l(\rho_1)+\rho_1 j_l'(\rho_1)\right) - n_1 n_2 j_l(\rho_1)\left(h_l(\rho_1)+\rho_1 h_l'(\rho_1)\right)}{n_1^2 h_l(\rho_1)\left(j_l(\rho_2)+\rho_2 j_l'(\rho_2)\right) - n_1^2 j_l(\rho_2)\left(h_l(\rho_1)+\rho_1 h_l'(\rho_1)\right)} \tag{3.28}$$

$$(a_o)^w_{lm} = -(a_o)^i_{lm}\frac{h_l(\rho_1)\left(j_l(\rho_1)+\rho_1 j_l'(\rho_1)\right) - j_l(\rho_1)\left(h_l(\rho_1)+\rho_1 h_l'(\rho_1)\right)}{h_l(\rho_1)\left(j_l(\rho_2)+\rho_2 j_l'(\rho_2)\right) - j_l(\rho_2)\left(h_l(\rho_1)+\rho_1 h_l'(\rho_1)\right)} \tag{3.29}$$

Obviously, for perfectly conducting sphere $(a_e)^w_{lm} = 0$ and $(a_o)^w_{lm} = 0$. The electromagnetic field is null inside the particle and the tangential components of the magnetic field are discontinuous on the boundary. This discontinuity induces surface currents (3.30) (also called surface plasmon) that behave as secondary source. In figure 3.2 a perfectly conductive sphere of radius $a = 3\lambda$ has been studied. The scattered intensity (a) seems to be in the forward direction, but if we look at the total intensity (b) we observe a shadow effect and backscattering. In fact, the scattered field observed in the forward direction (a) is the opposite of the incident field. The tangential component of the magnetic is represented in figure 3.2(c). The discontinuity at the sphere surface can be observed.

$$H_t^{in} - H_t^{out} = j_s \tag{3.30}$$

For finite conductive particle, there is a small depth at the surface of the particle where the electromagnetic field vanishes (skin depth). That makes possible the propagation of evanescent waves at the surface of the particle (The propagation direction is orthogonal to the direction of field decrease), this waves are also called surface plasmon.

The incident field

The incident wave is assumed to be plane and monochromatic. This wave must be expanded on the basis of spherical vectorial functions [20]. This expansion depends of polarization, see figure 3.3. (The i in mathematical formulae is the complex number such as $i^2 = -1$, but i as a superscript or subscript indicates that the value is linked to the incident wave).

$$(a)\ if\ \vec{E}^i(\vec{r}) = \exp(i\vec{k}.\vec{r})\vec{e}_2 \tag{3.31}$$

$$(a_{1o})^{i2}_{lm} = i^n \left[\frac{4\pi(2l+1)(l-m)!}{l(l+1)(l+m)!}\right]^{1/2} \frac{\sqrt{2}m}{\sin\theta_i} P_l^m(\cos\theta_i) \tag{3.32}$$

$$(a_{2e})^{i2}_{lm} = i^{n+1} \left[\frac{4\pi(2l+1)(l-m)!}{l(l+1)(l+m)!}\right]^{1/2} \frac{\sqrt{\epsilon_m}}{\sin\theta_i} \times \left[(l+1)\cos\theta_i P_l^m(\cos\theta_i) - (l-m+1)P_{l+1}^m(\cos\theta_i)\right] \tag{3.33}$$

$$(a_{1e})^{i2}_{lm} = (a_{2o})^{i2}_{lm} = 0 \tag{3.34}$$

if $\theta_i = 0$: $(a_{2e})^{i2}_{lm} = -i(a_{1o})^{i2}_{lm} = i^{l+1}\left[2\pi(2l+1)\right]^{1/2}\delta_{m,1}$. (Please, note that in the paper by Peterson and Ström [20] there is a mistake (minus sign); see demonstration appendix D.1)

$$(b)\ if\ \vec{E}^i(\vec{r}) = \exp(i\vec{k}.\vec{r})\vec{e}_1$$

$(a_{1e})^{i1}_{lm} = -i(a_{2e})^{i2}_{lm}$, $(a_{2o})^{i1}_{lm} = -i(a_{1o})^{i2}_{lm}$, $(a_{1o})^{i1}_{lm} = (a_{2e})^{i1}_{lm} = 0$

For circular polarization $(a_{1e})^i_{lm} = (a_{2e})^i_{lm}$ and $(a_{1o})^i_{lm} = (a_{2o})^i_{lm}$.
The coefficients a^i and a^s will be discussed further in section 3.5.

Proposed scattering modelling for an aggregate of spheres

In light scattering by only one sphere, the T-matrix can be easily found by applying

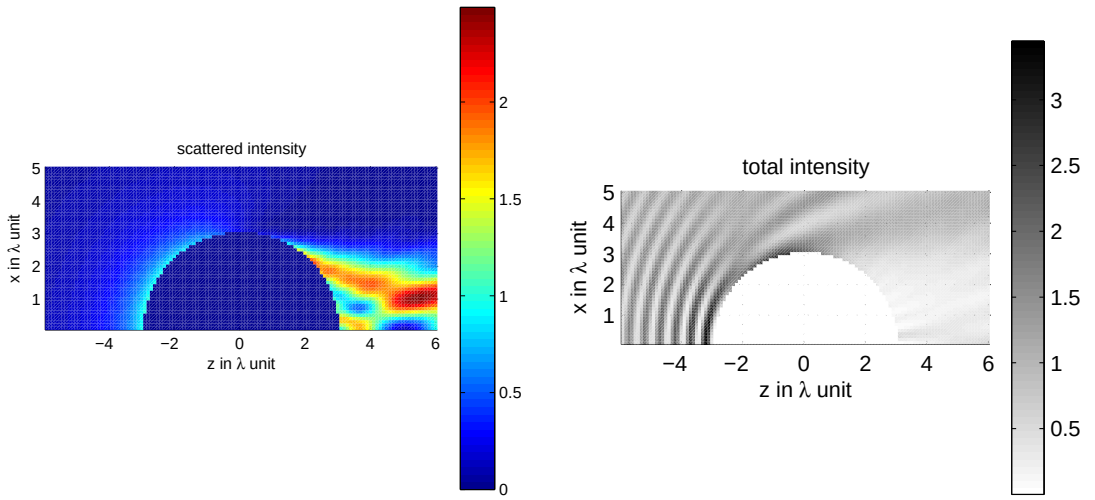

(a) (b)

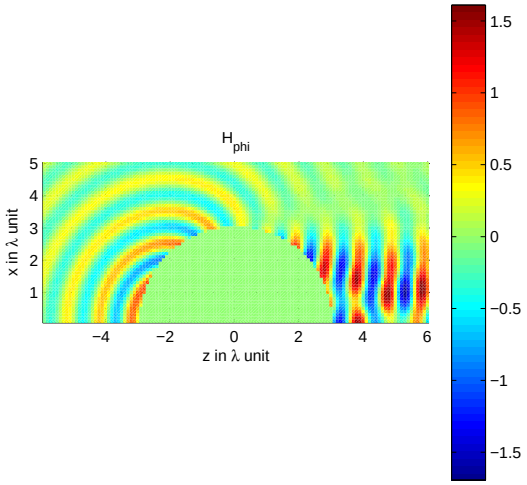

(c)

Figure 3.2: Perfectly conductive sphere of radius $a = 3\lambda$, $H_i = H_y$ and $k_i = k_z$.(a) scattered intensity, (b) total intensity, (c) tangential component of the scattered magnetic field H^s_φ

the boundary conditions, because the basis of functions used to expand the incident and scattered fields is made of the eigenmodes. The T-matrix is diagonal. When there are several spheres, we use the same basis of functions and we search the T-matrix which describes the linear relation between the expanded coefficients. But in this case the boundary conditions are more difficult to express because the expansion modes are not adapted to the geometry of the boundaries. That is the reason why an integral formulation of the electromagnetic solution will be used to express them. The method described in the next section is called the Extended Boundaries Conditions Method

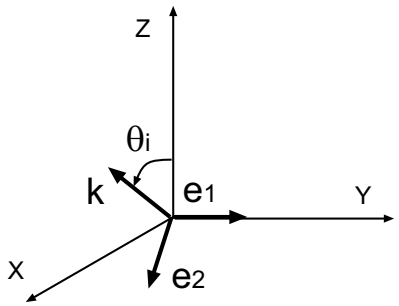

Figure 3.3: **k**, the propagation vector of the incident field is in the (O, x, z) plane. **e1** is an unit vector along the y axis. **e2** is an unit vector orthogonal to **k** and **e1**. $\vec{E}$ and $\vec{H}$ are in the $(O, e1, e2)$ plane.

(EBCM), after Waterman [19].

We will use the basis of spherical vectorial functions because this basis is adapted to spherical particles, but in the general case, the field can be decomposed on other basis of functions. These other basis can be interesting for other geometries of particles. They can also have easier translation matrix. As we will show the T-matrix can be generalized to aggregates of non-spherical particles.

3.3 The integral formulation of the electromagnetic solution

The scalar formulation

This section describes the integral formulation of the solution of Maxwell equations that are used to calculate the T-matrix. We will begin with the scalar formulation and finally outline the vectorial formulation.

We first begin by considering the electric field as a scalar value E with the temporal frequency ω. E must be a solution of the wave equation :

$$\Delta E(\vec{r'}) + k^2 E(\vec{r'}) = 0 \tag{3.35}$$

A method to find E is to use the Green function g. This function is the electric field created by a point source in $\vec{r'} = \vec{r}$ (see appendix A.3):

$$\Delta g(\vec{r'}, \vec{r}) + k^2 g(\vec{r'}, \vec{r}) = -\delta(\vec{r'} - \vec{r}) \tag{3.36}$$

where $\delta(\vec{r'} - \vec{r})$ is the three-dimensional Dirac function ($\delta = 1$ if $\vec{r} = \vec{r'}$ else $\delta = 0$). We can verify that $g_{\vec{r},k}$, given in formula (3.37), verifies the equation 3.35 for $\vec{r'} \neq \vec{r}$. The Green function is not defined in $\vec{r'} = \vec{r}$ but the normalized constant $1/(4\pi)$ is found by

integrating the equation 3.36 over a infinitely small sphere around $\vec{r}$ [18] (see appendix A.3).

$$g_{\vec{r},k}(\vec{r'}) = \frac{\exp(ik|\vec{r'} - \vec{r}|)}{4\pi|\vec{r'} - \vec{r}|} \tag{3.37}$$

By multiplying the equation (3.35) by g and the equation 3.36 by E and by subtracting them, we find :

$$g_k(\vec{r'}, \vec{r})\Delta E(\vec{r'}) - E(\vec{r'})\Delta g_k(\vec{r'}, \vec{r}) = \delta(\vec{r'} - \vec{r})E(\vec{r'}) \tag{3.38}$$

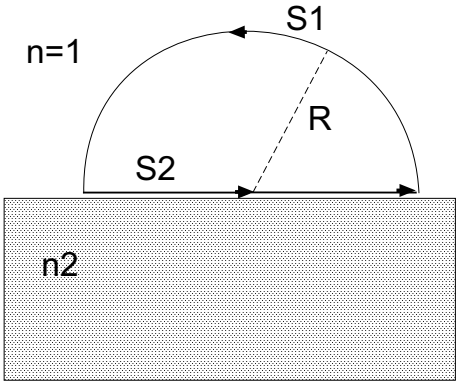

Figure 3.4: *2D representation of a 3D contour of integration. Case of a half-infinite medium.*

We can now integrate this equation on the volume V defined in figure 3.4 and with $dV' = r'^2 \sin\theta' dr' d\theta d\varphi$ a small volume element:

$$\iiint_V g_k(\vec{r'}, \vec{r})\Delta E(\vec{r'}) - E(\vec{r'})\Delta g_k(\vec{r'}, \vec{r})dV' = \iiint_V \delta(\vec{r'} - \vec{r})E(\vec{r'})dV' \tag{3.39}$$

$$= \begin{cases} E(\vec{r}) & \vec{r} \text{ outside V} \\ 0 & \vec{r} \text{ inside V} \end{cases} \tag{3.40}$$

This formulae can be modified by applying one of the Green theorems [83] that is:

$$\iiint_V (\phi\Delta\psi - \psi\Delta\phi)dV' = \iint_S (\phi\frac{\partial\psi}{\partial n} - \psi\frac{\partial\phi}{\partial n})dS'$$

Where S is the surface around the volume V, $\partial/\partial n$ is the differential along the normal direction of the surface and dS' a small surface element. $(\partial/\partial n)\ \phi dS' = \vec{\nabla}\phi.d\vec{S'})$. In our case we obtain:

$$\begin{cases} \vec{r} \text{ ouside S} & \vec{E}(\vec{r}) \\ \vec{r} \text{ inside S} & 0 \end{cases} = \iint_S g_k(\vec{r'}, \vec{r})\frac{\partial}{\partial n}E(\vec{r'}) - E(\vec{r'})\frac{\partial}{\partial n}g_k(\vec{r'}, \vec{r})dS' \tag{3.41}$$

Because of its linearity, the integral over S can be decomposed as the sum of integral over $S1$ and $S2$ as shown figure 3.4(a).

$$\begin{cases} \vec{r} \text{ ouside S} & \vec{E}(\vec{r}) \\ \vec{r} \text{ inside S} & 0 \end{cases} = \iint_{S1} (g\frac{\partial E}{\partial n} - E\frac{\partial g}{\partial n})dS' + \iint_{S2} (g\frac{\partial E}{\partial n} - E\frac{\partial g}{\partial n})dS' \quad (3.42)$$

When the radius of the contour of integration tends to infinity, the field integrated over $S1$ can only be the incident field because of the radiation condition that imposes that the scattered field would be zero at infinity. We obtain:

$$\begin{cases} \vec{r} \text{ ouside S} & \vec{E}(\vec{r}) \\ \vec{r} \text{ inside S} & 0 \end{cases} = E_i + \iint_{S2} g_k(\vec{r'}, \vec{r})\frac{\partial}{\partial n}E(\vec{r'}) - E(\vec{r'})\frac{\partial}{\partial n}g_k(\vec{r'}, \vec{r})dS' \quad (3.43)$$

This formulation shows that the total electric field, in a point outside the scattering object, can be expressed as the sum of the incident field and another term which is called the scattered field and which can be expressed as an integral of the total electric field at the surface of the scatterer.

The equation (3.43) inside the scattering object is called the extinction theorem [18]. A consequence of this theorem is that we can use the field at the surface of the scatterer to replace the incident field and to calculate the scattered field. The field at the surface of the scatterers is often described as surface currents [8].

In our case, with an ensemble of spheres, the same reasoning is done but with an integral over a surface as represented in figure 3.5 and by applying equivalent integral paths [83].

Equations (3.43) are the integral formulation of the electromagnetic solutions outside and inside the scatterers. We will now give a similar relation when the electromagnetic field is considered a vector.

The vectorial formulation

When the electric field is considered a vector, the equivalent of the Green function is more complex, it is an operator that will be written G_k [18]:

$$\vec{G}_k(\vec{r}, \vec{r'}) = ([I] + \frac{1}{k^2}[\nabla\nabla])g_k(\vec{r}, \vec{r'}) \quad (3.44)$$

where $I = \begin{vmatrix} 1 & 0 & 0 \\ 0 & 1 & 0 \\ 0 & 0 & 1 \end{vmatrix}$, $[\nabla\nabla] = \begin{vmatrix} \frac{\partial^2}{\partial x^2} & \frac{\partial^2}{\partial x \partial y} & \frac{\partial^2}{\partial x \partial z} \\ \frac{\partial^2}{\partial y \partial x} & \frac{\partial^2}{\partial y^2} & \frac{\partial^2}{\partial y \partial z} \\ \frac{\partial^2}{\partial z \partial x} & \frac{\partial^2}{\partial z \partial y} & \frac{\partial^2}{\partial z^2} \end{vmatrix}$ and g is the Green function (3.37).

When this operator is applied on a vector, the result is a vector. With these operators it is possible to have the same kind of relations as (3.43) with a vectorial electric field [18]:

$$\begin{cases} \vec{r} \text{ ouside S} & \vec{E}(\vec{r}) \\ \vec{r} \text{ inside S} & 0 \end{cases} = \vec{E}_i + \iint_S \vec{G}(k|\vec{r} - \vec{r'}|).\left(\vec{N} \times (\vec{\nabla} \times \vec{E})(\vec{r'})\right) d\vec{S'} + \iint_S \vec{\nabla} \times \vec{G}(k|\vec{r} - \vec{r'}|).(\vec{N} \times \vec{E}(\vec{r'}))d\vec{S'} \quad (3.45)$$

That could be written [18]:

$$\left\{ \begin{array}{ll} \vec{r} \text{ ouside S} & \vec{E}(\vec{r}) \\ \vec{r} \text{ inside S} & 0 \end{array} \right. = \vec{E}_i + \vec{\nabla} \times \left(\vec{\nabla} \times \iint_S \frac{i}{k} \vec{N} \times \vec{H}(\vec{r'}) g(k|\vec{r} - \vec{r'}|) dS' \right) + \vec{\nabla} \times \iint_S g(k|\vec{r} - \vec{r'}|) \vec{N} \times \vec{E}(\vec{r'}) dS' \quad (3.46)$$

where $\vec{N}$ is the normal to the surface and g the Green function.

This relation is called the $Huygens - Poincaré$ principle [20]. It is used by the T-matrix algorithm to calculate rigorously light scattering by several scatterers.

3.4 A demonstration of T-matrix algorithm

As we have seen in the previous chapter, there are several numerical algorithms to simulate light scattering. This section presents the principles of T-matrix algorithm that we have used for our main studies. In particular the Extended Boundary Condition Method (EBCM) that has been used to calculate the T-matrix and which is based on the integral formulation of electromagnetic solutions. The reasons why we have used it have already been explained at the end of the previous chapter, section 2.7. In the same section, the limitations of this algorithm and the conditions that must respect the scattered for being studied with this algorithm have been described. This algorithm

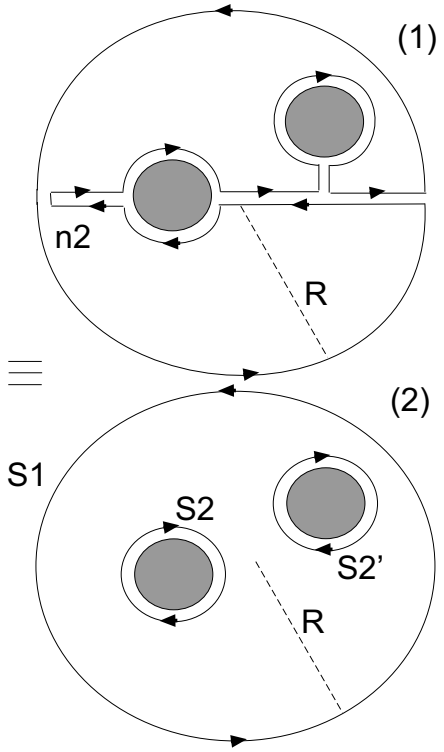

Figure 3.5: Two equivalent contours of integration for spheres.

allows us to extend the Lorenz-Mie theory and to compute light scattering by an aggregate of spheres (but also an aggregate of scatterers with arbitrary shape).

Principles
The EBCM is based on the Huygens-Poincaré principle (see equation 3.46) which was introduced in the previous section. This principle yields two equations. The first equation expresses the total electric field outside scatterers as the sum of the incident field and the tangential components of the electromagnetic field integrated over the surface of all scatterers. This second integrated term, where the Green function appears ($g(k|\vec{r}-\vec{r'}|) = \exp(ik|\vec{r}-\vec{r'}|)/(4\pi|\vec{r}-\vec{r'}|)$), is the scattered field. The second equation gives a relation between the incident field and the tangential components of the electromagnetic field integrated over the surface of all scatterers. By removing the tangential components of the electromagnetic field with the two equations, we find the relation between the incident and the scattered field.

In the Lorenz-Mie theory, that is for one dielectric sphere, the links between incident and scattered fields are found by applying the boundary conditions. The EBCM method is an extension of the Lorenz-Mie theory for several particles, that is the reason why the method is called Extended Boundary Condition Method. An other reason is that with the EBCM method, for several scatterers, the electromagnetic field at all point in space is expressed only as a function of the tangential components of the electric and magnetic fields at the boundaries of scatterers. However the EBCM and T-matrix method are often assimilated.

T-matrix calculation:
Outside the sphere the scattered field and the Green functions can be expanded on Spherical Vectorial Functions (SVF):

$$\vec{E^s}(\vec{r}) = \sum_n f_n \vec{\Psi}_n(\vec{r}) \tag{3.47}$$

$$g(k|\vec{r}-\vec{r'}|) = k \sum_n \vec{\Psi}_n(\vec{r}).\Re e[\vec{\Psi}_n(\vec{r'})] \tag{3.48}$$

For the expansion of the Green function (3.48), some conditions on $\vec{r}$ and $\vec{r'}$ must be verified if the particle is not a sphere [20]. We will not study this case.

In the Huygens-Poincaré formula (3.46), outside the sphere, the integral term describes the scattered field because $E^t = E^s + E^i$, thus:

$$\begin{aligned} \vec{E^s}(\vec{r}) = & \quad \vec{\nabla} \times \left(\vec{\nabla} \times \iint_S \frac{i}{k} \vec{N} \times \vec{H}(\vec{r'}) g(k|\vec{r}-\vec{r'}|) dS' \right) \\ + & \quad \vec{\nabla} \times \iint_S g(k|\vec{r}-\vec{r'}|) \vec{N} \times \vec{E}(\vec{r'}) dS' \end{aligned} \tag{3.49}$$

By using the expansion of the Green function and permuting $\sum$, $\int$ and $\vec{\nabla}$ we obtain:

$$\begin{aligned}\vec{E}^s(\vec{r}) = \quad & -1\sum_n \iint_S \left[\vec{N}\times\vec{H}(\vec{r'})\right]\vec{\nabla}\times\left(\vec{\nabla}\times\Re e[\vec{\Psi}_n(\vec{r'})]\right)dS'\vec{\Psi}_n(\vec{r}) \\ + \quad & ik\sum_n \iint_S \left[\vec{N}\times\vec{E}(\vec{r'})\right]\vec{\nabla}\times\Re e[\vec{\Psi}_n(\vec{r'})]dS'\vec{\Psi}_n(\vec{r}) \end{aligned} \tag{3.50}$$

But $\vec{\nabla}\times\left(\vec{\nabla}\times\Re e[\vec{\Psi}_n(\vec{r'})]\right) = k^2\Re e[\vec{\Psi}_n(\vec{r'})]$, thus by comparing (3.50) and (3.47) we find:

$$f_n = k^2\iint_S \left[ik^{-1}\vec{N}\times\vec{E}(\vec{r'})\right]\vec{\nabla}\times\Re e[\vec{\Psi}_n(\vec{r'})] - \left[\vec{N}\times\vec{H}(\vec{r'})\right]\Re e[\vec{\Psi}_n(\vec{r'})]dS' \tag{3.51}$$

Inside the sphere the incident field can be expanded on SVF:

$$\vec{E}^i(\vec{r}) = \sum_n a_n\Re e[\vec{\Psi}_n(\vec{r})] \tag{3.52}$$

In the Poincaré-Huygens formula (3.46), inside the sphere by using the expansion of the Green function and of the incident field, we can similarly find:

$$a_n = -k^2\iint_S \left[ik^{-1}\vec{N}\times\vec{E}(\vec{r'})\right]\vec{\nabla}\times\vec{\Psi}_n(\vec{r'}) - \left[\vec{N}\times\vec{H}(\vec{r'})\right]\vec{\Psi}_n(\vec{r'})dS' \tag{3.53}$$

If now we consider the easier case when the sphere is perfectly conductive: $\vec{N}\times\vec{E}(\vec{r'}) = 0$. If we expand $\vec{N}\times\vec{H}(\vec{r'})$ on the SVF (3.54) and use the identity (3.55),

$$\vec{N}\times\vec{H}(\vec{r}) = \sum_n \alpha_n k^{-1}\vec{N}\times\left(\vec{\nabla}\times\Re e[\vec{\Psi}_n(\vec{r})]\right) \tag{3.54}$$

$$Q_{nn'} = k\iint_S \vec{\nabla}\times\Re e[\vec{\Psi}_n(\vec{r})]\times\vec{\Psi}_{n'}(\vec{r})dS' \tag{3.55}$$

we can rewrite (3.51) and (3.53) as:

$$f_n = -\sum_{n'}\Re e[Q^t_{nn'}]\alpha_{n'} \tag{3.56}$$

$$a_n = \sum_{n'} Q^t_{nn'}\alpha_{n'} \tag{3.57}$$

or

$$\vec{f} = -\Re e[Q^t]\vec{\alpha} \tag{3.58}$$

$$\vec{a} = Q^t\vec{\alpha} \tag{3.59}$$

Thus we deduce that $\boxed{T = -\Re e(Q^t)(Q^t)^{-1}}$.

This formula is also true for a dielectric sphere [20].

The above formula is true in the general case but must now be adapted for several spherical scatterers. In this case, the EBCM used the **translation addition theorem** (see appendix C). This theorem gives the SVF expressed in a first coordinate system as a linear relation of the same functions expressed in a translated coordinate system (figure 3.6).

$$\vec{\Psi}_n(\vec{r}+\vec{d}) = \sum_{n,n'} \sigma_{n,n'} \Re e[\vec{\Psi}_{n'}(\vec{r})] \text{ if } |\vec{d}| > |\vec{r}| \tag{3.60}$$

$$\Re e[\vec{\Psi}_n(\vec{r}+\vec{d})] = \sum_{n,n'} R_{n,n'} \Re e[\vec{\Psi}_{n'}(\vec{r})] \tag{3.61}$$

What makes the analytical expression of boundary conditions possible in the Lorenz-

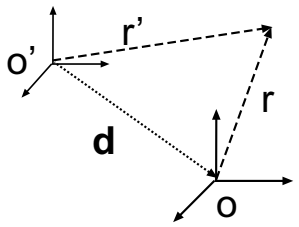

Figure 3.6: Translation of the coordinate frame from O' to O. $\vec{d}+\vec{r}=\vec{r'}$.

Mie theory is the fact that the coordinate center can be the center of the sphere. Thus the value of the eigenmodes at the surface are the SVF expressed for a constant radius. When there are several spheres, it is no longer possible. The translation addition theorem permits to solve this problem. The formulation of the T-matrix for 2 and more separated scatterers can be expressed in function of the T-matrix of each scatterer and is given appendix D.

The necessary adaptations of the T-matrix principles for allowing numerical computing are the cause of some limitations that are described and studied in the next section.

3.5 Convergence and limitations of the algorithm

Convergence
In order to compute the T-matrix, the basis of SVF must be truncated. The order of truncation L_{max} must be chosen to have a good convergence of the algorithm. This convergence must be verified after each simulation. Usually the number of orders L_{max} that must be taken into account is at least $2\pi a_{agg}/\lambda$ with a_{agg} the radius of the smallest virtual sphere that would contain the scatters [84, 20] (figure 3.7). This is true only if the used coordinates are centered on the aggregate.

What we have chosen to call *order* (L_{max}) in this dissertation is the maximum of variation of the index l and not the total number of used SVF as often. The advantage is

Figure 3.7: Example of smallest virtual sphere of radius a_{agg} containing all scatterers.

the physical link between this order and particle size. The relationship between L_{max} and the number of used SVF is given in the next section. This convergence criterium gives the minimum order that must be used in calculation.

Conditioning
Lmax is the minimum order that must be used in the expansion on SVF to have convergence. However another criterium gives the maximum order that can be used: If too many orders are used in calculation, the matrix inversion in the algorithm can be badly conditioned. Therefore the order of convergence must be reached before the matrix becomes badly conditioned, that is the reason why the global size of the aggregate of spherical particles that can be simulated is limited to several ten wavelengths. For larger aggregates, when the number of orders in computing increases, the matrix to inverse becomes badly conditioned before to obtain convergence.

Study of the Lorenz-Mie case
The study of the case of Mie scattering enables us to illustrate the convergence criterium on a simple case. In the case of the Lorenz-Mie theory, a single sphere of radius a is considered. Because the SVF (indexed by l and m) are the eigenmodes for one sphere, the T-matrix is diagonal. The minimum convergence criterium gives $1 \leq l \leq L_{max}$ with $L_{max} = ka$. We will try to justify this criterium. However, it can be first noted that if the incident angle of the plane wave is $\theta_i = 0$, so $m = 1$; whereas if $\theta_i \neq 0$, $0 \leq m \leq l$. In the two cases, the criterium $1 \leq l \leq L_{max}$ is the same and the scattered field has only be rotated, however the number of used SVF is not the same. This justifies why in this dissertation we call *order* the value L_{max} and not the total number of used SVF. Only L_{max} has a physical interpretation.

We can also note, in figure 3.8(a), that for a perfectly conductive sphere, the diagonal components of the T-matrix as a function of the particle radius are almost periodic, with a period $\lambda/2$. We also note that the coupling maximum value is equal to 1.
For a given radius of particle, this l^{th} diagonal component of the T-matrix is linked to the ratio of the incident SVF that will contribute to the scattered field. If a diagonal component is null, that means that the corresponding SVF does not contribute to light scattering. The figure 3.8(b) is a zoom of 3.8(a) for $0 < R < 1\lambda$. It can be observed

that before to be periodic as a function of the sphere radius, the diagonal components are null. The l^{th} diagonal component is null for sphere radius a such as $ka < l$. Therefore, if we consider a sphere with a radius a, all the SVF with an order $l > ka$ will not significantly contribute to light scattering. That is a justification of the convergence criterium $L_{max} = ka$. It can be noticed that L_{max} is the circumference of the aggregate in λ unit.

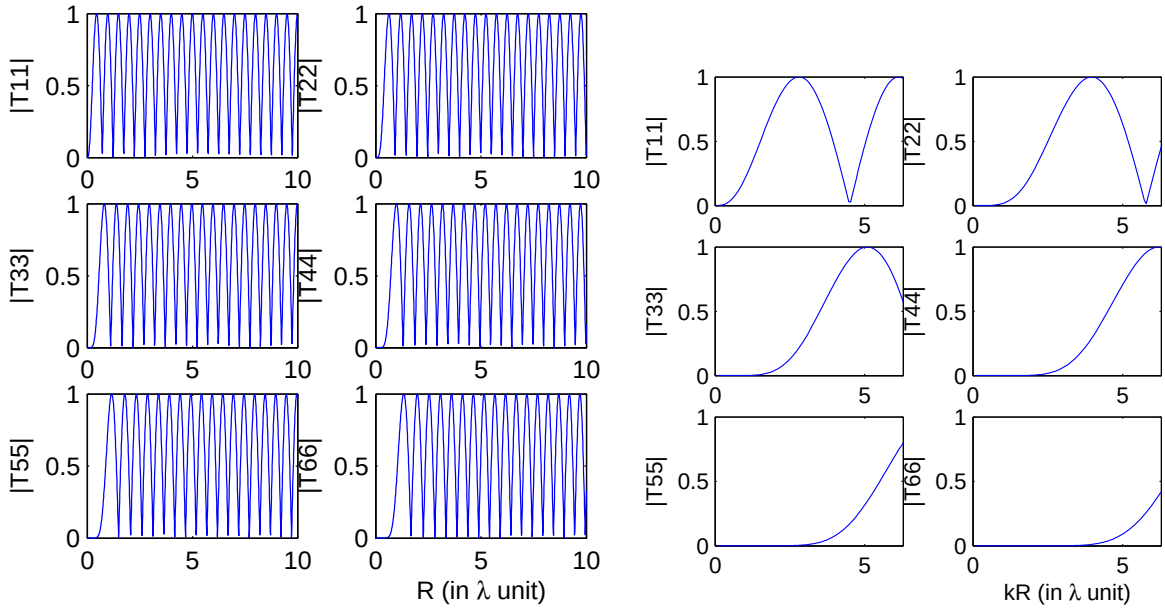

Figure 3.8: First 6 diagonal components of the T-matrix of a perfectly conductive sphere as function of its radius R. T11: diagonal component corresponding to $l = 1$

For dielectric spheres, in figure 3.9(a) we observe that the diagonal components of the T-matrix are periodic as well for perfectly conductive sphere, but with a more complicated period. The coupling maximum value are equal to one too and the same convergence criterium is observed ($L_{max} = ka$). A difference (see table 3.1) is that the period of variation of the diagonal components of the T-matrix as function of the radius of the dielectric sphere seems to depend of $(n-1)$ and is not always equal to $\lambda/2$ as for perfectly conductive sphere. n is the refractive index of the sphere .

Aggregates

The order of convergence for an aggregate of two identical spheres which centers are separated by a distance of 4 times their radius and with $\theta_i = 0$ is given in table 3.2. The convergence order appears to be $L_{max} \simeq 2ka_{agg}$, where a_{agg} is defined in figure 3.7. This order is independent of the refractive index of spheres. For example, for N aligned spheres of radius a, separated by a distance (center to center) d, $a_{agg} = (N-1)d + 2a$, therefore $L_{max} = 2k[(N-1)d + 2a]$.

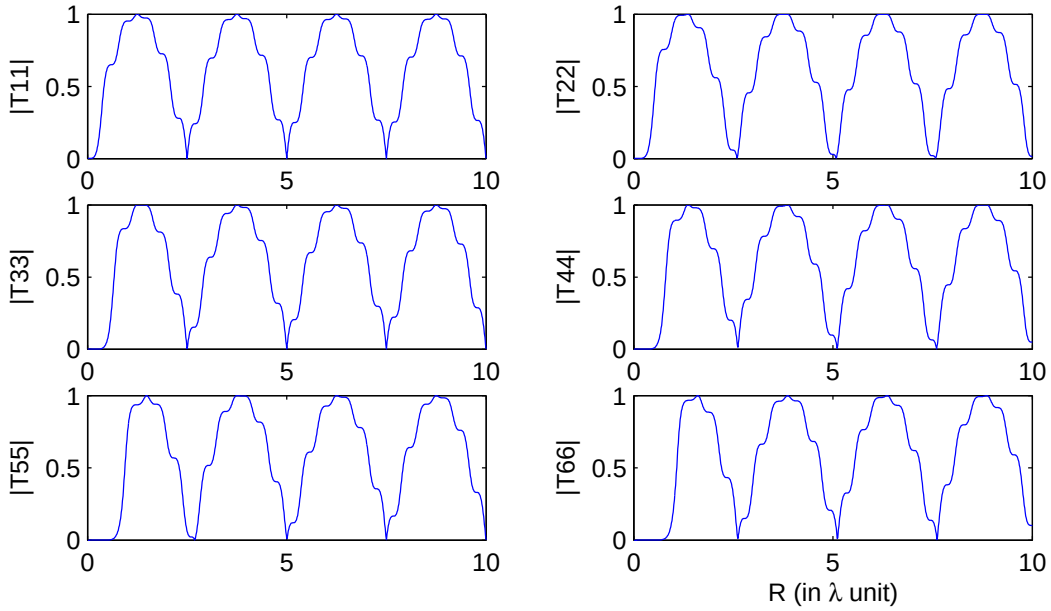

Figure 3.9: First 6 diagonal components of the T-matrix of a dielectric sphere with $n = 1.52$ as function of its radius.

Table 3.1: In figure 3.9, for a given refractive index of the sphere, all the diagonal components of the T-matrix $T_{ll}(a)$ have the same period. This table gives the period of these components as a function of the refractive index n of the sphere. A proportionality with $n - 1$ seems to appear.

n	n-1	period
2	1	$\lambda/2$
1.5	0.5	λ
1.25	0.25	2λ
1.2	0.2	$5\lambda/2$

Incident field expansion

The T-matrix approach needs the expansion of the incident field on SVF, that is a sum of functions. The mathematical convergence of this sum is not obvious as we will see and must be considered too. If $\theta_i = 0$, so only the SVF with $m = 1$ are needed. The expansion coefficients are given section 3.2 and are represented in figure 3.10(a). We observed that the absolute values of these coefficients increase when the order grows. Thus, such a sum does not converge in all space. However this sum converge uniformly in all finite space areas. The convergence of the incident field intensity in backward direction as a function of the order L_{max} for two different radii is represented in figure 3.10(b) and (c). We can observed that, for having convergence in a spherical area of radius R around the center, the needed order is approximatively $L_{max} = kR$. This local convergence is enough in our case, because the decomposition of the incident wave is used only at the boundaries of scatterers (or in the near field, if we want the total field

Table 3.2: Order of convergence for an aggregate of two identical spheres which centers are separated by a distance of 4 times their radius R and with $\theta_i = 0$ (independent of the refractive index)

sphere radius R	aggregate radius ρ	$k\rho$	convergence order
0.5λ	1.5λ	9	17
3λ	9λ	54	95
7λ	21λ	120	200

Table 3.3: Number of needed SVF in different cases. For a linear incident wave, this number is two times ($(e1, o2)$ or $(o1, e2)$) the number of couples (l, m).

θ_i	l and m variations	number of SVF
$\theta_i = 0$	$1 \leq l \leq L_{max}$, $m = 1$	$2L_{max}$
$\theta_i \neq 0$	$1 \leq l \leq L_{max}$, $0 \leq m \leq l$	$2\left(\frac{(L_{max}+1)(L_{max}+2)}{2} - 1\right)$

$E^t = E^s + E^i$ and not only the scattered field).

Convergence in the near field
This discussion and these convergence criteria are sufficient for the far field computation. However in this work, we have also considered the near field. For one sphere, the Lorenz-Mie theory is the rigorous one, that is the reason why we are also able to compute the near field.
For non spherical particles or for aggregates of particles, the Green function is used. This Green function is singular at its origin, that is the reason why there are limitations in its expansion on SVF [20]. Thus the **T-matrix does not allow us to compute the electromagnetic field inside the aggregate or in the near field**. The Point Matching Method (see section 2.6) and other iterative methods have been proposed to compute this near field [85].

3.6 Evaluation of computing time

Coupling and number of SVF
When the convergence order L_{max} is known, computing time can be estimated in function of the incident angle θ_i and of the geometry of the aggregate. This time is linked to the size of the matrix to compute. This size depends to the total number of SVF that must be used and to the possible couplings between these SVF. The number of needed SVF as function of θ_i is summarized in table 3.3. The possible couplings are summarized in table 3.4.

Computing time for the T-matrix
We have studied the computing time needed to calculate the T-matrix in function of the size parameter $x = ka$:

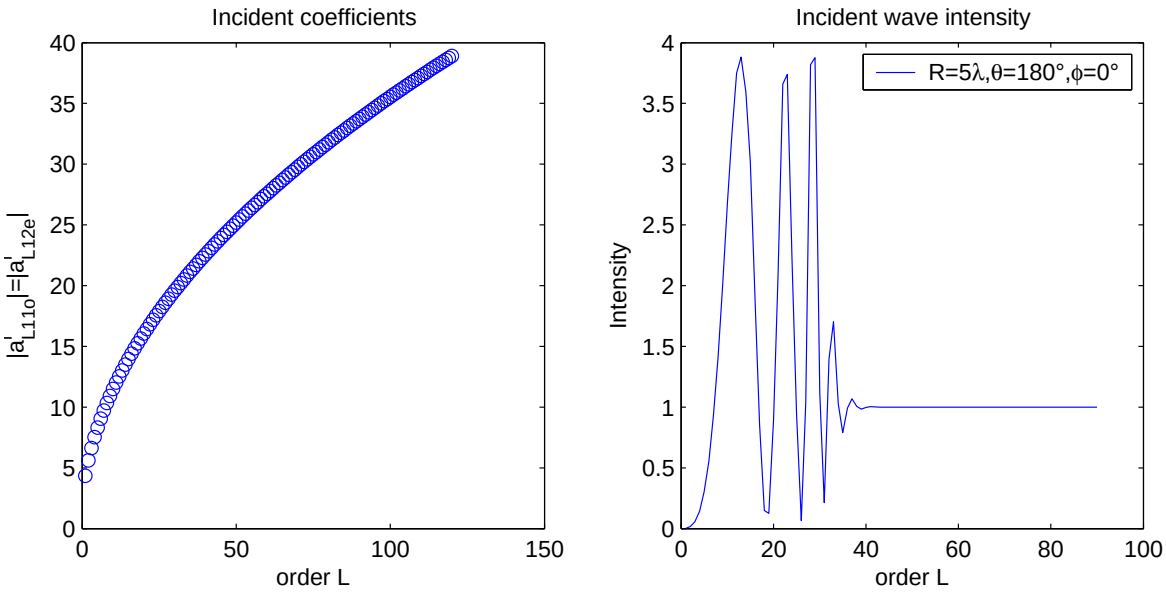

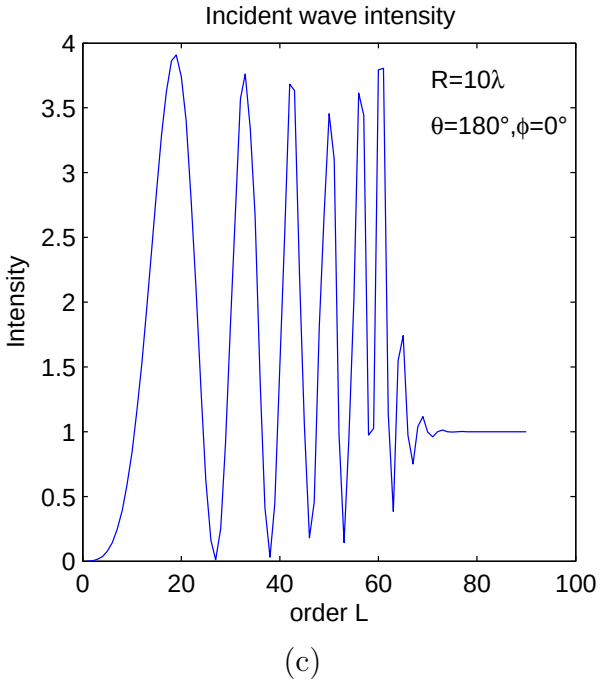

Figure 3.10: (a) Expansion coefficients of an incident plane wave on SVF in free space. $\theta_i = 0$, $H_i = H_y$ and $k_i = k_z$. (b) and (c) Incident intensity in backward direction for $R = 5\lambda$ (b) and $R = 5\lambda$ (c).

- for one sphere with $\theta_i = 0$ (figure 3.11a) only few seconds are needed,
- for one sphere with $\theta_i \neq 0$ (figure 3.11b), the computing time is plotted as a function of the order in figure 3.12(a). The time is in L_{max}^2 ($o(x^2)$),

Table 3.4: Possible couplings between SVF. $o1 \rightarrow e2$ means that the (a^i_{o1}) component of the incident wave has an influence on the component (a^s_{e2}) of the scattered wave.

Spheres number	Translation	Coupling
1	all	$\begin{cases} o1 \rightarrow o1 \\ e2 \rightarrow e2 \end{cases} = \begin{cases} o2 \rightarrow o2 \\ e1 \rightarrow e1 \end{cases}$
$N \neq 1$	z-axis	$\begin{cases} o1 \rightarrow o1 \\ o1 \rightarrow e2 \\ e2 \rightarrow e2 \\ e2 \rightarrow o1 \end{cases} = \begin{cases} o2 \rightarrow o2 \\ o2 \rightarrow e1 \\ e1 \rightarrow e1 \\ e1 \rightarrow o2 \end{cases}$
$N \neq 1$	others	$\begin{cases} o1 \rightarrow o1 \\ \rightarrow e2 \\ \rightarrow o2 \\ \rightarrow e1 \\ e2 \rightarrow e2 \\ \rightarrow o1 \\ \rightarrow e1 \\ \rightarrow o2 \end{cases} = \begin{cases} o2 \rightarrow o2 \\ \rightarrow e1 \\ \rightarrow e2 \\ \rightarrow o1 \\ e1 \rightarrow e1 \\ \rightarrow o2 \\ \rightarrow e2 \\ \rightarrow o1 \end{cases}$

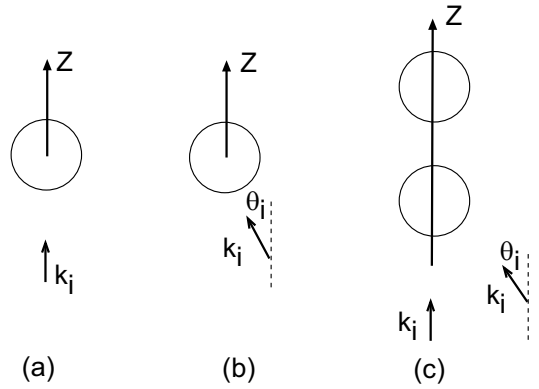

Figure 3.11: Geometrical description of sphere positions and possible incident wave vector Each case corresponds to particular possible couplings.

- for two spheres in the z-axis with $\theta_i = 0$ (figure 3.11c), computing time is plotted as a function of the expansion order L in figure 3.12(b). The time is in L^3_{max} $(o(x^3))$,
- for two spheres in the z-axis but with $\theta_i \neq 0$ (figure 3.11c), the computing time is similar to the case $\theta_i = 0$,
- the case of two spheres out of the z-axis has not been studied but is longer because of additional couplings.

Computing time for field reconstruction

We have also studied the computing time needed to calculate the field in rectangular spatial zones (20×20 pixels and 40×40 pixels). That is to sum the contribution of

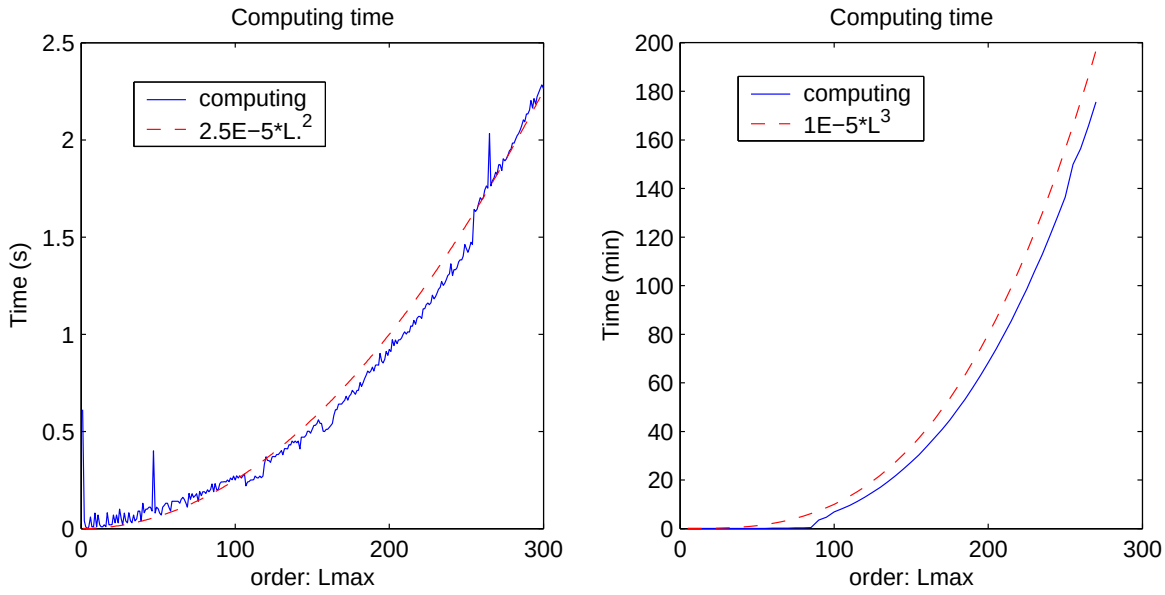

(a) For one sphere $\theta_i \neq 0$ (b) For two spheres $\forall\ \theta_i$

Figure 3.12: Computing time needed to calculate the T-matrix for one and two spheres according to the angle θ_i of the incident wave vector. The peaks in (a) are numerical artifacts. The difference between curves in (b) are only due to an additional constant.

each SVF for a given spatial zone. This time does not take into account the T-matrix calculation. The figure 3.13(a) shows for one sphere and incident angle $\theta_i = 0^o$ $(m = 1)$, that this time is in L^2_{max} $(o(x^2))$ where x is the size parameter of the aggregate. The figure 3.13(a) also shows that the computing time is also proportional to the surface of the considered spatial zone. The figure 3.13(b) shows that for one sphere but with $\theta_i \neq 0$ $(0 \leq m \leq l)$ the computing time is in L^5_{max} $(o(x^5))$ (this time is also proportional to the surface of the considered spatial zone). When it will be possible, for carrying out the post-treatment, we will try to use only the expansion coefficients on SVF and not the reconstructed field map, in order to reduce the computing time.

The computing time comparison with other algorithms has already been made, see in table 2.1.

3.7 Scattering phase function and cross sections

The following sections describe the calculations and the results for several useful physical parameters. The first two are the scattering phase function and the cross section.

Scattering phase function
In the far field, at a distance r of the scatterers, the scattered intensity distribution as function of phase angle is expressed as:

$$I(\theta, \varphi) = \frac{I_o F(\theta, \varphi)}{k^2 r^2} \tag{3.62}$$

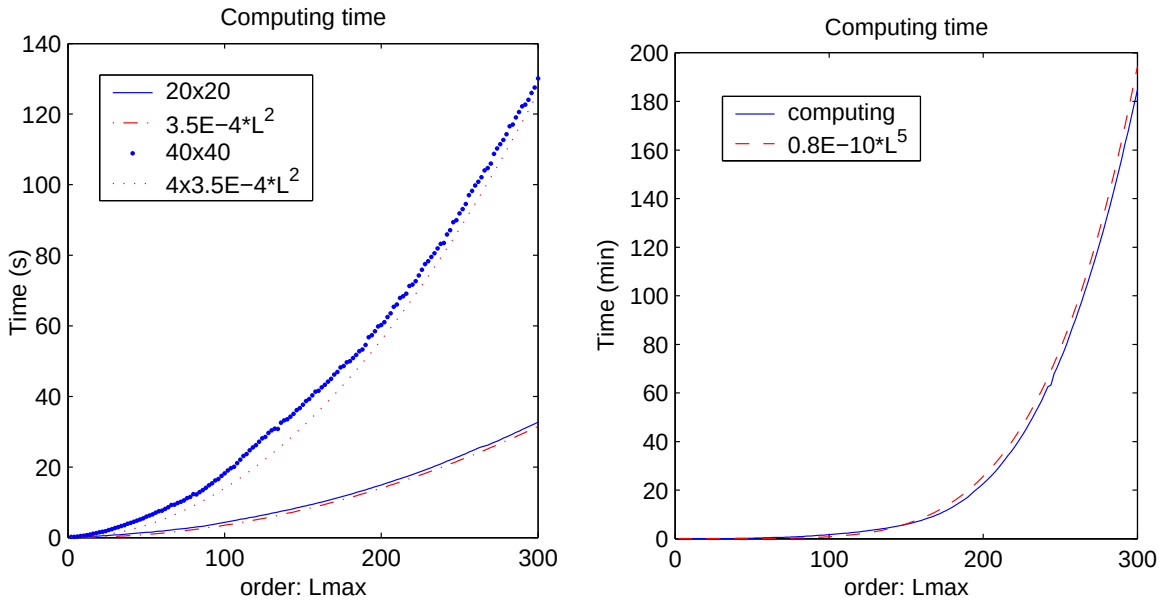

(a) For one sphere ($\theta_i = 0$) (b) For one sphere ($\theta_i = 90^o$) $20x20$

Figure 3.13: Computing time needed to calculate the field in a rectangular spatial zone (20×20 or 40×40) in several cases for one sphere and regression laws.

$F(\theta, \varphi)$ is the *scattering phase function*, it can be normalized by dividing by $k^2 C_{sca}$, where C_{sca} is the scattering cross section (see below). In this case $\int F_N(\theta, \varphi) d\Omega = 1$.

The angle between the incident and the scattered light is called the *phase angle*. The normalized scattering phase function can be interpreted (in a Monte-Carlo algorithm for example) as the density of probability describing the probability that a ray of an incident plane wave would be scattered in a particular direction (solid angle). Note that the normalization constant C_{sca} is the scattering cross section.

Cross section

The scattering cross section C_{sca} is defined as an area that reduces the power of incoming radiations due to scattering mechanism. If this area is multiplied by the incident flux, we must obtain the total power that is scattered.

$$C_{sca} = \frac{1}{k^2} \iint F(\theta, \phi) \sin\theta d\theta d\phi \tag{3.63}$$

The absorption cross section C_{abs} has the same definition but related to the loss due to absorption. When a beam of light goes through a scattering medium, a part of the incident flux is not transmitted. This part has been absorbed or scattered (figure 3.14) and can yield extinction of the beam. Therefore, the *extinction cross section* C_{ext} is defined as the sum of the scattering and absorption cross section:

$$C_{ext} = C_{sca} + C_{abs} \tag{3.64}$$

We also define the *albedo* of a particle or an aggregate as $w = \frac{C_{sca}}{C_{ext}}$.

Scattering cross section is not easy to measure, that is the reason why physicists prefer to use *backscattering cross section* C_{back}:

$$C_{back} = \lim_{r\to\infty} 4\pi r^2 |\tilde{E^s}|^2/|\tilde{E^i}|^2 \tag{3.65}$$

with $\vec{E^s}$ the scattered field in the backward direction ($\alpha = 180^o$) and with $\vec{r}$ the position vector.

The cross sections are often normalized dividing by πa^2 with a the radius of the scatterer.

Energy Balance
Because the part the incident flux, that is not transmitted through a scattering medium, is described by the extinction cross section, this cross section can be found by measuring the intensity in the far field, in the forward direction (figure 3.14). Such a measurement is possible only if there is a high extinction, else the sensor will be saturated by the incident light.

The incident wave is assumed to be an unpolarized plane wave.

$$E_i(z,t) = E_{0i} e^{ikz-\omega t}$$

Far from the aggregate, the scattered field is:

$$E_s(\vec{r},t) = E_{0i} S(\theta,\varphi) \frac{e^{ikr-\omega t}}{ikr}$$

In the forward direction ($\theta = 0, \varphi = 0$), the total field is

$$E_t(0) = E_i(0) + E_s(0) = E_{0i} e^{ikz-\omega t}(1 + S(0)\frac{e^{ikr-ikz}}{ikr})$$

If the observation point r is far from the scatterer and in the forward direction ($x, y \ll z$) so $r = z + (x^2+y^2)/(2z)$:

$$E_t(0) = E_{0i}(1 + S(0)\frac{e^{ik(x^2+y^2)/(2z)}}{ikz})$$

$$I_t(0) = |E_t(0)|^2 = I_{0i}(1 + \frac{2}{kz}\Re e\left[S(0)e^{ik(x^2+y^2)}\right])$$

($|1+a+ib|^2 = (1+a)^2+b^2 = 1+2a+a^2+b^2 \simeq 1+2a$ because $a^2+b^2 = |S(0)|^2/(kz)^2 \simeq 0$)
If the detector is in the z-axis and if light is integrated in the (x,y) plane on a surface Σ, the measured power P is:

$$\begin{aligned} P &= \int_\Sigma I_t(0)dxdy \\ &= I_{0i}\left(\Sigma - \frac{2}{kz}\Re e[S(0)\int_\Sigma e^{ik(x^2+y^2)/(2z)}dxdy]\right) \\ &= I_{0i}(\Sigma - \frac{4\pi}{k^2}\Re e[S(0)]) \end{aligned}$$

But

$$P = I_{0i}(\Sigma - C_{ext})$$

Thus we find the Van de Hulst formula [3]:

$$\boxed{C_{ext} = \frac{4\pi}{k^2}\Re e[S(0)]} \tag{3.66}$$

If we use (3.66) to calculate C_{ext}, the checking of the relation (3.64) is equivalent to

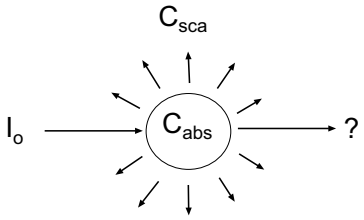

Figure 3.14: Energy conservation: $C_{ext} = C_{sca} + C_{abs}$.

the verification of energy conservation.

Discussion of cross section values
To have a better understanding of cross section, we study some simple examples. The first is the scattering cross section of a perfectly conductive sphere as function of its radius. In figure 3.15(a) we observed that the normalized scattering cross section is very small in the Rayleigh case and that for larger sphere is reached the constant value of 2. This means that, if we are not in the Rayleigh case, the scattering cross section of a perfectly conductive sphere is approximatively equal 2 times its geometric cross section.

Now if we consider dielectric spheres, the normalized scattering cross section for dielectric spheres is more complex because of the resonance with the cavity mode inside the sphere. In figure 3.15(b), which shows the scattering cross section of a dielectric sphere with a refractive index $n_2 = 1.2$ as function of its radius, this resonance can be observed. Diffraction effects increase when the sphere radius increases. This cross section also tends to reach 2 for large spheres. In order to explain this limit, which is called the **the extinction paradox** [3], we can consider that one part of the plane incident wave goes through the particle and the other part, outside the particle, is diffracted because of the obstacle (figure 3.16). This second diffraction is equivalent to the diffraction by a hole because of the Babinet theorem. Each of these two scattering process corresponds to a normalized cross section of 1 (one interaction with the geometrical cross section), the sum makes 2. (figure 3.15).

The incident flux I_o may create an *radiation pressure* F_r on the particles in the direction of propagation of the incident wave (supposed here to be in the z direction). This phenomenon has been first described by Debye [86]. The cross sections can be used

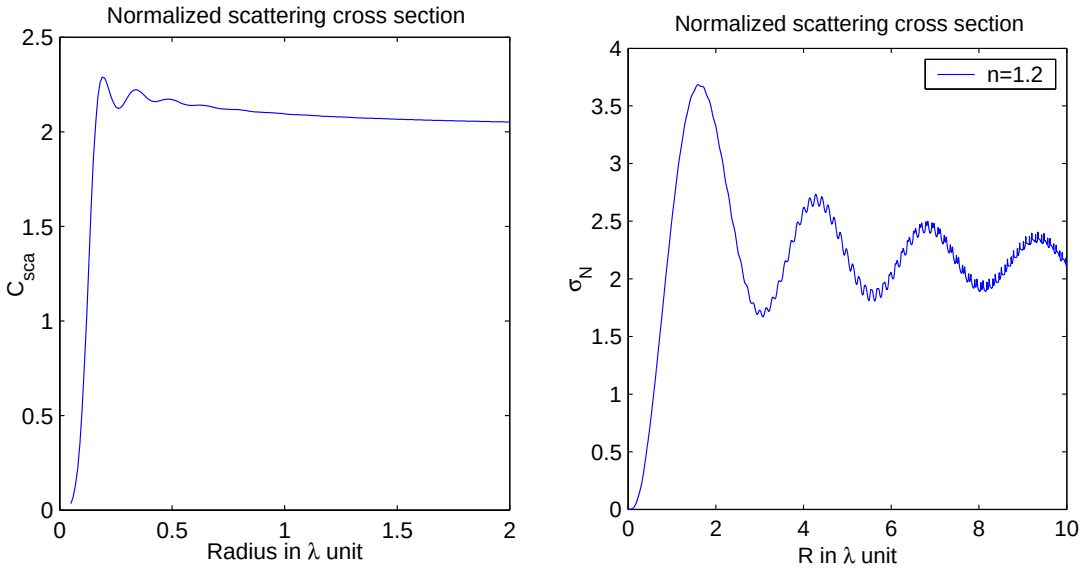

(a) (b)

Figure 3.15: Normalized scattering cross section as function of its radius of (a) a perfectly conductive sphere (b) a dielectric sphere with refractive index $n_2 = 1.2$. For a large sphere C_{sca} tends to 2.

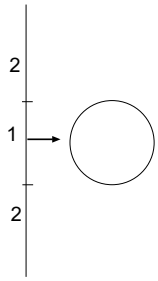

Figure 3.16: Schematic explanation of why the normalized cross section approaches to 2 when the sphere is large.

to calculate this radiation pressure [3]. If the extinction cross section is C_{sca} and the scattering phase function is $F(\theta, \varphi)$:

$$F_r = \frac{I_o C_{pr}}{c} \tag{3.67}$$

with $C_{pr} = C_{ext} - 1/k^2 \iint F(\theta, \varphi) \cos\theta d\Omega$.

3.8 Analysis of the polarization response of an aggregate

The polarization response of an aggregate for polarized or unpolarized incident wave has a great interest to obtain information concerning its shape and symmetries.

Stokes parameters
Stokes parameters (S_0, S_1, S_2, S_3) can be used to describe polarization state of the scattered wave, when this wave is transverse, that is in the far field.

$$S_0 =< E_\phi E_\phi^* > + < E_\theta E_\theta^* > \tag{3.68}$$
$$S_1 =< E_\phi E_\phi^* > - < E_\theta E_\theta^* > \tag{3.69}$$
$$S_2 =< E_\phi E_\theta^* > + < E_\theta E_\phi^* > \tag{3.70}$$
$$S_3 = i(< E_\theta E_\phi^* > + < E_\phi E_\theta^* >) \tag{3.71}$$

<> is for the temporal mean. Stokes parameters are often normalized by divided by S_0.
Stokes parameters do not describe a vectorial space (in mathematics), that is why we will not speak about Stokes vectors but about Stokes parameters.

The degree of polarization is defined as, $\sqrt{S_1^2 + S_2^2 + S_3^2}/S_0$ and is a value between 0 and 1. Degree equal to 1 corresponds to a total polarized field, whereas degree equal to 0 corresponds to a unpolarized light.

Some examples of Stokes parameters:
(1,1,0,0) corresponds to a linear polarization,
(1,-1,0,0) corresponds to a linear polarization orthogonal to the first,
(1,0,1,0) corresponds to a linear polarization rotated through 45^o from the first,
(1,0,0,1) corresponds to a circular left polarization,
(1,0,0,-1) corresponds to a circular right polarization,
(1,0,0,0) corresponds to a non polarized light.
(In some books, Stokes parameters are noted (I,Q,U,V)).

Stokes parameters can be added, because an unpolarized wave can be described as a succession in time of light considered as polarized during a shorter time than the integration time. Detectors measure quadratic values but are assumed to be linear in time. So an unpolarized wave can be modelled as the sum of two polarized fields with Stokes parameters (1,-1,0,0) and (1,1,0,0).

Mueller matrix and ellipticity
The relation between polarization of the incident and the scattered waves can be described by the Mueller Matrix. This 4x4 matrix also depends on the incident direction, on the scattering directions and on the wavelength. Mueller matrix can also be used for partially polarized incident wave. In the general case, the 16 components of this Matrix are not independent. If the polarization degree of the scattered wave is 1, Mueller matrix can be expressed as function of the amplitude matrix, so the Mueller matrix M can be expressed in function of 4 complex values or 8 real values. If the Mueller matrix is normalized by its $M(1,1)$ components, the matrix only depends of 8-1=7 independent values. Thus, 16-7=9 relations between its 16 components can be expressed. However if some additional symmetries are considered (aggregate symmetries), others additional relations can be expressed [3]. If an independent scattering occurs (that is

without phase effect), the Mueller Matrix can also be added.

The polarization can also be described by its axis and its ellipticity [8, 13]. If A_{large} and A_{small} are respectively the large and the small axis of the polarization ellipse:
$\vec{E} = \vec{P} + i\vec{Q} = (\vec{A}_{large} + i\vec{A}_{small}) \exp(i\kappa)$

$\vec{P} = \Re e[\vec{E}]$
$\vec{Q} = \Im m[\vec{E}]$
$\kappa = \text{angle}\left((|\vec{P}|^2 - |\vec{Q}|^2 + 2i\vec{P}.\vec{Q}) / \sqrt{(|\vec{P}|^2 - |\vec{Q}|^2)^2 + 4(\vec{P}.\vec{Q})^2} \right)$

$\vec{A}_{large} = \vec{P}\cos\kappa + \vec{Q}\sin\kappa$
$\vec{A}_{small} = -\vec{P}\sin\kappa + \vec{Q}\cos\kappa$

Polarization conservation
We often use the linear polarization degree as $P = S1/S0$ or the contrast of linear polarization $\frac{S1-S2}{\sqrt{S1^2+S2^2}}$
For a two spheres aggregate and for two particular cases of incident wave directions (figure 3.17), the linear polarization degree is represented in figure 3.18) as a function of the observation direction (and for a linearly polarized incident wave). The scattered light is linearly polarized in the white regions, unpolarized in the black ones and has an elliptic polarization in the gray regions. We can observe that the polarization of the scattered light as a function of the observation direction is quite complex in the general case. However white lines can be observe in figure 3.18): for a linear polarized incident wave, the scattered field stays linear in the symmetry planes of the aggregate when $(\vec{k}, \vec{E}^i)$ or $(\vec{k}, \vec{H}^i)$ are also in these planes (example in figure 3.17 and 3.18). There are

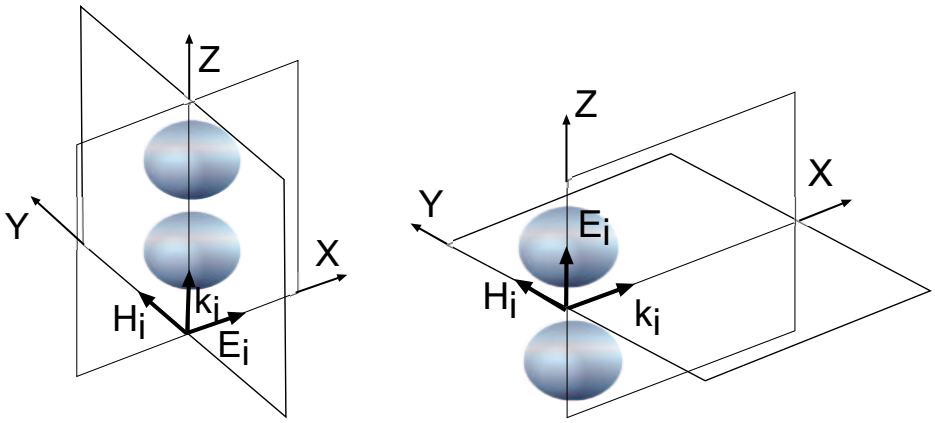

(a) (b)

Figure 3.17: Example for 2 spheres of planes where the scattered wave polarization is linear for two incident linear polarized wave.

not a lot of studies of polarization response of the scattered wave when the incident wave has a circular polarization. In Rayleigh scattering the polarization is conserved in the main direction (forward and back). In Mie scattering, the polarization is conserved in the forward direction ($\alpha = 0^o$). A comparison of depolarization between linear and

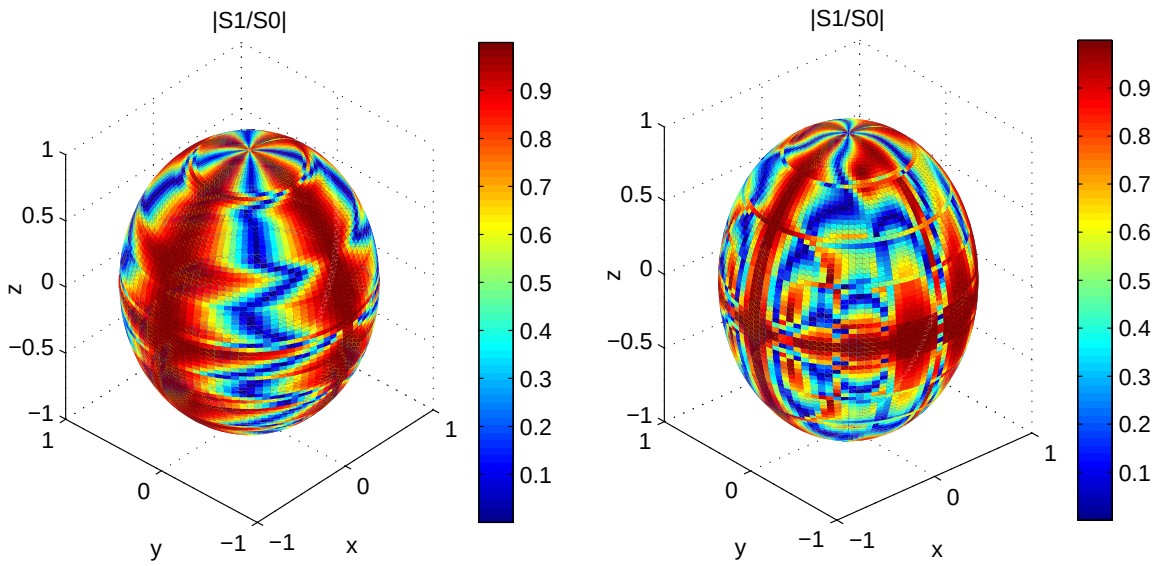

(a) geometry of figure 3.17(a)

(b) geometry of figure 3.17(b)

Figure 3.18: Linear polarization degree, $|S1/S0|$, in the far field as a function of the direction of observation for two different geometries (a) and (b) described in figure 3.17. The scatterer is made of 2 spheres $a = \lambda$, $n = 1.5$, $d = 4\lambda$. We observe that the scattered field stays linear (white regions) in the $(\vec{k}, \vec{E}^i)$ and $(\vec{k}, \vec{H}^i)$ planes, because these planes are also the symmetric planes of the couple of particles.

circular incident polarization has been made for aggregate of several size in reference [87].

Chapter conclusion

In this chapter, we have presented the main tools and algorithms that will be used in our studies of scattering phenomena that occur in the near field. The two algorithms allow to find rigorous solution of Maxwell equations in the case of light interaction with spherical particles. The Lorenz-Mie theory will be used in the next chapter to study the intensity map in the near field around a single dielectric particle. The T-matrix will be used in chapter 5 to study the consequence in the far field of electromagnetic couplings between close particles.

Chapter 4

Application: The Photonic Jet

To have a better physical understanding of multiple scattering, a great interest is in the study of interactions between particles. Whereas light scattering is generally measured in the far field, the interactions between particles take place in the near field, that is within the aggregates. For this reason, we start by studying the intensity profile in the near field, just around the particle. Moreover, in order to be able to find physical interpretations, we will begin with the simplest case of only one sphere. Our notations are reminded in figure 4.1. In this section the refractive index of the medium around is supposed to be $n_1 = 1$ and no absorption is taken into account ($\sigma_2 = 0$).

Our interest for this simple case can also be explained by another reason. Chen and Taflove [22] have recently shown that micrometer-size cylinders were able to concentrate visible light in the near field. Our aim was to investigate what will happen with micrometer-size dielectric spheres in similar cases and what are the influences of sphere parameters on this concentration of light.

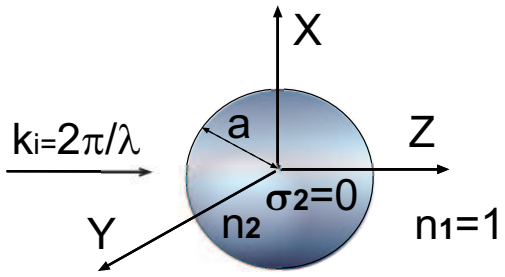

Figure 4.1: Notations to describe the micro-spherical lens. $n_1 = 1$ and $\sigma_2 = 0$. k_i is the incident wave vector, a and n_2 are respectively the radius and the refractive index of the sphere.

4.1 A photonic jet

We will first define what a photonic jet is. Recently simulations have shown that an infinite dielectric cylinder [22] with a ten wavelength diameter was able to focus light and to reach the diffraction limit. Depending on its refractive index the focus point (defined here as the intensity maximum on the optical axis) can be inside or outside the cylindrical micro-lens, but when the focus point is just on its surface an interesting phenomenon occurs. Along a distance of propagation of one or two wavelengths in front of the focus point, the Full-Width-Half-Maximum (FWHM) (defined in figure 4.2) of the beam stays smaller than the wavelength and the beam locally reaches a very high intensity. The focus point reaches the diffraction limit. This beam has been called a *photonic jet* by Taflove [22] because of the analogy between the high speed gradient which is characteristic of a jet in fluidic mechanic and the observed high light flux gradient (top of figure 4.5).

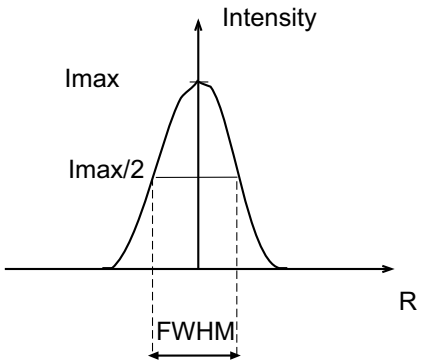

Figure 4.2: Definition of the FWHM of a beam. R is the radial position in a plane transverse to the propagation axis.

Chen and Taflove [22] have used a FDTD method (see section 2.6) to simulate this focusing of light by a cylinder. This method has several limitations [16]:

- the required computational memory is large, therefore, calculations are often limited to 2-dimensional cases,
- the sampling grid makes the boundaries of objects difficult to describe,
- the sampling grid anisotropy introduces numerical dispersion. Because of the grid, the light velocity is not exactly the same in all directions,
- because FDTD simulates the evolution of field in time, a long computing time is needed to obtain the stationary state.

Because of these reasons, we prefer to use the Lorenz-Mie theory (see section 3.2) that makes it possible to rigorously carry out the 3-dimensional calculations.

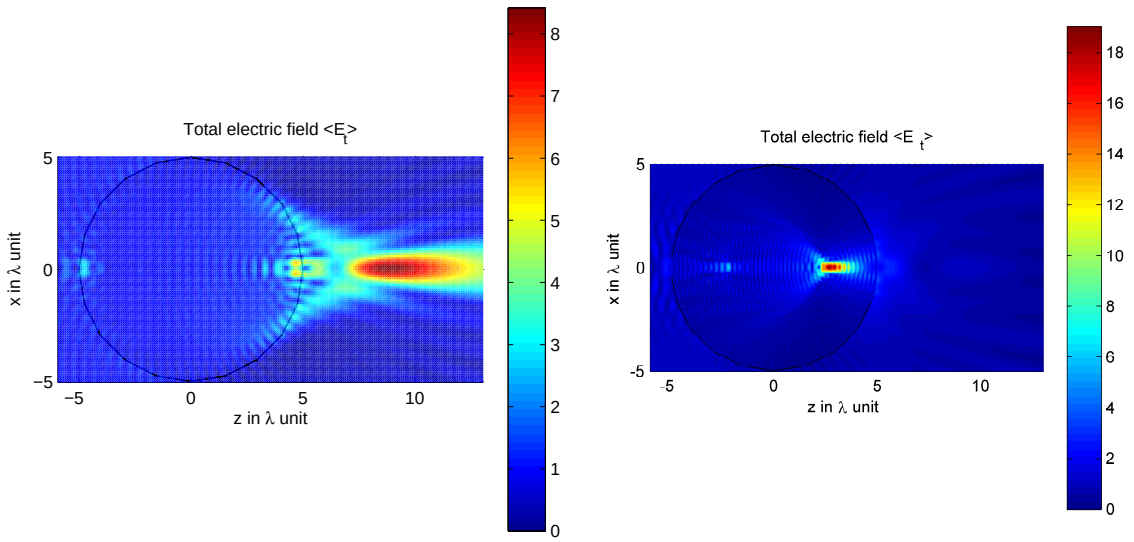

(a) $n_2 = 1.2$ (b) $n_2 = 2.5$

Figure 4.3: Focusing of an incident plane wave ($H_i = H_y$ and $k_i = k_z$) by a dielectric sphere of index n_2 and radius $a = 5\lambda$ ($L_{max} = 40$).

As we see in figure 4.3, our simulations show that a ten wavelength diameter sphere is also able to focus an incident plane wave and to locally concentrate intensity. According to its refractive index the focus point can be outside (a) or inside (b) the sphere. The figure 4.5 also shows that the FWHM of the focus point can be smaller than the wavelength. Therefore the photonic jet also exists for spherical dielectric particles [15].

This possibility to concentrate light in the near field with a few wavelength diameter dielectric particle is almost unknown, probably because we usually consider their ability to scatter light in the far field. Usually, only the scattered field (and not the total electric field) and only the field outside the sphere is computed. For example in figure 4.4, the scattered field is represented for a sphere of 5 wavelengths radius and refractive index n_2=2.5, whereas the total electric field (scattered field + incident field) is represented in figure **??**b. The focusing can be observed only in the second one. A second reason, as we will see, is that the **high** energy concentration occurs only in specific cases.

We have observed, as it will be explained in the next sections, that two different effects must be distinguished:

- the possibility to reach a high intensity concentration outside the sphere,
- the possibility to have a subwavelength focused beam along a large distance of propagation.

In order to demonstrate and to understand why these two effects cannot be optimized together and why they happen, we will study the influence of the sphere parameters

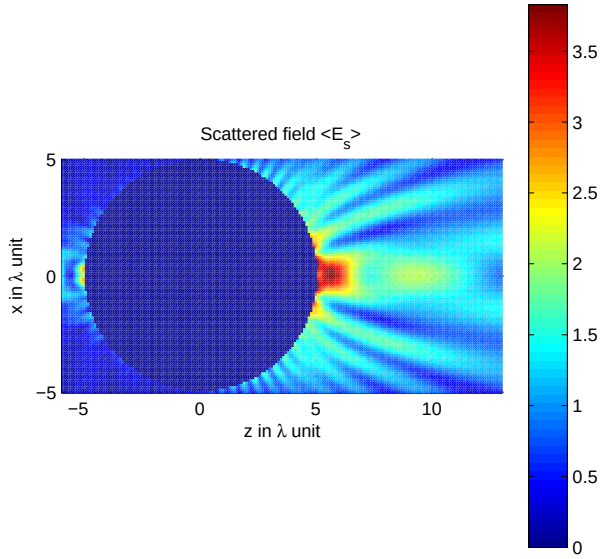

Figure 4.4: Electric field scattered by a dielectric sphere of index $n_2 = 2.5$ and radius $a = 5\lambda$ of an unitary plane wave ($H_i = H_y$ and $k_i = k_z$). Only the field outside the particle is represented.

on the photonic jet.

4.2 Focusing with a micro-spherical lens

For large spherical lens, the thick lens formula [88] in geometrical optics gives the focus position according to the refractive index n_2 and the diameter D of the sphere:

$$f = n_2 D/(4(n_2 - 1)) \tag{4.1}$$

However, this law does no work for few wavelength diameter spheres. The focus position is calculated as a function of the refractive index for several sphere radii and the results are depicted in figure 4.6. The focus is defined here as the intensity maximum on the optical axis, its position is measured from the sphere center.

Figure 4.7 represents the difference of position in wavelength unit between the rigorously calculated focus and the theoretical geometrical focus (4.1) according to the refractive index and for several radii. For small refractive indexes, the increase of difference is due to the fact that the focus point was no more in the studied space area. The focus point was too far from the spherical lens.

For large refractive indexes ($n > 2$) the focus point is in the dielectric sphere. Figure 4.8 shows the difference between the calculated focus and the theoretical geometrical focus for a large refractive index (asymptotic value) according to the radius. The theoretical position of the focus point would be $a/2$ in geometrical optics. This difference

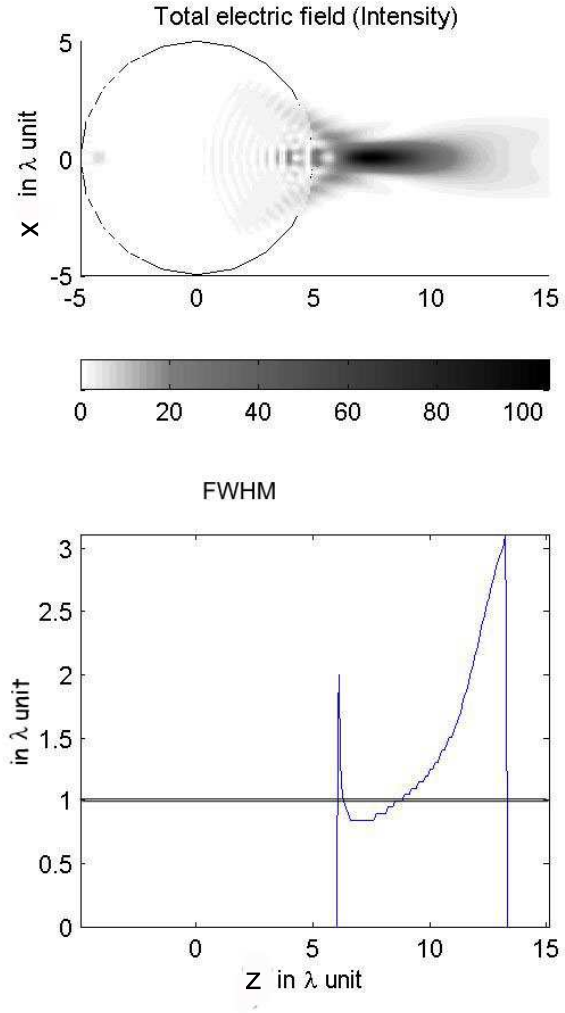

Figure 4.5: Electric field intensity $H_i = H_y$ and $k_i = k_z$ (top) and FWHM (down) of a dielectric sphere of index $n_2 = 1.3$ and radius $a = 5\lambda$. The focused beam is smaller than the wavelength.

seems to be proportional to the radius (proportional to $a/4$).

Our study confirms that the geometrical laws cannot be applied for such small spherical lens. We have found how to correct the focus position law for large refractive indexes and we have given the curves which describe the focus positions for small refractive indexes according to the radius.

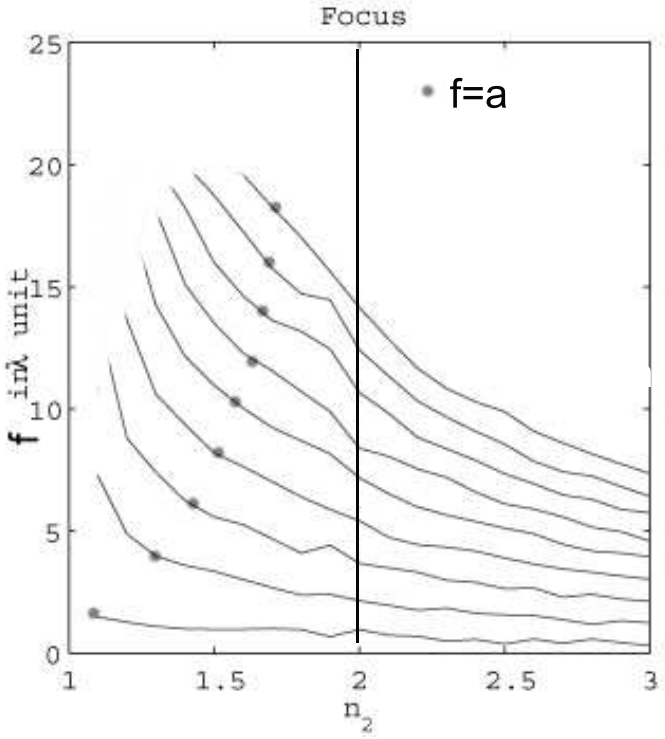

Figure 4.6: Focus position as a function of the refractive index for several sphere radii a. At the bottom $a = 2\lambda$, then $a = 4\lambda$, until $a = 18\lambda$ at the top. The points • show the case when the focal point is just on the sphere surface.

4.3 High intensity concentration

We have observed that was possible to concentrate energy with dielectric spheres. Next, we would like to determine where the focus point must be to obtain the highest intensity outside the sphere. For several different radii ($a = 2\lambda$, $a = 3\lambda$, $a = 5\lambda$, $a = 15\lambda$), we calculated the intensity maximum outside the sphere as a function of the refractive index of the sphere. The highest intensity outside the sphere is reached when the focus point is just on the surface of the sphere (coherent with paper [22] of Chen and Taflove which deals with infinite cylinder). If we want to focus on the surface of a spherical lens, the geometrical law (4.1) gives that the index has to be 2. However our simulations for spheres with a radius of a few wavelengths, where geometric laws are not valid, show that the refractive index has to smaller than 2. This index tends to 2 for large sphere (see • $f = a$ in figure 4.6).

In figure 4.9 the index n_2 has been chosen in order to locate the focus point on the surface of the sphere. In this figure the sphere radius a is 5λ and the refractive index n_2 is 1.63. There is no absorption. We observed that for any given unitary incident plane wave, the intensity maximum outside the sphere is locally multiplied by more than 200 as it would be without sphere.

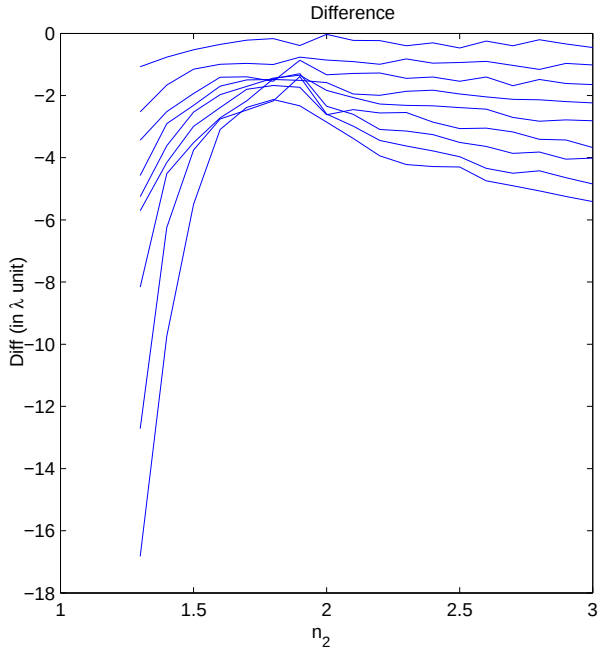

Figure 4.7: Difference of focus position between electromagnetic computing (fig. 4.6) and geometrical law (4.1) for several sphere radii a, according to the refractive index n_2. At the bottom $a = 2\lambda$, then $a = 4\lambda$, until $a = 18\lambda$ at the top.

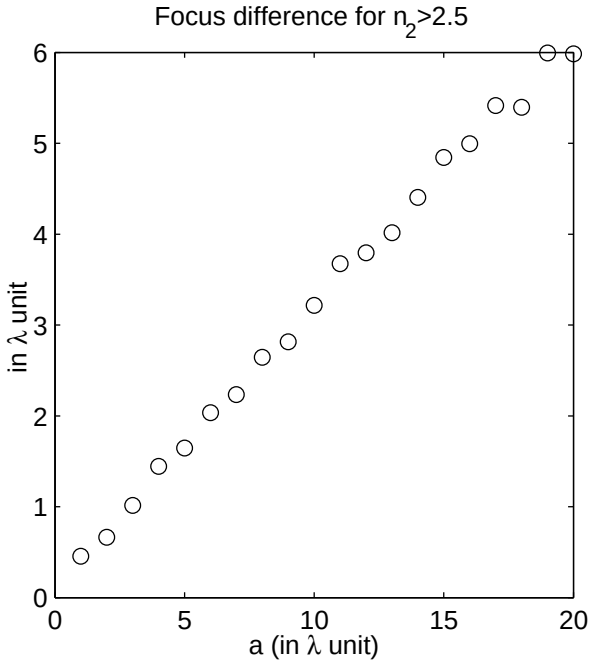

Figure 4.8: Difference between the calculated focus and the theoretical geometrical focus for a large refractive index (n_2>2.5, asymptotic value).

This focused beam outside the sphere, called photonic jet, has a FWHM smaller than the wavelength along approximatively one wavelength in the direction of propagation.

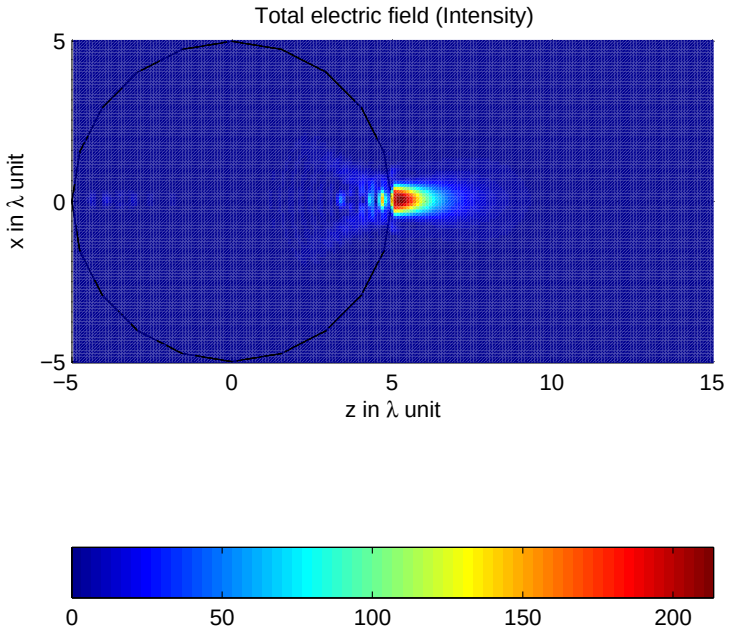

Figure 4.9: Intensity of the total electric field for a sphere with $a = 5\lambda$ and $n_2 = 1.63$. Calculations have been made with $L_{max} = 45$ and the incident plane wave is $H_i = H_y$ and $k_i = k_z$.

However it is no in this case, when the focus point is on the surface and when the highest intensity outside the sphere is reached, that the beam stays along the longest distance of propagation with a width smaller than the wavelength.

4.4 Subwavelength focusing with a dielectric sphere

It is also important to know under what conditions the photonic jet width stays smaller than the wavelength along the longest distance of propagation. In order to determine this, calculations were carried out for several sphere radii. The distance along which the photonic jet stays smaller than the wavelength as a function of the refractive index is depicted in figure 4.13. The FWHM is not always easy to compute because the intensity maximum in the transverse planes ($z = z_o$ planes) is not always on the optical axis: see for example in figure 4.10, near of the sphere surface.

We observe that if we want a focused beam with a FWHM smaller than the wavelength along the longest distance of propagation and with an intensity over the half global maximum, we must not focus on the sphere surface but just in the front of it. For example, we should focused round one wavelength ahead for a sphere of radius $a = 5\lambda$. The refractive index must be around $n_2 = 1.3$ in this case. As we observe in figure 4.10 the beam width stays smaller than the wavelength because of the proximity of the focus point with the sphere surface. However, this phenomenon does not permit

us to reach an intensity as high as by focusing on the surface.

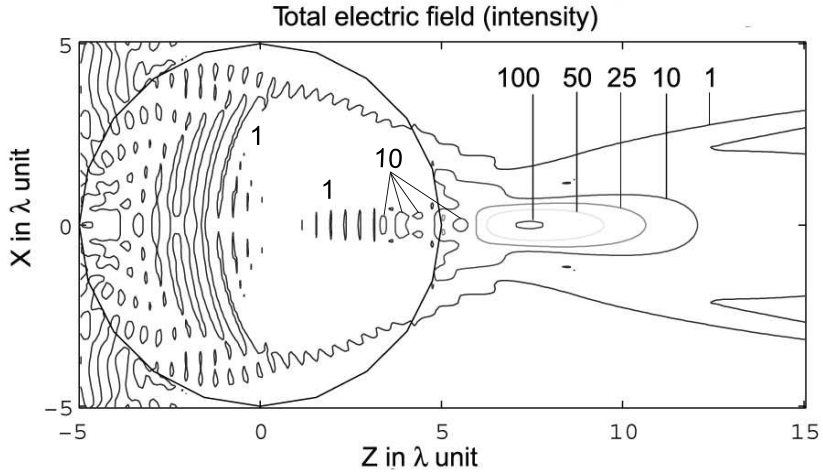

Figure 4.10: Electric field intensity for a sphere with $a = 5\lambda$ and $n_2 = 1.3$, a sub-wavelength FWHM is observed. Calculations have been made with $L_{max} = 45$ orders and the incident plane wave is $H_i = H_y$ and $k_i = k_z$.

The possibility of reaching or of going beyond the diffraction limit is not new, it is used in various applications [89] as SNOM microscopy [90][91], microscopy using near-field probes [92], immersion lens microscopy [93][94]. This limit is true in the scalar far field approximation [8]. In this case, the diffraction half-angle caused by a physical aperture of diameter D can not be smaller than $1.22\lambda/D$ [8]. If we consider the intensity FWHM at the focus distance f of a lens, it can not be smaller than $1.02\lambda f/D = 1.02\lambda/NA$ with $NA = D/f$ (figure 4.11). If we want the focus point to stay outside the sphere, NA, the numerical aperture, can not be larger than 2. For a photonic jet, we reach this diffraction limit.

4.5 Basic properties of the photonic jet

The optical properties of this photonic jet is important to know in order to identify their differences with geometrical laws and to be able to use it for possible applications. We have already published the details of this study in [15]. This section will outline the fundamental results obtained for photonic jets.

Influence of the refractive index
As demonstrate in the previous sections, if the refractive index is too high (n>2, figure 4.3b), the focus point will be inside the sphere, the forward scattering decreases and several lateral scattering orders appear. If the refractive index is too small, the focus point is far out of the sphere (figure 4.3a), scalar approximation can be used and the focus point cannot be smaller than the wavelength. We have already explained what

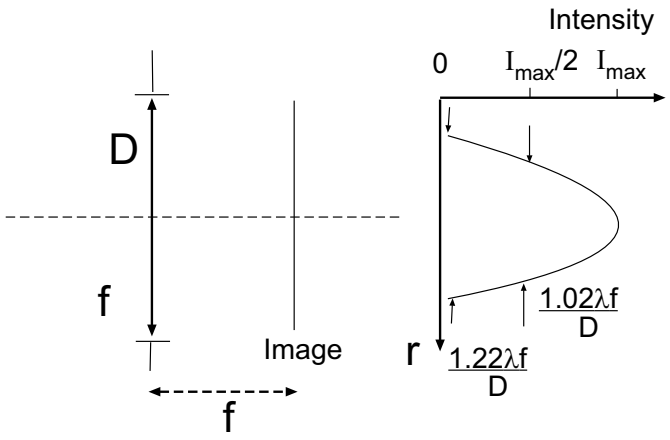

Figure 4.11: Abbe's law for an imaging system of focus f and aperture D. Image by a lens of a point placed at infinity.

happens in the two interesting cases when the focus point is just on the surface of the sphere (maximum intensity outside the sphere) and when it is just in the front of the sphere (longest distance of propagation with a width smaller than the wavelength).

Influence of the radius
There is not photonic jet in the Rayleigh case ($ka < 1$) because in this case, in the near field, the intensity maximum is not on the optical axis [23]. There are two maxima at two sides of the particle as illustrated in figure 4.12.
The photonic jet can be created with small ($a \simeq \lambda$), but also with large spheres ($a > 20\lambda$). When a sphere is larger, the refractive index required to focus on the surface will increase from 1.6 to 2. With such an index the width of the beam will stay smaller than the wavelength along around 2 wavelengths of propagation.

For sphere radii where $ka > 1$, it will be possible to have a beam width smaller than the wavelength along the longest distance of propagation, if the refractive index is around 1.3. This distance of propagation under the wavelength may have to increase when the radius becomes larger, but the adapted refractive index stays the same. Figure 4.13 shows for several radii and according of the refractive index of the sphere, the distance of propagation where the beam FWHM stays under the wavelength and has an intensity over the half global maximum. The figures 4.15 and 4.16 show that this possibility to have a beam width smaller than the wavelength is also true for larger sphere ($a = 15\lambda$).

The properties of the focus point as a function of the refractive index and of the radius of the sphere are summarized in table 4.1.

Polarization
What is the influence of the incident wave polarization and how the photonic jet is polarized?
The 3D vectorial calculations make it possible to see that, due to the linear incident

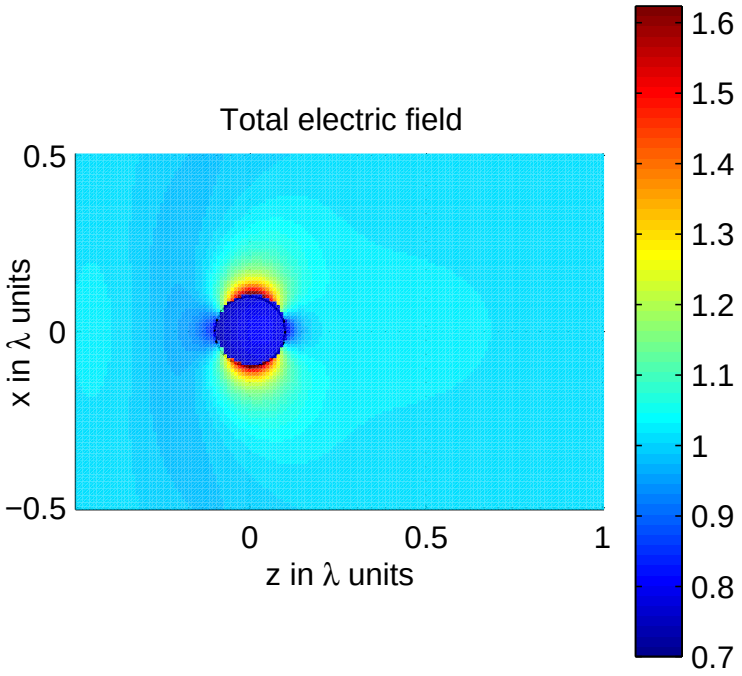

Figure 4.12: Total electric field around a dielectric sphere of radius $a = 0.1\lambda$ and optical index $n_2 = 1.5$, for an incident field: $H_i = H_y$ and $k_i = k_z$: In the Rayleigh case there are two maxima at two sides of the particle.

polarization of the incident wave, the photonic jet has not a cylindrical symmetry as in geometrical optics (figure 4.14).
However the photonic jet has a cylindrical symmetry when the incident wave has a circular polarization or if the wave is unpolarized.

The photonic jet corresponds to the total electromagnetic field in the forward direction z. In all the studied cases (incident wave with a general elliptic polarization), we have observed that the photonic jet has the same polarization of the incident beam (that is, in the forward direction). This is a known property far from the sphere[3], but it is also true for near field distribution in the front of the particle. The value of the E_r component of the electric field is zero in the forward direction z as it can be deduced from equations (3.20) and (3.21). However that is not necessary the case in other directions (see for example figure 4.18). Therefore in the near field, the scattered wave is not necessarily transverse and when the wave is not transverse, the usual definition of polarization (see section 3.8) can not be used.

Next, the influence of the refractive index and of the radius of the sphere on the photonic jet are studied. We have changed these two parameters and we have observed the field around the dielectric sphere.

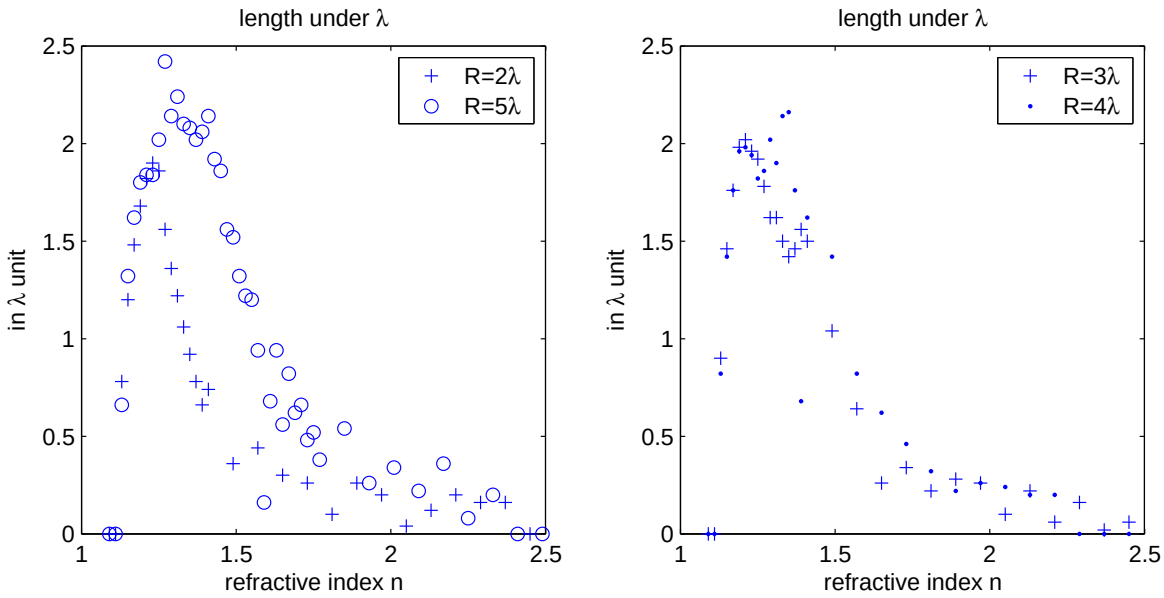

Figure 4.13: Distance along the z-axis (see geometry in figure 4.1) where the FWHM stays smaller than the wavelength and the intensity over the half global maximum for 4 radii. The curves are regular only for small indexes because for larger indexes a near field effect occurs: the global intensity maximum, which is close to the sphere, jumps from a local maximum of a stationary case to another when the refractive index changes.

4.6 Near field effect

We would like to understand why a dielectric sphere is able to focus a beam with a width smaller than the wavelength and to highly concentrate energy.

First, we want to show that these particular properties are not due to the small size of the particles. We have often studied small particles because the number of needed orders in computing increases dramatically with the size of the sphere (see section 3.6). In figure 4.15 the field forward a larger sphere ($a = 15\lambda$) is computed for the refractive index $n_2 = 1.3$ for which the beam width must stay smaller than the wavelength along

Table 4.1: Properties of the focus point as a function of the refractive index n_2 and of the radius a of the sphere. ($n_1 = 1$).

n_2	$0.5\lambda < a < 20\lambda$		$a > 20\lambda$	
	position	property	position	property
1.2	far from the sphere	-	far from the sphere	-
1.3	behind the sphere	longest distance $< \lambda$	behind the sphere	longest distance $< \lambda$
1.6	on the surface	highest intensity	-	-
2	inside the sphere	-	on the surface	highest intensity
2.2	inside the sphere	-	inside the sphere	-

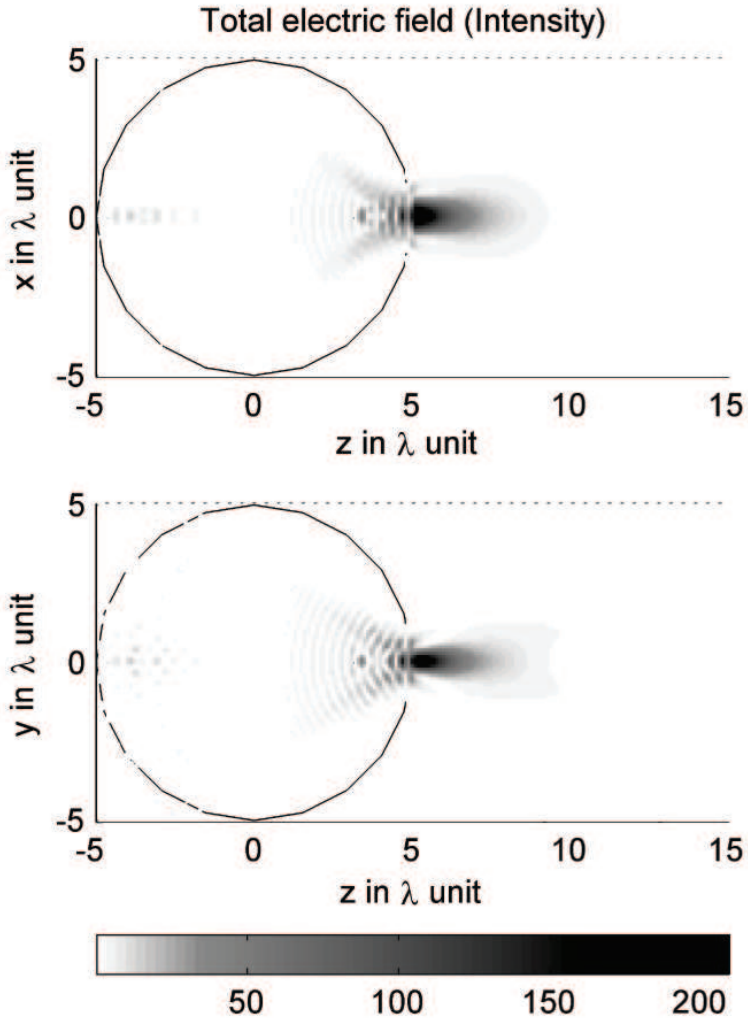

Figure 4.14: Intensity profile of the total electric field for a sphere with $a = 5\lambda$ and $n_2 = 1.63$ in two orthogonal planes. Calculations have been made with $L_{max} = 45$ and the incident plane wave is taken as $H_i = H_y$ and $k_i = k_z$.

the longest distance of propagation. We can effectively observe in figure 4.16 that the FWHM of this beam stays smaller than the wavelength along several wavelengths. In figure 4.17 the field forward a sphere with the same size ($a = 15\lambda$) is computed but for the refractive index $n_2 = 1.9$ for which the focus must be on the sphere surface and for which the intensity concentration must be maximum. The predicted high energy concentration is effectively observed. Therefore the photonic jet can also be created with large spheres (here a=15λ).

This possibility to have a beam with a width smaller than the wavelength agrees with the diffraction limit and seems to be a near field effect. First, we must explain what is called **the near field** in this discussion. We use *near field* in opposition to *the far field*. An area is in the far field when its distance with the scattered is far compared

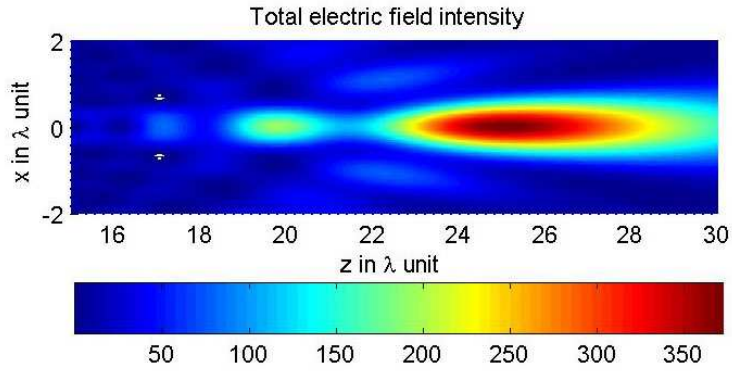

Figure 4.15: Total electric field intensity forward a sphere of radius $a = 15\lambda$ and index $n_2 = 1.3$. $H_i = H_y$ and $k_i = k_z$. The sphere is centered in $z = 0$.

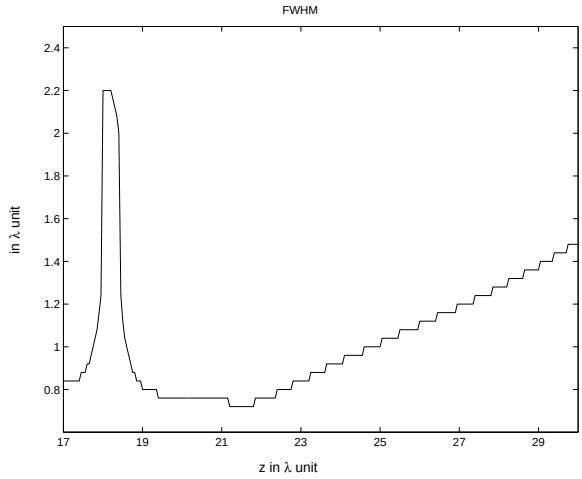

Figure 4.16: FWHM of the beam forward a sphere of radius $a = 15\lambda$ and index $n_2 = 1.3$. The discontinuities are only due to the space sampling. The sphere is centered in $z = 0$.

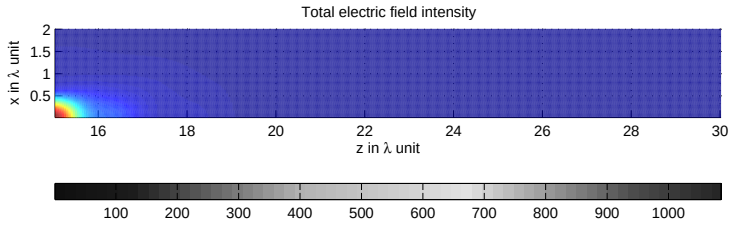

Figure 4.17: Total electric field intensity forward a sphere of radius $a = 15\lambda$ and index $n_2 = 1.9$. $H_i = H_y$ and $k_i = k_z$. The sphere is centered in $z = 0$.

to the wavelength, compared to the particle sizes and compared to the aggregate sizes. When these three conditions are verified, it can be demonstrated that the field will be transverse. Figure 4.18, we have represented the 6 components of the electromagnetic field for a sphere of radius 5λ and refractive index $n_2 = 1.63$. We know that a photonic jet is created (see the electric field intensity in figure 4.9). What we observe in figure

4.18 is that the E_r component is not zero everywhere. In the near field, close to the particle, the electromagnetic field is not transverse. We can also observe, in figure 4.19, for the sphere of radius 15λ and refractive index 1.3, that several local intensity maxima are forward the sphere. There is not a monotone intensity decrease in the near field.

The fact that the E_r component is not zero in the near field is not compatible with the scalar far field approximation used to demonstrate the Abbe limit. That is the reason why the diffraction limit has no meaning in this case. If we look at the E_r expression in formulae (3.20) and (3.20), its decrease is in $1/r^{1/2}$, whereas the other components decrease as $1/r$. The E_r component will be zero in the far field. However for a dielectric sphere without absorption, this component is not an evanescent wave, because the E_r component alone does not obey to the propagation equation and its associated wave vector is not complex. This particular field is a whispering gallery mode.

We may have evanescent waves for a metallic sphere with finite conductivity. In this case the complex wave vector would be parallel to the sphere surface and the evanescent wave would be a stationary state at the surface (plasmon). We have not studied this case. When the wave vector k is a complex value, the SVF are no more an orthogonal basis, the study is more difficult. The same difficulties occur if the incident wave is evanescent [95, 96, 97]. However, we have not studied this case either.

4.7 Applications of the photonic jet

The photonic jet can have several important applications. It can be used for surface materials laser processing. It may allow a larger precision. For example transparent submicrospheres have already been used to make holes in silicon or BK7 [23]. Spheres are put on the surface material to process. Thus, the incident plane wave is concentrated by each sphere and allows to make a hole in the substrate. These holes can then be observed by microscopy. Because in this example, report in [23], experiments were in the Rayleigh case, two holes were carried out under each sphere (explication in figure 4.12).

Another interest would be for optical data storage [98]. The higher resolution can be used to improve storage capacity. Spheres can be used as near field lens able to concentrate energy in a volume with a size smaller than the wavelength. By this mean, more data could be stored on a given surface. Philips has begun to work on such near-field systems for data storage [99].

If a high intensity concentration is reached in the near field and if the medium around the dielectric sphere can have non-linear responses, these responses may be enhanced.

Another application would be the improvement of optical microscopy. The photonic jet makes observations of details smaller than the wavelength possible. But in all these applications, the interaction between the sphere and the object (substrate, storage disc,

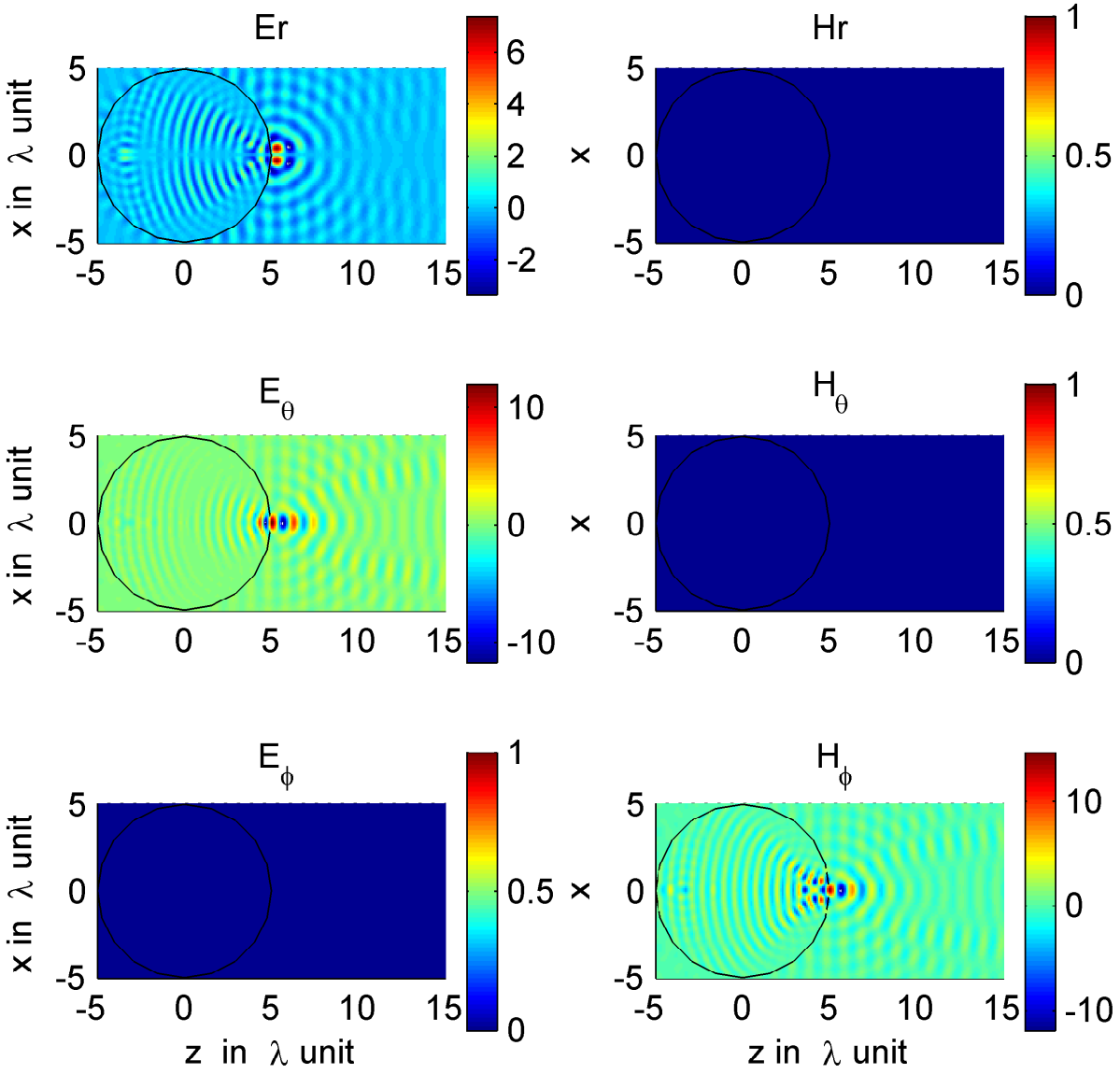

Figure 4.18: Electromagnetic field components around a dielectric sphere of radius $a = 5\lambda$ and index $n_2 = 1.63$ ($L_{max} = 115$). $H_i = H_y$ and $k_i = k_z$.

etc.) cannot be neglected. The focus point is near of the sphere surface, resonances can occur. But in particular cases, this electromagnetic interaction between sphere and object can be directly used. For example, this would make the detection of nanoparticles possible and could have a particular interest in biology [100] (see below). We have presented such applications for biology in conference [25].

Detection of nano-particles with the photonic jet

How to detect nanoparticles, for example antibodies, by using a sphere of a few microns diameter, for example silicate beads (see in figure 4.20)? A nanoparticle does not scat-

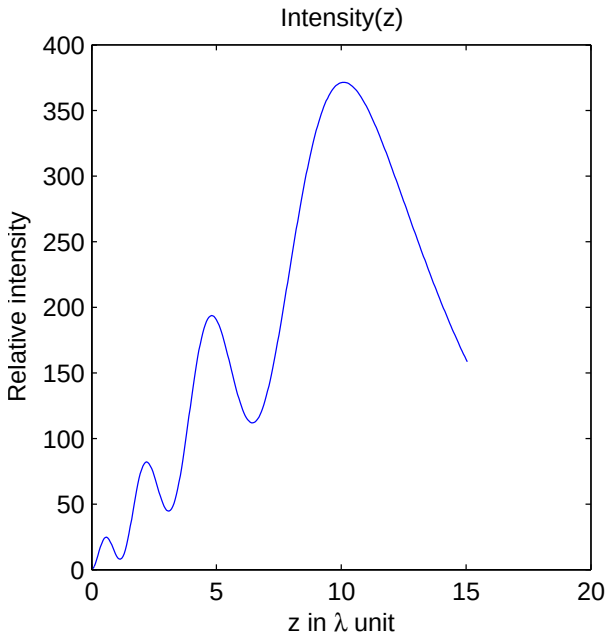

Figure 4.19: Total electric field intensity on the optical axis forward a sphere of radius $a = 15\lambda$ and index $n_2 = 1.3$. $H_i = H_y$ and $k_i = k_z$.

ter enough light to be detectable by actual sensors. If a microsphere is added beside the nanoparticle, the light scattered by the nanoparticle will be very small compared with the light scattered by the microsphere. That is the reason why, in general, if a nano and a micro particle scatter light together, the measured scattered light will be the one of the microparticle (see in figure 4.20 with k_{i2}). But in the particular case, when the nanoparticle is just in the photonic jet created by the microparticle (see in figure 4.20 with k_{i1}), the incident light is concentrated on the nanoparticle and strong interactions between the two particles will occur. This has been reported in [24]. In this case, simulations predict a large enhancement of backscattering. Without nanoparticle, only the light backscattered by the microsphere is detected. When a nanoparticle, an antibody for example, goes through the photonic jet created by the microsphere, an enhancement of backscattering may be observed.
We have tried to simulate such cases with the T-matrix algorithm developed during the thesis. We have observed backscattering changes, however the problem is appeared to be badly conditioned (too important numerical errors occur during matrix inversion) probably because the sizes of the two particles are too different. Chen and Taflove do not speak about such a problem in their paper [24]. Their algorithm may be more adapted.

Chapter conclusion

In this chapter, photonic jet phenomena has been described in depth. This study (published in [15]) has allowed us to describe properties and to identify engineering

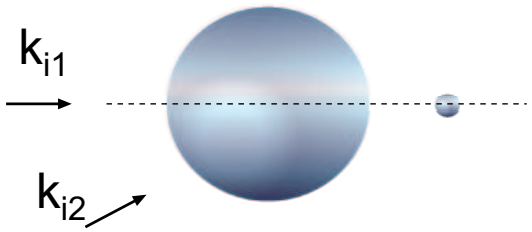

Figure 4.20: If a nano-particle is beside a micro-sphere, according to the incident wave vector direction, the nano-particle will be detectable (k_{i1}) or not (k_{i2}) (in backscattering).

interests of near field focusing by dielectric spheres. We have described some possible engineering applications of sub-wavelength focusing and of the possible high energy concentration.
This work is also interesting from the point of view of light scattering. Light scattering is observed in the far field, yet when multiple scattering occurs, the energy couplings take place in the near field. If we consider an aggregate of spherical particles close together, this study of the photonic jet lets us imagine what kind of intensity map (caustics) can appear inside the aggregate. Stationary states with energy maxima may appear inside the aggregate and may have influence on the light scattered in the far field.

In the next chapter, these electromagnetic couplings will be studied for a simple case of bi-sphere. The fields in the far field will be considered because the T-matrix algorithm does not allow us to calculate the fields inside the aggregate.

Chapter 5

Bi-spheres couplings

As explained in chapter 1, the comprehension of elementary physical phenomena when electromagnetic couplings between two particles occur, has a great interest when light scattering is used to find the statistical description of media containing a large amount of particles [101]. It is particularly true when the particles size can be compared with the wavelength and for new applications where the studied media can be made out of very dense non-spherical particles (powders for instance). In these cases, particles are close together. As explained in the previous chapter, if a single particle is able to concentrate energy in the near field area, we can image the importance of electromagnetic couplings between close particles. The methods based on the Lorenz-Mie theory (see section 3.2) and which consider that each particle only scatters the incident light, can not be used for several close particles. Each particle also scatters the light scattered by the others. In these materials, multiple and dependent scattering occur. New algorithms were developed to study multiple scattering, but also to take into account the shape of particles and the statistical behavior of the medium (see section 2.6). Unfortunately, because of the high complexity of interactions between particles, it is often difficult with these algorithms to identify the elementary physical phenomena.

By studying coupled spherical particles, we want to point out the elementary physical phenomena that are observed. A review of studies which deal with two or more particles behavior as a function of their properties can be found in **??**. In our case, calculations are computed with the T-matrix algorithm (see section 3.4). The scattering response is described by scattering diagram (that is the scattering phase function) and normalized backscattering cross section (NBSCS). Interferences are observed in the far field and the differences between single and multiple scattering are discussed. The main physical phenomena that have been observed are described (they have been presented in conference PIERS 2005 [14]).

5.1 Transition between single and multiple scattering

We will first study the transition between single and multiple scattering. The geometrical description and the coordinates are represented in figure 5.1. The incident wave is supposed to be a monochromatic plane wave of wavelength λ in free space and

with a wave vector orthogonal to the common axis of the two particles ($\theta_i = 90^o$ and $k_i = k_x$). Its polarization is linear: for a given k_i wave vector in the (O,x,z) plane, two linear polarizations are distinguished $E_i = E_y$ (Electric field along the y-axis) or $H_i = H_y$ (magnetic field along the y-axis). The other polarizations can be described as a composition of these two linear ones. The particles are identical spherical particles with a radius a such as $ka = 2$. Particles are small, their size can be compared with the wavelength but, they are not in the Rayleigh scattering regime. α is the angle of observation (the phase angle).

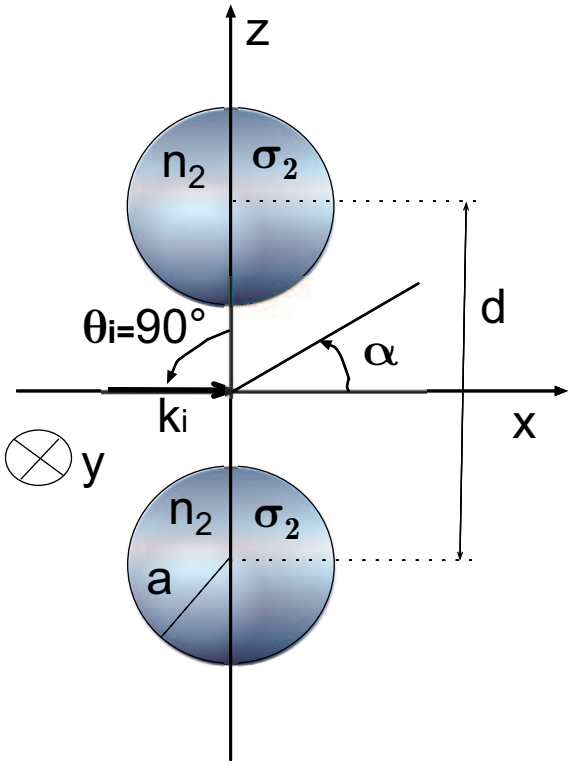

Figure 5.1: Geometrical description of the couple of particles considered.

In order to study the transition between single and multiple scattering, the normalized backscattering cross section (NBSCS) of the couple of spherical particles is computed as a function of the distance between their centers (figure 5.2 and 5.3). The backscattering cross section (BSCS) is defined as $\lim_{r\to\infty} 4\pi r^2 |\vec{E}_s|^2/|\vec{E}_i|^2$ with $\vec{E}_s$ the scattered field in the back direction ($\alpha = 180^o$) and with $\vec{r}$ the position vector. This cross-section is normalized (NBSCS) by dividing by the geometrical section of one sphere πa^2. By analogy the forward scattering cross section (FSCS) has the same definition but with $\vec{E}_s$ the scattered field in the forward direction ($\alpha = 0^o$). It can also be normalized to obtain NFSCS.

We can see in figure 5.2 for perfectly conductive spheres and in figure 5.3 for dielectric spheres, that when the distance d between the two particles is small, the NBSCS oscil-

number of spheres	kd	NBSCS	NFSCS	4πBSCS	4πFSCS
1	-	1	5.16	4	20.6
number of spheres	kd	NBSCS	NFSCS	πBSCS	πFSCS
2	45	4	20.59	4	20.55
2	10	5.2	17.86	5.2	17.84

Table 5.1: NBSCS and NFSCS for one and two spheres with $ka = 2$ and $\sigma_2 = \infty$. $\theta_i = 90^o$ ($k_i = k_x$) and $H_i = H_y$.

lates with a period $kd = 2\pi$. That is to say that the backscattering is maximum when the distance which separates the two particles is a fair number of λ.
It can also be noticed that when kd becomes larger, that is to say when particles are remote, the NBSCS reaches a constant value that is four times the NBSCS of one sphere (see table 5.1 for perfectly conductive spheres and table 5.2 for dielectric spheres).
The results also suggest that the polarization of incident field has no influence on the convergence value but changes the distances kd for which resonances occur. In fact, the asymptotical value of the NBSCS corresponds to constructive interferences of the two particles considered as two circular Young slits. This analogy, as we will see, can be extended to the scattering diagram, not only in single scattering but also when multiple scattering occurs.

The convergence value of backscattering for large kd corresponds to single scattering, whereas the oscillations are due to multiple scattering. We are in single or in multiple scattering according to the distance d between the particles.

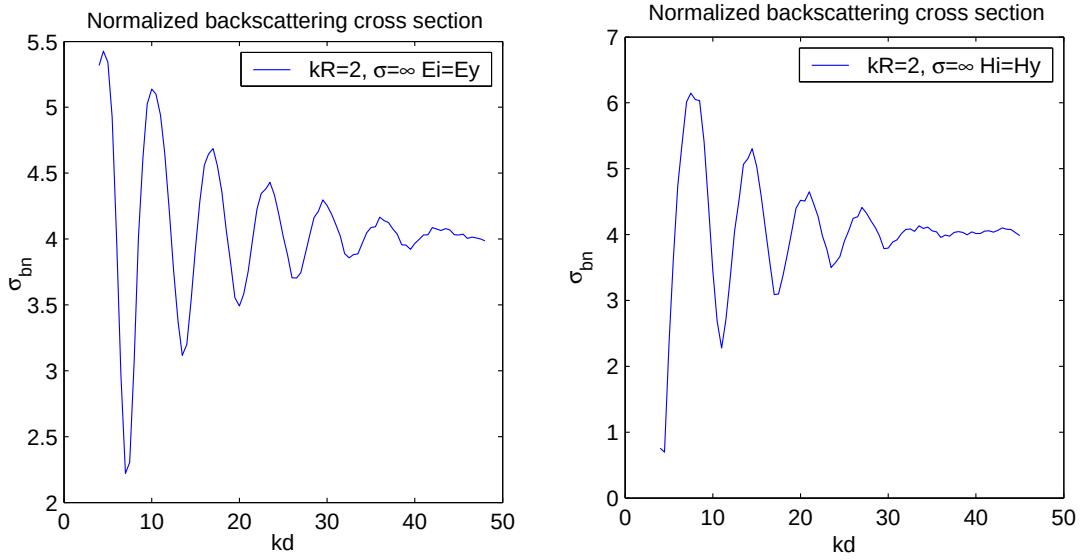

(a) $Ei = Ey$ (b) $Hi = Hy$

Figure 5.2: Normalized backscattering cross section of two spheres with $ka = 2$, $\sigma_2 = \infty$, $\theta_i = 90^o$ ($k_i = k_x$) and two incident linear polarizations.

number of spheres	kd	NBSCS	NFSCS	4πBSCS	4πFSCS
1	-	0.093	2.97	1.17	37.3
number of spheres	kd	NBSCS	NFSCS	πBSCS	πFSCS
2	45	0.372	11.88	1.17	37.3
2	10	0.34	11.7	1.07	36.7

Table 5.2: NBSCS and NFSCS for one and two spheres with $ka = 2$ and $n_2 = 1.5$. $\theta_i = 90^o$ ($k_i = k_x$) and $E_i = E_y$.

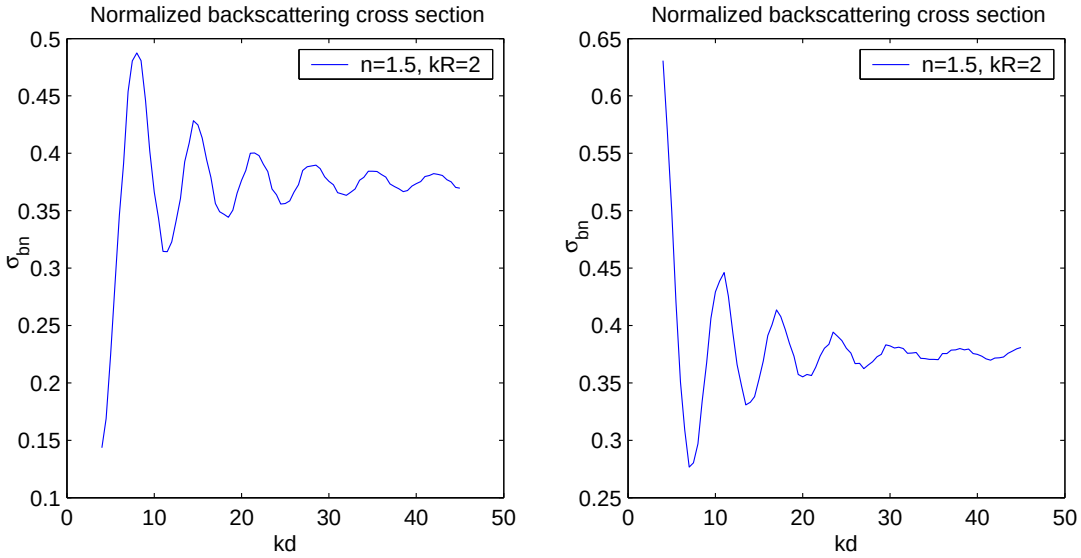

(a) $E_i = E_y$ (b) $H_i = H_y$

Figure 5.3: Normalized backscattering cross section of two spheres with $ka = 2$, $n_2 = 1.5$, $\theta_i = 90^o$ and two incident linear polarizations.

5.2 Circular Young slits for perfectly conducting spheres

We will first consider the case of perfectly conductive sphere ($\sigma_2 = \infty$). The Young slits configuration that we consider for comparison, is two circular holes in an opaque screen. The holes have the same radius a of the spheres and are separated by the same distance d as the distance between the two spheres centers, as illustrated in figure 5.4(b). The screen is supposed to be orthogonally illuminated by an incident plane wave and light is diffracted to the far field. The interferences pattern in the far field is given by formula (5.1). In this formula the first function corresponds to the diffraction by one hole (the Airy function) and the second to the interferences between the two holes [8]. I_0 is the incident field intensity:

$$I(\alpha) = 4I_0 \left(\frac{J_1(ka \sin \alpha)}{ka \sin \alpha} \right)^2 \cos^2\left(\frac{kd \sin \alpha}{2}\right) \tag{5.1}$$

For circular Young slits, the formula (5.1) shows that in the back direction ($\alpha = 180^o$), no phase-shift between the two holes has to be considered. The scattered field measures

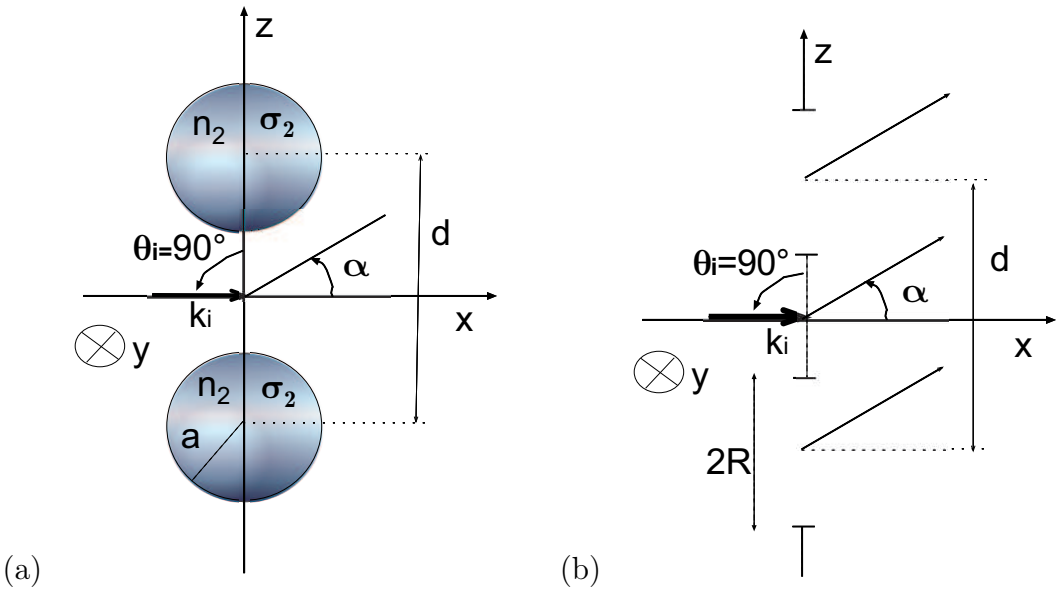

Figure 5.4: (a) Geometrical description of the couple of particles. (b) Equivalent circular Young slits

four times the amplitude of the incident field because of constructive interferences. This value does not depend of kd. This case corresponds to the curve NBSCS (figure 5.2(a)) when $kd > 45$. In this case the two particles can be considered as independent coherent sources. We are in a single scattering regime.

In order to extend this analogy to the other angles of observation α, the scattering diagram is simulated with the T-matrix algorithm, in this case ($kd = 45$) and is compared in figure 5.5 with the interferences pattern of circular Young slits in forward and backward directions for the two linear incident polarizations. The scattering diagram is defined as $f(\alpha) = \lim_{r\to\infty}(kr)^2|\vec{E_s}|^2/|\vec{E_i}|^2$ in the forward $-90^o < \alpha < 90^o$ and in the backward $90^o < \alpha < 270^o$ directions, for the two linear incident polarizations $E_i = E_y$ and $H_i = H_y$. In figure 5.5, the same period of interferences and a similar diffraction curve are observed. Differences are observed only for large phase angles α. The intensity maximum I_o in formula 5.1 is 4π times the scattering cross section of one sphere, because of the definitions of the used cross section and the scattering phase function, and because no coupling is assumed.

For $kd = 45$, it is still in single scattering. The same comparison can be made in a case where multiple scattering cannot be neglected ($kd < 45$). The result is presented in figure 5.6 for $kd = 10$. The periods of interferences and the diffraction curves are also similar in curves (a)(b) and (d), but the intensity maximum is no more dependent of the light scattering by one sphere (I_o). Thus, when multiple scattering occurs, the comparison with circular Young slits can still be used but with an intensity maximum that depends of kd. In figure 5.6, I_{max} is π times the scattering cross section of the two spheres (see figure 5.2). This π coefficient is only due to the difference of definition between the scattering phase function and the used cross section.

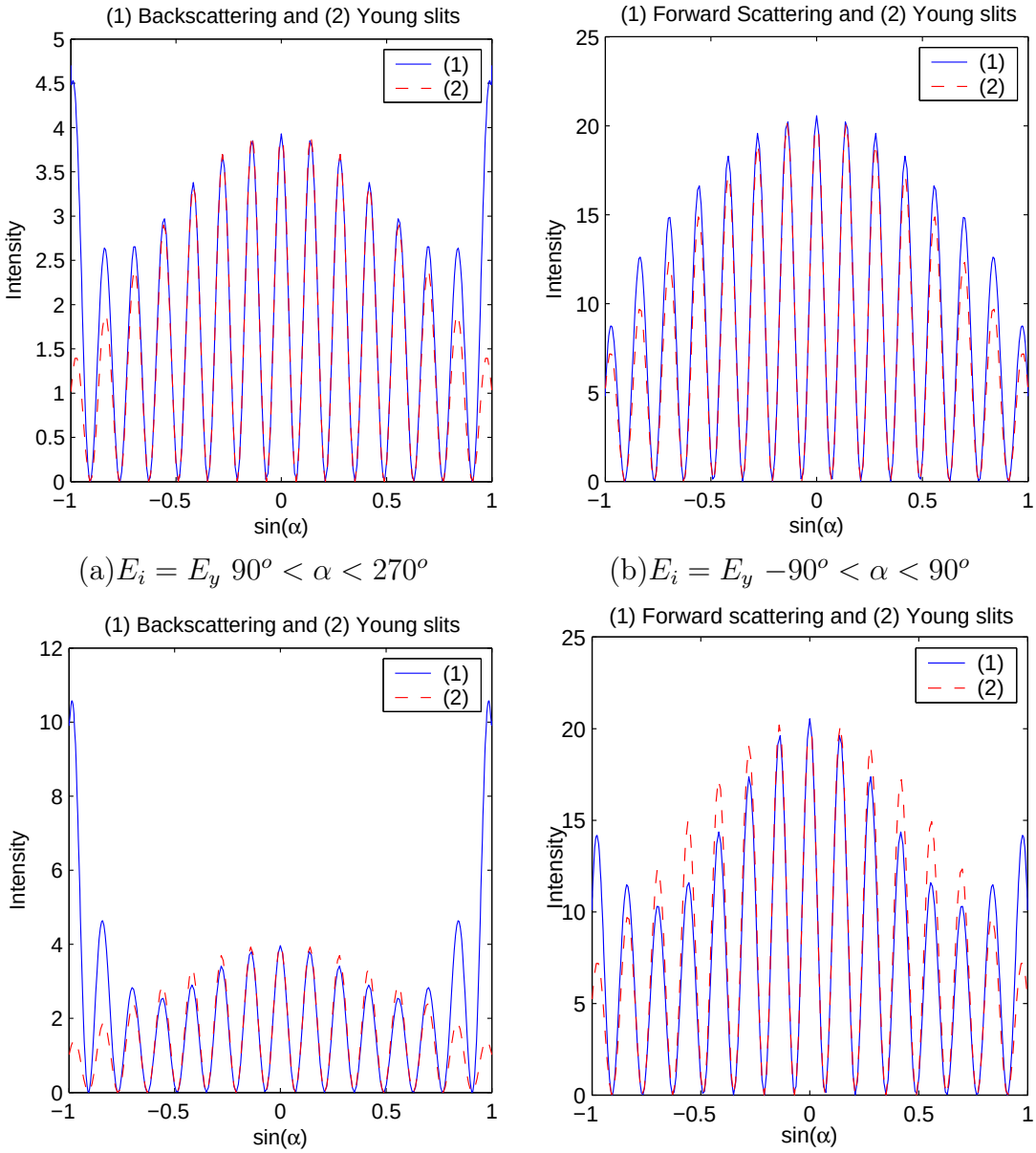

(a)$E_i = E_y$ $90^o < \alpha < 270^o$ (b)$E_i = E_y$ $-90^o < \alpha < 90^o$

(c)$H_i = H_y$ $90^o < \alpha < 270^o$ (d)$H_i = H_y$ $-90^o < \alpha < 90^o$

Figure 5.5: Comparison between circular Young ($-$ $-$) slits and single scattering ($-$). $ka = 2$, $\sigma_2 = \infty$, $\theta_i = 90^o$ ($k_i = k_x$), $kd = 45$, for the two linear incident polarizations.

As seen in figure 5.6 (c), the agreement observed between light scattering and circular Young slits interferences is not good. These cases are rarely observed and occur only in multiple scattering regimes. They correspond to the cases when the scattering global intensity maximum is not for $\alpha = 0$.

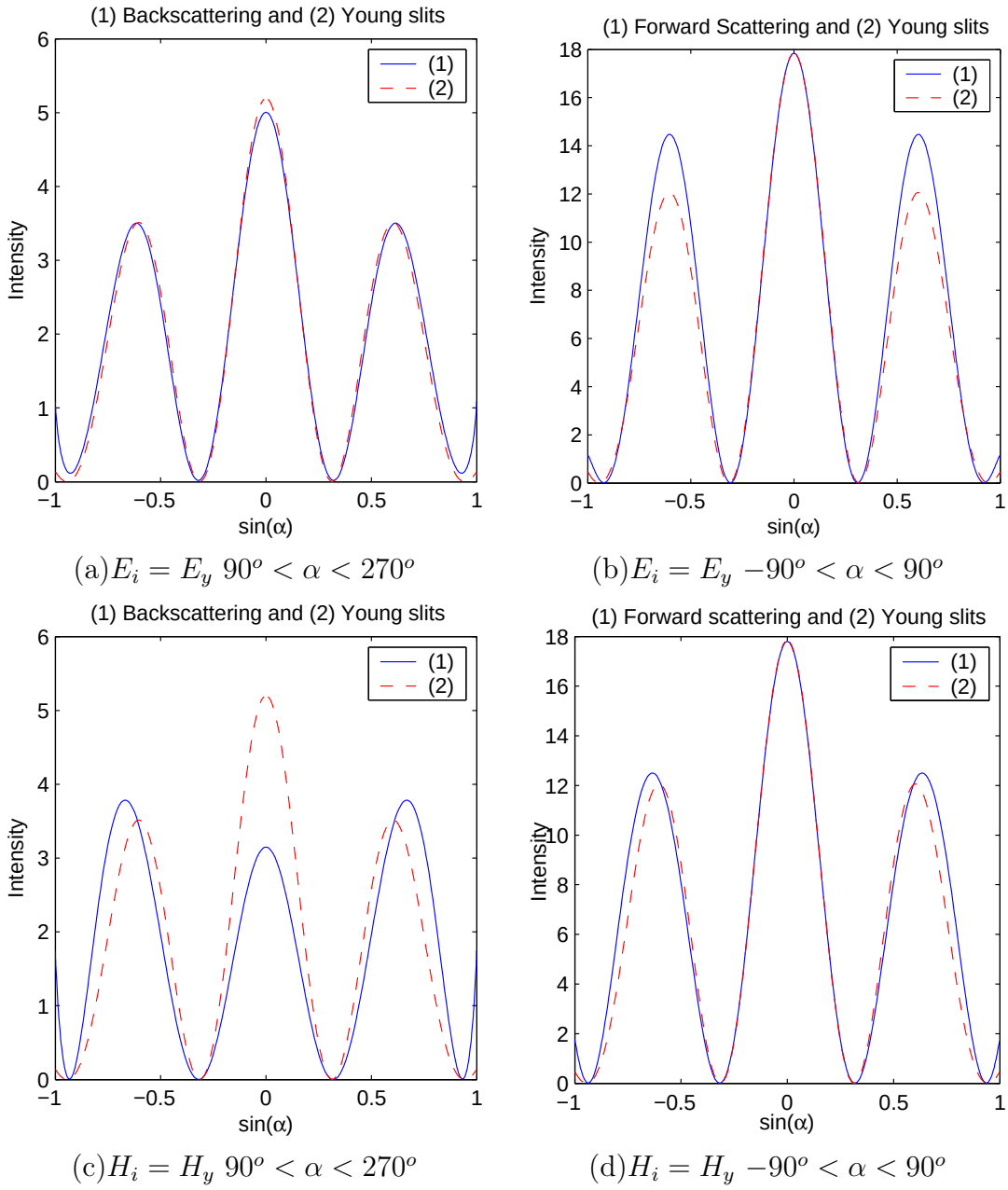

(a)$E_i = E_y$ $90^o < \alpha < 270^o$ (b)$E_i = E_y$ $-90^o < \alpha < 90^o$

(c)$H_i = H_y$ $90^o < \alpha < 270^o$ (d)$H_i = H_y$ $-90^o < \alpha < 90^o$

Figure 5.6: Comparison between circular Young slits and forward scattering. $ka = 2$, $kd = 10$, $\sigma_2 = \infty$, $\theta_i = 90^o$ ($k_i = k_x$), for the two incident polarizations.

5.3 Circular Young slits for dielectric spheres

We have also considered the case of dielectric spheres. The geometry of the couple of spheres and the comparison between circular Young slits is the same as represented in figure 5.4. However in this case, the refractive index of the spheres is $n_2 = 1.5$ and the conductivity is $\sigma_2 = 0$.

In figure 5.7(a), a good agreement is forward in the forward direction when $kd = 45$,

which is a single scattering regime. I_o in formula (5.1) is equal to 4πNFSCS as in backward direction. In figure 5.7(b), a similar good agreement is observed in the forward direction for $kd = 10$; but this case is considered as multiple scattering. As for perfectly conductive spheres, I_o depends of kd and is equal to π times the NFSCS of the couple of spheres (table 5.2). The results for a couple of dielectric spheres in the forward direction are similar to the ones of perfectly conductive spheres.

However, in the backward direction, the agreement is not good between light scat-

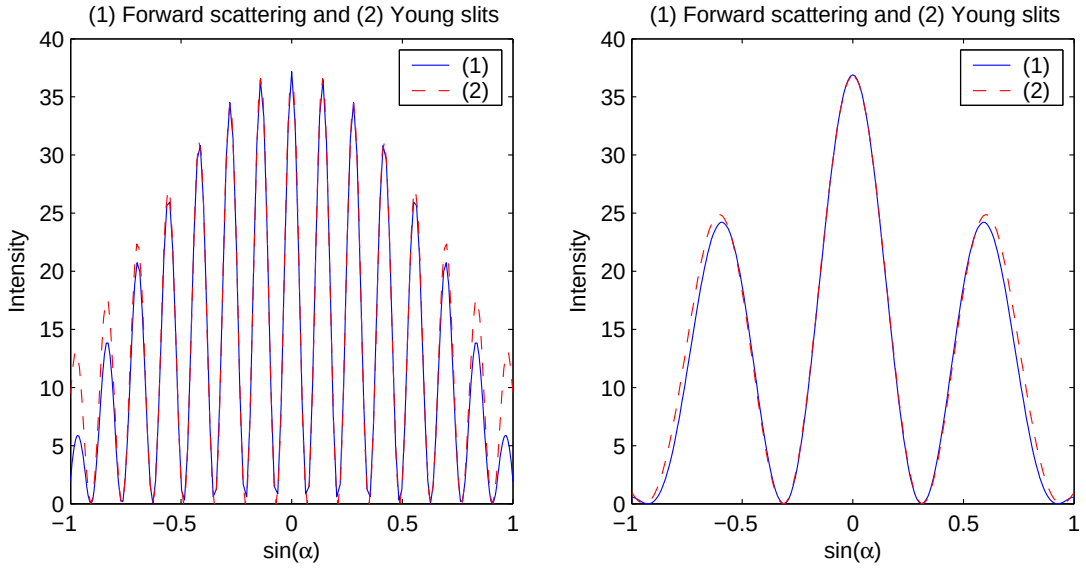

(a) $kd = 45$ (single scattering) (b) $kd = 10$ (multiple scattering)

Figure 5.7: Comparison between circular Young slits and forward scattering. $ka = 2$, $kd = 10$ or $kd = 45$, $n_2 = 1.5$, $\theta_i = 90^o$ ($k_i = k_x$) and $E_i = E_y$.

tering by the couple of dielectric spheres and the equivalent circular Young slits in multiple scattering ($kd = 10$) or also in single scattering ($kd = 45$) (see figure 5.8). In this figure, we also observe the disagreement due to the diffraction function (the Airy function). That is the reason why, a coefficient β has been included in the function describing the intensity interferences of circular Young slits (see formula 5.2).

$$I(\alpha) = 4I_0 \left(\frac{J_1(k\beta a \sin\alpha)}{k\beta a \sin\alpha} \right)^2 \cos^2\left(\frac{kd \sin\alpha}{2}\right) \tag{5.2}$$

Different β coefficient should be used to have a good agreement in single scattering ($kd = 45$); $\beta = 1.6$ yielded acceptable results for this case. Then, additional comparisons were made with circular Young slits in multiple scattering ($kd = 10$) with the same β coefficient. A good agreement is observed in figure 5.9, where I_o is π times the NBSCS of the two spheres.
For a couple of dielectric spheres, in the backward direction, the equivalent circular Young slits must have a larger radius than the one of the spheres. However, as for the other cases, the transition between single and multiple scattering only changes the

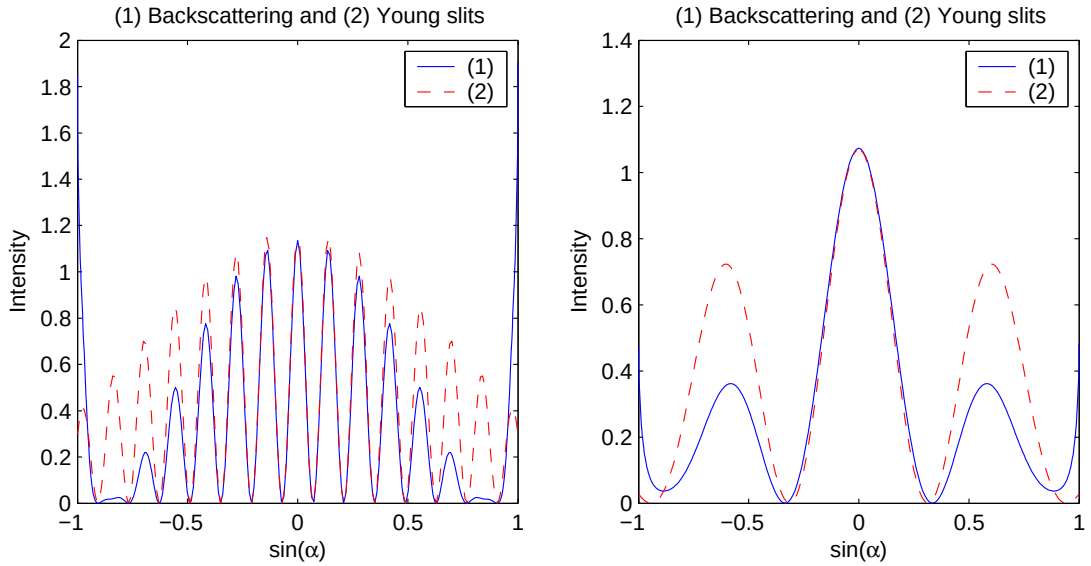

(a) $kd = 45$ (single scattering) (b) $kd = 10$ (multiple scattering)

Figure 5.8: Comparison between circular Young slits and backscattering. $ka = 2$, $kd = 45$ or $kd = 10$, $n_2 = 1.5$, $\theta_i = 90^o$ ($k_i = k_x$) and $E_i = E_y$.

intensity maximum I_0, that is the ratio of the incident flux that is scattered.

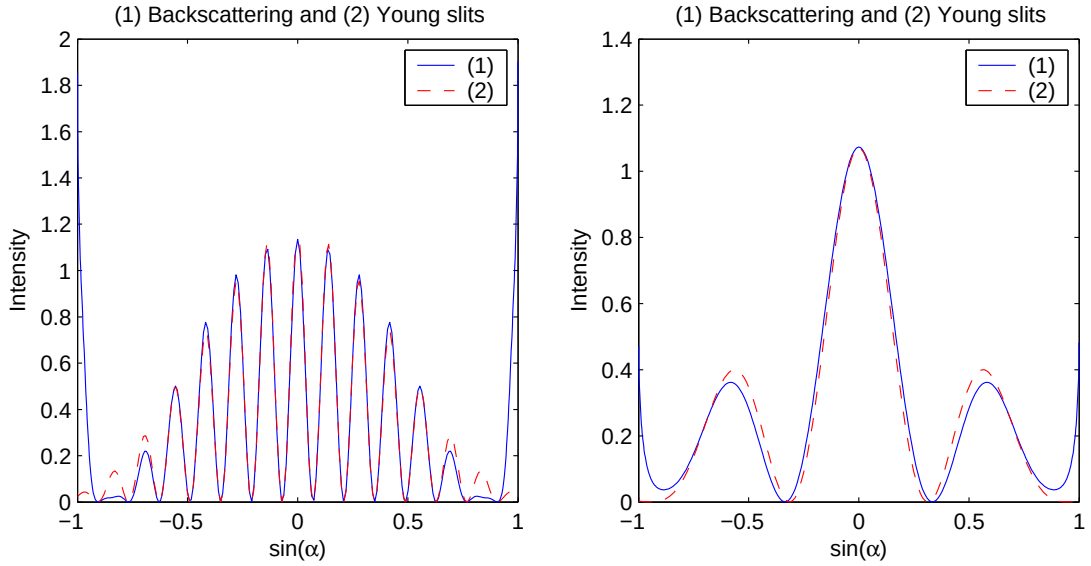

(a) $kd = 45$ (single scattering) (b) $kd = 10$ (multiple scattering)

Figure 5.9: Comparison between circular Young slits and backscattering. $ka = 2$, $kd = 45$ or $kd = 10$, $n_2 = 1.5$, $\theta_i = 90^o$ ($k_i = k_x$) and $E_i = E_y$.

5.4 Perot-Fabry and shadow effect

We have studied the couple of particles with another orientation of the wave vector k_i. In this section, k_i is in the axis of the two spheres (see in figure 5.10). The incident wave is linearly polarized. Because of the cylindrical symmetry, a change in the direction of the polarization of the incident field only rotates the result.

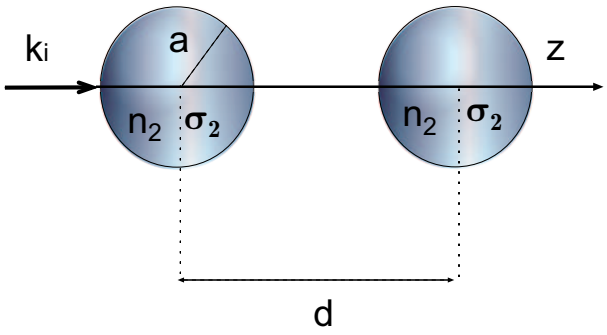

Figure 5.10: Geometrical description of the couple of spheres. The incident wave vector is parallel to the axis of the two spheres.

Figure 5.11 represents the backscattering cross section of such a couple of particles when these particles are perfectly conductive. We observe that when the distance between particles d is large, the curves become sinusoidal with a constant amplitude and a period $\lambda/2$ of d. On the other hand, if the distance between particles d is small, the amplitude of the sinusoidal curves change, thus the amplitude decreases when particles are closer.

When kd is large, we are in single scattering. The backscattering is the interferences of light scattered by each particle. Each particle scatters the incident light independently of the other sphere. The phase-shift between the light scattered by each particle is $2\pi \times 2d/\lambda$.
The decrease of the sinusoidal amplitude in multiple scattering (kd small) can be interpreted as a shadow effect. The second sphere may scatter less light because of its position (see figure 3.2 in section 3.2).

The same simulations have been carried out with two dielectric spheres. The geometry is the same as in figure 5.10. There is no conductivity $\sigma_2 = 0$, the refractive index is $n_2 = 1.5$, the radius is a such as $ka = 2$. The backscattering cross section as a function of the distance d between the particles is represented in figure 5.12.

For large kd the same sinusoidal curve with period $\lambda/2$ of d is observed. This is single scattering regime and the explanation is the same as for the case of conductive spheres. In multiple scattering, when kd is small, no shadow effect are observed, probably because light goes through the first particle and is not "stopped." Inversely

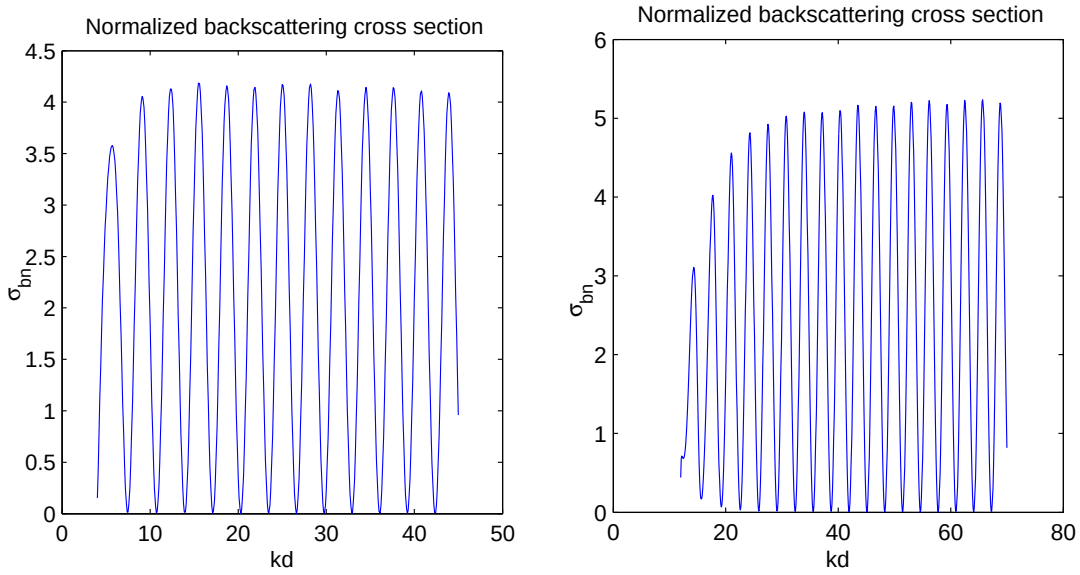

(a) $ka = 2$ (b) $ka = 6$

Figure 5.11: Backscattering cross section as a function of kd. $ka = 2$ or $ka = 6$, $\sigma_2 = \infty$, $\theta_i = 0^o$ $(k_i = k_z)$.

to a shadow effect the sinusoidal amplitude increases: The couple of spheres seems to behave as a Perot-Fabry interferometer. We would like to explain this analogy. In a Perot-Fabry interferometer, light is reflected by two mirrors which are the limits of a cavity. High transmissions are observed when the cavity size is equal to a fair number of half-wavelengths. In the system of two dielectric particles aligned in the propagation direction, each sphere is like a partial reflector. When the particles are close, a cavity seems to be created. At the resonances of this cavity, a maximum of transmission in the backward direction (but also in the forward direction) increases the initial interference.

What we have observed, is that when the incident wave vector is parallel to the axis of a couple of spherical particles, single and multiple scattering must be distinguished. In single scattering, the backscattering is the interferences of the light scattered independently by each particle. This is the same for dielectric or perfectly conductive spheres. However in multiple scattering, the electromagnetic couplings are not the same for dielectric or perfectly conductive spheres. For perfectly conductive spheres, a shadow effect is observed and makes the backscattering intensity decreases, whereas for dielectric spheres a Perot-Fabry effect is observed and makes the backscattering intensity increase.

5.5 Summary

We have used the normalized backscattering cross section to distinguish single and multiple scattering. The particles considered were perfectly conductive spheres and dielectric spheres and their radii were comparable with the wavelength.

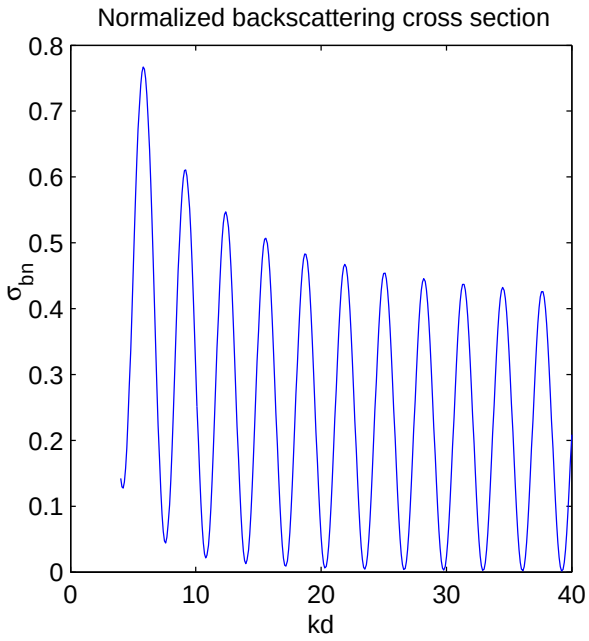

Figure 5.12: Backscattering cross section as a function of kd. $ka = 2$, $n_2 = 1.5$, $\theta_i = 0^o$ ($k_i = k_z$).

We have first studied the case when the incident wave vector was orthogonal to the spheres. In this case, we have shown that when only single scattering occurs, the scattering diagram in forward and backward directions of a couple of spherical particles can be compared with the interferences pattern of two circular holes in a screen. In this case, the radius of the holes are the same than the one of the spheres if the spheres are perfectly conductive and the distance between the centers of the holes is the same as the one between the centers of the spheres. For dielectric spheres the equivalent radius can be larger. When the spheres are closer, multiple scattering occurs and the comparison with circular Young slits can also be used but with an intensity maximum that depends on the distance between the two holes. In these cases, multiple scattering only changes the energy couplings. That is to say the ratio of the incident flux that is scattered.

We have also studied the backscattering of a couple of spheres when the incident wave vector is parallel to the axis of the spheres. In single scattering, light scattered by each sphere of the couple of dielectric and perfectly conductive spheres interfere. The phase-shift in backward direction depends on the distance between their centers. However in multiple scattering, a shadow effect makes the interferences amplitude decrease for perfectly conductive spheres, whereas for dielectric spheres a Perot-Fabry effect makes the interferences amplitude increase.

These comparisons with circular Young slits and Perot-Fabry have been used to analyze the coupling of light by a couple of particles in single but also in multiple scattering.

This makes it possible to explain physically the interactions between light and such a couple of particles, that is for example to distinguish interferences pattern, diffraction effects and multiple scattering phenomena.

For an incident wave vector orthogonal to the couple of spheres, in multiple scattering, when electromagnetic couplings occur between the two perfectly conductive spheres, the physical phenomena are similar to the ones described by Ebbesen [102]. In Ebbesen experiment, the intensity that goes through N close circular holes in a metallic film can be larger than N times the transmitted intensity of one hole. In our case, the scattering intensity of two close spheres can be larger than two times the intensity scattered by one sphere. In the two cases, this non-linearity is due to electromagnetic couplings, electromagnetic couplings between the particles in our case and electromagnetic couplings between holes in the Ebbesen experiment. For the perfectly conductive spheres, the coupled waves are the plasmons which are on the surface of each sphere.

Finally, the importance of couplings between close particles, that was suggested in the previous chapter has been confirmed. Moreover physical interpretations of these couplings have been proposed.

Chapter 6

Conclusions and perspectives

The objective of this dissertation has been to study theoretically the interactions between visible light and micrometer-sized particles, that is to consider diameter that can be compared with the wavelength. In particular the near field phenomena, that is intensity distribution around dielectric particles and electromagnetic couplings between close particles, have been pointed. In this chapter, the main contributions of this work are summarized and possible improvements and recommendations for future research are outlined.

6.1 The main contributions

First, basic knowledge on light scattering were summarized; the Rayleigh scattering and the Lorenz-Mie theory were explained. These two models correspond to single scattering by spherical particles. Their known properties have been simulated. These scattering cases have allowed us to define the main physical properties and concepts used later on.

The next step was to describe the T-matrix algorithm that is considered an extension of the Lorenz-Mie theory. This integral method makes the simulation of several non-spherical particles possible. We have used this algorithm to simulate small aggregates of two spherical particles. This algorithm has also allowed us to study multiple scattering, that is, the electromagnetic couplings between close particles.

Our first main result is the rigorous demonstration of the possibility to reach the diffraction limit and to highly concentrate energy in the near field of a dielectric spherical particles. This demonstration has been carried out by applying the Lorenz-Mie theory in the near field. The focused beam is called a photonic jet. This innovative model has been inspired by a paper describing the FDTD simulations of Chen and Taflove on cylindrical particles [22]. These new possibilities of focusing are valid for large spheres (geometrical domain) and also for very small spheres when they are not in the Rayleigh regime. If k is the wave vector and a the sphere radius, ka must be larger than unity. The basic properties of this photonic jet has been studied and recently published in Optics Letters [15]. The interaction of light with a single sphere, when

the sphere has a radius size that can be compared with the wavelength, was considered as well known. That was true in the far field (light scattering), but not in the near field.

This better understanding of light interactions with one dielectric spherical particle in the near field can have several applications that have been described. The photonic jet can be used to detect nano-particles with visible light, to carry out more accurate laser processing, to improve optical data storage capacities, and so on. The second interest of this result is to ask us questions about multiple scattering: what is the intensity map in the near field around an aggregate of particles? What is the intensity map inside an aggregate? What is the influence of this near field intensity on light scattering? For example, a photonic jet inside an aggregate could cause radiation pressure or non-linear effects. The T-matrix does not allow us to compute the field inside the aggregate nor in the near field, that is the reason why the far-field effects of the electromagnetic coupling between close particles is reported.

Our second main result was the physical description of electromagnetic couplings between two particles [14]. The comparison between light scattering intensity by two particles with the interferences pattern of equivalent circular Young slits has allowed us to describe light scattering intensity as interferences, diffraction and energy couplings. The particle shape induces a diffraction effect. In dependent scattering, the distance between particles induces phase-shifts and interference effects. When the particles are far enough from the others, there is single scattering. The total scattered power is the sum of the power scattered by each particle. When particles are close together, multiple scattering occurs. If the spherical particles are orthogonal to the incident wave vector, similar diffraction and interference effects may occur but the interactions between particles will mainly change the total power that will be scattered. If the spherical particles are parallel to the axis of the incident wave vector, a shadow effect occurs for perfectly conductive spheres and makes the interferences intensity decrease, whereas for dielectric spheres a Perot-Fabry effect makes it increase. In these analogies, we considered only the intensity distribution in the far field. The generalization of this analogy for more particles and for other properties as polarization will be carried out in future studies.

6.2 Perspectives

Other studies and several improvements after this work could be done in the future and are described in this section.

Photonic jet
Several investigations could be carried out to understand the photonic jet:

- it would be interesting to measure with a probe by using near field microscopy the presence of the photonic jet forward a dielectric sphere,

- the possibility to carry out a near field optical system with several micro-particles

could be studied,

- the various applications of the photonic jet could be developed (we have already started to study the possibility of non linear-effects enhancement),

- the influence of the dielectric sphere absorption on the photonic jet could be interesting to explore,

- the electromagnetic couplings between one sphere and what is around could be done (subtract, nano-particles, etc.). These couplings will play an important role for possible applications (data storage for example),

- the consequence of roughness on the sphere surface may be studied.

Electromagnetic coupling
To have a better understanding of electromagnetic couplings, our work can be extended:

- the comparison between light scattering intensity and circular Young slits can be extended to linear aggregates, random aggregates and more general particles (dielectric with absorption),

- the comparison can be made by considering polarization properties and not only scattering intensity,

If the extension of this analogy can be carried for complex aggregates, it would be useful to have physical interpretations of multiple scattering phenomena. However probably that cannot be used as a simplified model. The electromagnetic couplings are complex and need rigorous electromagnetic algorithms. The interest of this analogy is mainly to give a physical sense to observations and simulations.

Multiple scattering
In order to have a better understanding of multiple scattering and to be able to predict light scattered by large complex aggregates, some improvements have to be done:

- in experimental measurements, a better knowledge of the samples may be interesting (optical properties, shapes, size distribution of studied particles). For example, image processing could be interesting to reconstruct 3-dimensional particles by using several angles of view of microscopic observations,

- the negative polarization in backscattering is still not well understood (see section 2.4),

- computations of intensity profiles inside the aggregates could probably be used to understand some multiple scattering effects. For example, the possibility of local energy concentration may cause non-linear effects,

- an other interest could be in the transition between regular (periodic) aggregate of particles to random aggregate, to study the influence of defects in photonic crystals,

- the identification of proteins in solution by light scattering will be possible to study in the Photonics Systems Laboratory (LSP) with Novartis. The theoretical predictions could probably be done with the coded T-matrix algorithm [103].

We will investigate several of these developments in the future.

6.3 Modelling improvements for dense media of particles

In the previous section, discussions deal with interactions of light with particles or aggregates of particles. However, for rigorous simulations of the interactions of light with dense media of particles, new algorithms must be developed.

It would be useful to have a rigorous algorithm to simulate larger aggregates of particles. Current algorithms are not able to simulate aggregates whose parameter size x would be larger than 100. We have started thinking such an iterative algorithm to simulate larger aggregates. The medium can be divided into small regions where the T-matrix could be computed. We can assume that for a given region, interactions occur only with the regions just around. The iterative process can be used to take into account these interactions with the near regions. We will try to go on to develop such a method. Perhaps new field effects will be observed.

Another idea to improve the T-matrix algorithm would be to find a better basis of functions for the expansion of the electromagnetic fields. The spherical vectorial functions are adapted to the geometry of spherical particles. This choice makes the calculation of the T-matrix for one sphere easily possible. However the translation theorem for these functions is not so easy and is one of the causes of the size limitation. With an other basis of functions, perhaps the T-matrix calculation of one particle will be more complex, but the translation will be easier. In fact, for non-spherical particles the T-matrix calculation is already difficult with SVF and must often be numerically carried out.

However if a such rigorous algorithm was developed and was able to simulate very large aggregates or dense media of particles, we would still need a realistic description

of the medium, including positions, sizes and properties of all particles. Such a description can only be made as statistics. That is the reason why, perhaps, *new statistical solutions* of Maxwell equations must be found.

Bibliography

[1] OSA. *The Collected Optics Papers of Lord Rayleigh.* Optical Society of America, 1994.

[2] S. Berthier. *Les couleurs physiques des insectes.* Springer, 2003.

[3] H.C.Van de Hulst. *Light scattering by small particles.* Dover publications, 1981.

[4] V. Haudebourg. *Propriété de diffusion lumineuse de particules en suspension : transition du régime de Mie à celui d'aggrégats. Utilisation de l'expérience CODAG/LSU.* PhD thesis, Paris VI University: Marie Curie, 2000.

[5] E. Hadamcik, J.B. Renard, A.C. Levasseur-Regourd, and J.C. Worms. Laboratory light scattering measurement on natural particles with the progra2 experiment: an overview. *Journal of Quant. Spect. and Radia. Transf.*, 79:679–693, 2003.

[6] J.C.Worms. Study of the optical and mechanical properties of regolith with the icaps facility. *Advance Space Results*, 31(12):2527–2535, 2003.

[7] Lord. Rayleigh. On the light from the sky, its polarization and colour. *Phil.Mag*, XLI:107–120, 1871. see next reference.

[8] Born and Wolf. *Principle of optics.* Pergamon Press, 1980.

[9] Beiträge zur optik trüber medien, speziell kolloidaler metallösungen. *Ann. d. Phys.*, 25(4):377–445, 1908. translation in the 2 next references.

[10] M.P.Menguc and R.K.Iyer. Modeling of radiative transfer using multiple spherical harmonics approximations. *Jour. of Quant. Spect. and Rad. Trans.*, 39(6):445–461, 1998.

[11] R.Viskanda and M.P.Menguc. Radiative heat transfer in combustion systems. *Progress in energy and combustion sciences*, 13:97–160, 1987.

[12] A.J.Fowler and M.P.Menguc. Propagation of focused and multibeam laser energy in biological tissue. *Trans. of the ASME, Jour. of Biomech. Eng.*, 122(5):534–540, 2000.

[13] M.I.Mishchenko, J.W.Hovenier, and L.D.Travis. *Light Scattering by Non-spherical Particles: Theory, Measurements, and Applications*. Academic Press, San Diego, 2000.

[14] S.Lecler, Y.Takakura, and P.Meyrueis. Electromagnetic coupling of light within a couple of particles in interaction, 2005.

[15] S.Lecler, Y.Takakura, and P.Meyrueis. Properties of a 3d photonic jet. *Optics Letters*, 30(19), 2005.

[16] A. Taflove. *The Finite-Difference Time Domain Method*. Artech House, 1995.

[17] E.M.Purcell and C.R.Pennypacker. Scattering and absorption by non-spherical dielectric grains. *Astrophysic Journal*, 186, 1973.

[18] J.A.Kong. *Electromagnetic wave theory*. EMW Publishing Cambridge, Massachusetts, USA, 2005.

[19] P.C.Waterman. Symmetry, unitary, and geometry in electromagnetic scattering. *Physical review D*, 3(4):825–839, 1971.

[20] B.Peterson and S.Ström. T-matrix for electromagnetic scattering from an arbitrary number of scatterers and representations of e(3). *Physical review D*, 8(10):3661–3678, 1973.

[21] Z.Ivezic and M.P.Menguc. An investigation of dependent/independent scattering regimes using a discrete dipole approximation. *International Journal of Heat and Mass Transfer*, 39(4):811–822, 1996.

[22] Z. Chen and A. Taflove. Photonic nanojet enhancement of backscattering of light by nanoparticles: a potential novel visible-light ultramicroscopy technique. *Optics Express*, 12(7):1214–1220, 2004.

[23] H.J. Munzer, M. Mosbacher, M. Bertsch, J. Zimmermann, P. Leiderer, and J. Boneberg. Local field enhancement effects for nanostructuring of surfaces. *Journal of microscopy*, 202(1):129–135, 2001.

[24] X. Li, Z. Chen, A. Taflove, and V. Backman. Optical analysis of nanoparticles via enhanced backscattering facilitated by 3-d photonic nanojets. *Optics Express*, 13(2):526–533, 2005.

[25] S.Lecler, Y.Takakura, and P.Meyrueis. Generation of a 3d photonic nanojet to enhance scattering of light by nanoparticles: interest for microscopy, 2005.

[26] C.F.Bohren and D.R.Huffman. *Absorption and Scattering of Light by Small Particles*. JohnWiley, New York, 1983.

[27] G. Mie. *Contributions to the optics of turbid media, particularly of colloidal metal solutions*. Royal Aircraft Establishment-Lit-Trans, Translation in 1976.

[28] G. Mie. *Contributions on the optics of turbid media, particularly.* Sandia Laboratories, Albuquerque, New Mexico SAND78-6018. National Translation Center, Chicago, ILL, Translation 79-21946, Translation in 1978.

[29] L.Lorenz. On the identity of the vibrations of light with electrical currents. *Philos. Mag.*, 34:287–301, 1867.

[30] M.Kerker. *The scattering of light and other electromagnetic radiation.* Academic Press, New York, 1969.

[31] M.A. Morgan and K.K. Mei. Finite-element computation of scattering by inhomogeneous penetrable bodies of revolution. *IEEE Trans. Antennas Propag.*, 27, 1979.

[32] P.P. Silvester and R.L. Ferrari. *Finite-element for electrical engineering.* Cambridge Univ. Pres, New York, 1996.

[33] S.K.Yee. Numerical solution of initial boundary value problems involving maxwell equations in isotropic media. *IEEE Trans. Antennas Propag.*, 14(5):302–307, 1966.

[34] P.Yang, K.N.Liou, M.I.Mishchenko, and B.C.Gao. Efficient finite difference time domain scheme for light scattering by dielectric particles: application to aerosols. *Applied Optics*, 39(21):3727–3737, 2000.

[35] K.Lumme and J.Rahola. Light scattering by porous dust particles in the discrete-dipole approximation. *Astrophysical Journal*, pages 653–667, April 1994.

[36] B.M.Nebecker, J.L.de la Pena, and E.D.Hirlemann. Comparison of the discrete dipole approximation and modified double interaction model methods to predict light scattering from small features on surface. *Journal of Quantitative Spectroscopy and Radiative Transfer*, 70:749–759, 2001.

[37] M.I.Mishchenko, L.D.Travis, and D.W.Mackowski. T-matrix computations of light scattering by nonspherical particles: a review. *J. Quant. Spectrosc. Radiat. Transfer*, 55(5):535–575, 1996.

[38] J. Maxwell. *A Treatise on Electricity and Magnetism.* Dover, 1 ed.1873, 1954.

[39] L.Zuppiroli, M.N.Bussac, and C.Grimm. *Traité des couleurs.* Presses polytechniques et universitaires romandes, 2001.

[40] M.A.Naboulsi, H.Sizun, and F.de-Fornel. Fog attenuation prediction for optical and infrared waves. *Optical Engineering*, 43(2):319–329, 2004.

[41] A.Compte. *Traité philosophique dŠastronomie populaire.* Librairie Arthème Fayard - Corpus des oeuvres de philosophie en langue française, 1985 (1844).

[42] B.Montcel, R.Chabrier, and P.Poulet. Detection of cortical activation with time-resolved diffuse optical methods. *Applied-Optics*, 44(10):1942–1947, 2005.

[43] P.R. Smith, O. Kusmartseva, and R. Naimimohases. Evidence for particle shape sensitivity in the correlation between polarization states of light scattering. *Optics Letters*, 26(16), 2001.

[44] J.Harthong. Alternative theory of diffraction by modulated media. *JOSA-A*, 8(1):3–10, 1991.

[45] B.Kress. *Optimisation du calcul et de la fabrication d'éléments optiques diffractifs en vue de leur intégration dans des micro-systèmes : une approche de CAO/CFAO.* PhD thesis, LSP-ULP-Strasbourg.

[46] B.Kress and P.Meyrueis. *An Introduction to Planar Diffractive Optics and Related Technology.* John Wiley & Sons, 2000.

[47] Y.Takakura. *Une méthode d'étude de la diffusion photonique par des surfaces rugueuses.* PhD thesis, LSP-ULP-Strasbourg.

[48] A.Bony. *Mesure de rugosité par microscope électronique et diffusion lumineuse.* PhD thesis, LSP-ULP-Strasbourg.

[49] E. Zubko, Y. Shkuratov, and M. Hast. Backscattering and negative polarization of agglomerate particles. *Optics Letters*, 28(17), 2003.

[50] C.M.R.Platt. Lidar observation of a mixed-phase altostratus cloud. *J. Appl. Meteorol.*, 16, 1977.

[51] R.Greenler. *Rainbows, halos and Glories.* Cambridge Univ. Press, 1990.

[52] P.G.Martin. *Cosmic Dust.* Oxford Univ. Press, 1978.

[53] M.I.Mishchenko. Light scattering by randomly oriented axially symmetric particules. *JOSA-A*, V.8:871–882, 1991. [Errata V.9 p.497,1992].

[54] H. Kimura. Light scattering properties of fractal aggregates: numerical calculations by a superposition technique and the discrete dipole approximation. *Journal of Quantitative Spectroscopy and Radiative Transfer*, 70:581–594, 2001.

[55] M. Schnaiter and G. Wurm. Experiments on light scattering and extinction by small, micrometer sized aggregates of sphere. *Applied Optics*, 41(6), 2002.

[56] Y.Kuga and A.Ishimaru. Retroreflectance from a dense distribution of spherical particles. *JOSA-A*, 1(8):831–835, 1984.

[57] S.Kaasalainen, J.Piironen, K.Muinonen, H.Karttunen, and J.Peltoniemi. Laboratory experiments on backscattering from regolith samples. *Appl. Opt.*, 41(21):4416–4420, 2002.

[58] B. Lyot. Polarization of the moon and of the planets mars and mercury. *Comptes rendus de lŠAcadémie des Sciences. Reprinted with commentary in A Source Book in Astronomy and Astrophysics, 1900-1975, Kenneth R. Lang & Owen Gingerich, eds. (Harvard Univ. Press, Cambridge, MA, 1979)*, 178:1796–98, 1924.

[59] Y.G.Shkuratov, N.V.Opanasenko, and M.A.Kreslavsky. Polarimetric and photometric properties of the moon: telescopic observations and laboratory simulations. 1. the negative polarization. *Icarus*, 95(2):283–299, 1992.

[60] B.Goidet-Devel, J.B.Renard, and A.C.Levasseur-Regourd. Polarization of asteroids. synthetic curves and characteristic parameters. *Planetary-and-Space-Science*, 43(6):779–786, 1995.

[61] M.G.Tomasko et al. The descent imager/spectral radiometer (disr) experiment on the huygens entry probe of titan. *Space-Science-Reviews*, 104(1-4):469–551, 2002.

[62] M.G.Tomasko et al. Properties of dust in the martian atmosphere from the imager on mars pathfinder. *Journal-of-Geophysical-Research*, 104(E4):8987–9007, 1999.

[63] Ch.Leinert and E.Pitz. Zodiacal light observed by helios throughout solar cycle no.21: stable dust and varying plasma. *Astronomy-and-Astrophysics*, 210(1-2):399–402, 1989.

[64] J.B.Renard, A.C.Levasseur-Regourd, and R.Dumont. Properties of interplanetary dust from infrared and optical observations. ii. brightness, polarization, temperature, albedo and their dependence on the elevation above the ecliptic. *Astronomy-and-Astrophysics*, 304(2):602–608, 1995.

[65] J.Blum and R.Schrapler. Structure and mechanical properties of high-porosity macroscopic agglomerates formed by random ballistic deposition. *Physical-Review-Letters*, 93(11), 2004.

[66] B.A.S.Gustafson and L.Kolokolova. A systematic study of light scattering by aggregate particles using the microwave analog technique: Angular an wavelength dependence of intensity an polarization. *J. Geophys. Res.*, 104:31711–31720, 1999.

[67] A.L.Aden and M.Kerker. Scattering of electromagnetic waves from two concentric spheres. *J. Appl. Phys.*, 22:1242–12463, 1951.

[68] J.R.Wait. Electromagnetic scattering from a radially inhomogeneous sphere. *Appl. Sci. Res. Sect. B*, 10:441–450, 1963.

[69] J.R.Wait. Scattering of a plane wave from a circular dielectric cylinder at oblique incidence. *Can. J. Phys.*, 33:189–195, 1955.

[70] C.S.Kim and C.Yeh. Scattering of an obliquely incident wave by a multilayered ellipsoidal lossy dielectric cylinder. *Radio Sci.*, 26:1165–1176, 1991.

[71] S.Asano and M.Sato. Light scattering by spheoridal particle. *Appl. Opt.*, 14:29–49, 1975.

[72] Gerrit Mur. Absorbing boundary condition for the finie-difference approximation of the time-domain electromagnetics-field equations. *IEEE Transaction on electromagnetic compatibility*, Vol.23:377–382, november 1981.

[73] J.P. Berenger. A perfectly matched layer for the absorption of electromagnetics waves. *Journal of computational physics*, Vol.114:185–200, 1994.

[74] T.A.Nieminen, H.Rubinsztein-Dunlop, and N.R.Heckenberg. Calculation of the T-matrix: general considerations and application of the point-matching method. *J. Quant. Spectrosc. Radiat. Transfer*, pages 1019–1029, September 2003.

[75] M.F.Iskander, H.Y.Chen, and J.E.Penner. Optical scattering and absorption by branched chains of aerosols. *Appl. Opt.*, 28:3083–3091, 1989.

[76] F.Borghese, P.Denti, and R.Saija. *Scattering from model nonspherical particles*. Springer, 2003.

[77] A.Moroz. Density-of-states calculations and multiple-scattering theory for photons. *Physical Review B Condensed-Matter*, 51(4):2068–2081, 1995.

[78] W.Kohn and N.Rostoker.

[79] J.Korringa. Solution of the schrodinger equation in periodic lattice with an application to metallic lithium. *Physica*, 13, 1947.

[80] J.M.Song, C.C.Lu, and W.C.Chew. MLFMA for electromagnetic scattering by large complex objects. *IEEE Trans. Antennas Propagat.*, 45(10):1488–1493, 1997.

[81] Z. Chen, A. Taflove, and V. Backman. Concept of equiphase sphere for light scattering by nonspherical dielectric particles. *Journal of Optics of America A*, 21(1), 2004.

[82] Y.G.Shkuratov and Y.S.Grynko. Light scattering by media composed of semitransparent particles of different shapes in ray optics approximation: consequences for spectroscopy, photometry, and polarimetry of planetary regoliths. *Icarus*, 173(1):16–28, 2005.

[83] J.Harthong. *Cours d'analyse mathématique*. http://moire.u-strasbg.fr, 2004.

[84] O.R.Cruzan. Translation addition theorem for spherical vector wave functions. *Quaterly of applied mathematics*, 20(1):33–40, 1962.

[85] H. Xu. Calculation of the near field of aggregates of arbitrary spheres. *Journal of Optics of America A*, 21(5), 2004.

[86] P.Debye. Der lichtdruck auf kugeln von beliebiegen material. *Ann. Phys.*, 30:57–136, 1909.

[87] D.Biscount, C.Brosseau, A.S.Martiney, and J.M.Schmitt. Depolarization of multiply scattered waves by spherical diffuser: influence of the size parameter. *Physical Review E*, 49(2), 1994.

[88] W.T. Welford. *Aberration of optical systems.* Adam Hilger Ltd, 1986.

[89] F. De Fornel. *Evanescent waves, from newtonian optics to atomic optics.* Springer, 2000.

[90] D.W. Pohl, W. Denk, and M. Lanz. *Applied Physic. Letters.*, 44, 1984.

[91] R.C. Reddick, R.J. Warmack, and T.L. Ferrell. *Physic Review B*, 39(1):767–70, 1989.

[92] E. Betzig and J.K. Trautman. *Science*, 257(189), 1992.

[93] S.M. Mansfield and G.S. Kino. *Applied Physic Letters*, 57(24):2615–16, 1990.

[94] B.B. Goldberg, S.B. Ippolito, L. Novotny, Zhiheng-Liu, and M.S. Unlu. *IEEE-Jour. of Select. Top. in Quant. Elec.*, 8(5):1051–9, 2002.

[95] P.C.Chaumet, A.Rahmani, F.de-Fornel, and J.P.Dufour. Evanescent light scattering: The validity of the dipole approximation. *Physical Review B: Condensed Matter*, 58(4):2310–2315, 1998.

[96] G.Videen, M.M.Aslan, and M.P.Menguc. Characterization of metallic nanoparticles via surface wave scattering: A. theoretical framework and formulation. *Jour. of Quant. Spect. and Rad. Trans.*, 93(1-3):195–206, 2005.

[97] M.M.Aslan, M.P.Menguc, and G.Videen. Characterization of metallic nanoparticles via surface wave scattering: B. physical concept and numerical experiments. *Jour. of Quant. Spect. and Rad. Trans.*, 93(1-3):207–217, 2005.

[98] Myung-Bok-Lee, M. Kourogi, K. Tsutsui, N. Atoda, and M. Ohtsu. *Applied optics*, 38(16), 1999.

[99] F.Zijp, M.B.van-der-Mark, J.I.Lee, and C.A.Verschuren et al. Near-field read-out of a 50-gb first-surface disc with na=1.9 and a proposal for a cover-layer-incident, dual-layer near-field system, 2004.

[100] E. Betzig, M. Kourogi, K. Tsutsui, N. Atoda, and M. Ohtsu. *Optics Letters*, 20(3), 1995.

[101] J.B.Renard, J.C.Worms, T.Lemaire, and al. Light scattering by dust particules in microgravity: polarization and brightness imaging with the new version of the progra2 instrument. *Applied Optics*, 41(4), 2002.

[102] T.W.Ebbesen, H.J.Lezec, H.F.Ghaemi, T.Thio, and P.A.Wolff. Extraordinary optical transmission through sub-wavelength hole arrays. *Nature (London)*, 391(6668):667–669, 1998.

[103] S.Lecler, Y.Takakura, and P.Meyrueis. A model to describe light scattering from material made of sensitized proteins, 2004.

[104] P.W.Zhai, Y.K.Lee G.W.Kattawar, and P.Yang. Implementating the near to far field transformation in the fdtd method. *Applied Optics*, 43(18), 2004.

[105] H.T. Miyazaki, H. Miyazaki, and K. Miyano. Anomalous scattering from dielectric bispheres in the specular direction. *Optics Letters*, 27(14), 2002.

[106] M. Abramovitz and I.A. Stegun. *Handbook of mathematical functions.*

[107] J.Reichardt, S.Reichardt, M.Hes, and T.J.McGee. Correlations among the optical properties of cirrus-cloud particles: microphysical interpretation. *Journal-of-Geophysical-Research*, 107(D21):AAC8–1–12, 2002.

[108] K.Muinonen, L.Lamberg, P.Fast, and K.Lumme. Ray optics regime for gaussian random spheres. *Journal-of-Quantitative-Spectroscopy-and-Radiative-Transfer*, 57(2):197–205, 1997.

[109] A.R.Edmonds. *Angular momentum in quantum mechanics.* Princeton Univ. Press, Princeton USA, 1957.

[110] E.U.Condon and G.H.Shortley. *The theory of atomic structure in spectra.* Cambridge university press, USA, 1935 (1991).

[111] MP.Menguc and R.K.Iyer. Modeling of radiative transfer using multiple spherical harmonics approximations. *Jour. of Quant. Spect. and Rad. Trans.*, 39(6):445–461, 1998.

Webography:

[Web1] *www.esf.org/jcw/progra2.htm* and *http://progra2.cnrs-orleans.fr* official web sites of PROGRA 2

[Web2] *http://www.scatlab.com/index.html* free code for Mie theory computing.

[Web3] *www.astro.ufl.edu/ elsnews/* newsletters and mailing-list about light scattering by particles.

[Web4] *http://www.t-matrix.de/* Electromagnetic scattering program by Thomas Wriedt: News about light scattering, links to several algorithm codes.

[Web5] *http://www.astro.princeton.edu/ draine/DDSCAT.6.0.html* DDA code of B.T.Braine and P.J.Flatau (Princeton University Observatory and California Space Institute) :The Discrete Dipole Approximation for Scattering and Absorption of Light by Irregular Particles :

[Web6] *http://www.giss.nasa.gov/ crmim/t_ matrix.html* T-matrix code of M.I.Mishchenko and D.W.Mackowski (Respectively NASA and Auburn University).

[Web7] *http://mathworld.wolfram.com/* to find mathematic formulae.

[Web8] *http://plasma-gate.weizmann.ac.il/369j.html* website where the 3-Symbol of Wigner can be computed.

Glossary

ABC: Absorbing Boundaries Conditions
BSCS: BackScattering Cross Section
CCA: Cluster-Cluster Aggregation
CPA: Cluster-Particle Aggregation
DDA: Discrete Dipole Approximation
EBCM: Extended Boundary Condition Method
FDTD: Finite Difference Time Domain
FSCS: Forward Scattering Cross Section
FEM: Finite Element Method
FWHM: Full Width Half Maximum
ISS: International Space Station
LDR: Lattice Dispersion Relation
LSP: Photonic System Laboratory
MoM: Method of Moment
NBSCS: Normalized BackScattering Cross Section
NFSCS: Normalized Forward Scattering Cross Section
PML: Perfectly Matched Layer
PPM: Point Matched Method
SVF: Spherical Vectorial Functions
SVM: Separation Variable Method

Notations

$\epsilon_o = 1/(36\pi 10^9)$ the permittivity in farad/meter

$\mu_o = 4\pi 10^{-7}$ the magnetic permeability in henry/meter

a radius of the smallest volume than contains the scatterer. The radius if the scatterer is a sphere.

λ incident wavelength.

$k = 2\pi/\lambda_o$ the wave vector in free space.

$x = ka$ is the size parameter.

c celerity of light in free space.

ω temporal pulsation.

n refractive index of the particle when this particle is in free space.

σ_2 conductivity of a medium.

(r, θ, φ) spherical coordinates, see figure 2.3(b).

α is the phase angle, that is the angle between the incident wave vector and the scattered one.

$H_i = H_y$ linear polarized incident wave whose magnetic field is along the y direction. $\vec{k}$ is in the (O, x, z) plan and is described by θ_i.

$E_i = E_y$ linear polarized incident wave whose electric field is along the y direction. $\vec{k}$ is in the (O, x, z) plan and is described by θ_i.

θ_i describes the direction of the incident wave vector in the plan (O, x, z), $\theta_i = (\vec{z}, O, \vec{k})$.

$C_{sca}, C_{ext}, C_{abs}$ are respectively the scattering, extinction and absorbtion cross sections.

$\vec{\psi}_n$ are the SVF (see appendix B).

$\Re e[A]$ is the real part of a matrix A.

$\Im m[A]$ is the imaginary part of a matrix A.

A^t is the transposed matrix of A but transposition without conjugation.

$\sigma_{nn'}$ and $R_{nn'}$ are the translation matrixes for SVF (see appendix C).

A^* is the conjugate value of the complex matrix A.

a^i, a^s, a^w are the expansion coefficient on SVF of respectively the incident field, the scattered field and the field inside the particle.

i in mathematical formulae is the complex number such as $i^2 = -1$, but i in exponent indicates that the value is linked to the incident wave. No confusion is possible.

Appendix A

Electromagnetism

This appendix deals with electromagnetism story, Maxwell equations and special tools for electromagnetism studies.

A.1 The birth of electromagnetism

The main steps for understanding what is light and the birth of electromagnetism are summarized. A lot of other dates and physicists' names could have been added. It is only a fast overview of a very long and complex evolution on which a great number of scientists have worked.

XVIIth: is light particle or a wave?
1621 Refractive law and reflexion (Snell) (1637 Descartes).
1675 Light described by rays. Particle theory of light (Newton).
1690 Light described as wave (Huygens).

XVIIIth: charges and magnets
1752 Demonstration with a kite that storm light is made of "electrical fire" (Benjamin Franklin).
1785 Electrostatic law (Cavendish and Coulomb).
Measure of the electrostatic strength with a distortion balance (figure A.1). Two charged metallic spheres are used, one is static, the other is on a torsion fiber. The torsion of the fiber gives the strength.
1791 Magnetostatic law: same experiment with magnet (Coulomb).
1797 Diffraction by a hole (Young and after Fresnel).
1800 First electrical battery (Volta).
Stack of copper and zinc discs separated by cloth impregnated of diluted sulfuric acid.

XIXth: Birth of electromagnetism
1820 Magnetic phenomenon due to an electrical current (Hans Christian Oersted).
Observation of a compass change of orientation a when a current goes through a wire at proximity.
1820 Jean-Baptiste Biot and Félix Savart found the law describing the strength applied

on a charge by a magnetic field.
1820 A strength appears on a conductive circuit in a magnetic field when a current goes through this circuit. Concept of current and voltage (Ampere).
1826 The Ohm law. Concept of resistivity (Ohm).
1831 Induction (Faraday).
A magnetic field is able to produce an electric current. He demonstrated this principle of induction in 1831. Faraday expressed the electric current induced in the wire in terms of the number of lines of strength that are cut by this wire.
1835 Self-induction (Faraday and Henry).
An intense magnetic field can rotate the plane of polarized light in a medium.
1845 Law for current and voltage at a electrical node of a circuit (Kirchhoff).
1846 Diamagnetism (Faraday).
1850 Foucault currents.
1873 Treatise on Electricity and Magnetism of James Clerk Maxwell.

XXth: quantum optic, holography, photonic techniques.

The most important experiment is probably the one of Oersted in 1820, because it is the first that shows the link between the electric field and the magnetic field.

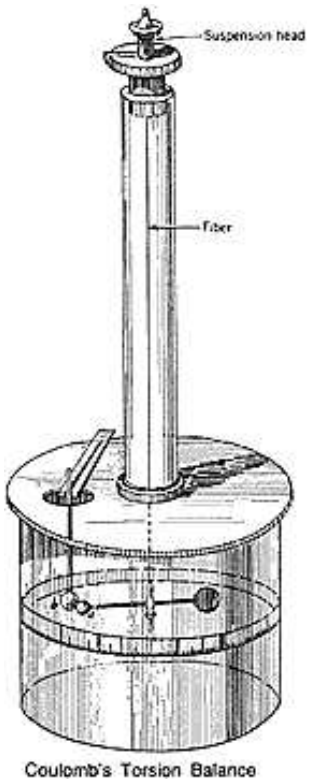

Figure A.1: Distortion balance of Coulomb. The forces between charged spheres create a proportional distortion in the fiber.

A.2 Maxwell equations

In numerical computing, real numbers have to be truncated and this truncation can create numerical error. That can cause false results when an operation is made between two numbers which are very different, a big number and a small number for example. This problem can occur when Maxwell equations are computed.

Maxwell equations in usual notation (International System notations):

$$\begin{cases} \text{curl}\vec{H} = -i\omega\epsilon\vec{E} \\ \text{curl}\vec{E} = i\omega\mu_o\vec{H} \end{cases} \tag{A.1}$$

In this case the absolute values of E and H differ in a proportion of 10^3. Other better convention can be used.

Notation adapted to numeral computing. In this case the absolute values of E and H are comparable:

$$\begin{cases} \text{curl}\vec{H} = -kn^2\vec{E}' \\ \text{curl}\vec{E}' = k\vec{H} \end{cases} \tag{A.2}$$

with

$$\begin{cases} k = i\omega/c \\ \vec{E}' = c\epsilon_o\vec{E} = 1/(c\mu_o)\vec{E} \end{cases}$$

A.3 The Green function

The Green function is used to find the solutions of the propagation equation by using the integral methods (see section 3.3). This section explains how is found the Green function for the scalar propagation equation.

The Green function g verifies:

$$\Delta g(r') + k^2 g(r') = -\delta(r') \tag{A.3}$$

where $\delta(r')$ is the three-dimensional Dirac function ($\delta = 1$ if $r' = 0$ else $\delta = 0$).

We can verify that for $\vec{r'} \neq 0$ a solution is:

$$g_{\vec{r'},k}(\vec{r}) = C\frac{\exp(ik|\vec{r'}|)}{|\vec{r'}|} \tag{A.4}$$

C is a constant. The Green function is not defined in $\vec{r'} = 0$, but to find C we can integrate the equation A.3 over the small sphere around $r' = 0$ when the radius δ of this sphere tends to zero [18].
We have:

$$\iiint_V -\delta(r')dV' = -1 \tag{A.5}$$

$$\begin{aligned}\iiint_V k^2 g(r')dV' &= 4\pi k^2 \int_0^\delta r'^2 g(r')dr' \\ &= C4\pi k^2 \int_0^\delta r' e^{ikr'} dr' \end{aligned} \tag{A.6}$$

which vanishes when δ tends to zero because the integral result will be proportional to δ^2. And we have, by applying the Gauss theorem [18]:

$$\begin{aligned}\iiint_V \Delta g(r')dV' &= \iint_{r=\delta} \frac{\partial}{\partial r} g(r')dS' \\ &= -C4\pi \end{aligned} \tag{A.7}$$

Therefore, in order to verify equation A.3, C must be equal to $1/(4\pi)$.

Notations
The definition of the Green function is not the same in all references:
in the Born & Wolf, $g = \frac{e^{ik|\vec{r}-\vec{r'}|}}{|\vec{r}-\vec{r'}|}$
in the Kong and in this thesis, $g = \frac{e^{ik|\vec{r}-\vec{r'}|}}{4\pi|\vec{r}-\vec{r'}|}$
In the paper of Peterson and Strom [20], $G = \frac{e^{ik|\vec{r}-\vec{r'}|}}{4\pi k|\vec{r}-\vec{r'}|}$

Appendix B

Spherical vectorial functions

The spherical vectorial functions (SVF), written Ψ_n, are the solution of the vectorial Helmholtz equation in spherical coordinates. These functions are described in section 3.2, they contain Bessel functions and Legendre polynoms. The origin of SVF and some properties of spherical harmonic functions are presented in this appendix. Formulae can be found in [106] or in [Web7].

B.1 Electro-Magnetic waves in Spherical coordinates

Change of coordinates:
We will first write some mathematical operators and the scalar Helmholtz equation in the spherical coordinates.

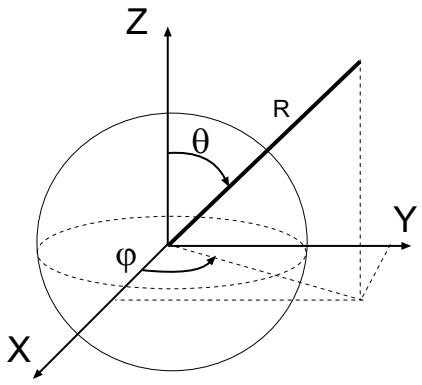

Figure B.1: Change of coordinates.

$$\left| \begin{array}{l} x = r\cos\varphi\cos\theta \\ y = r\cos\varphi\sin\theta \\ z = r\sin\varphi \end{array} \right.$$

If these equations are differentiated and rewritten with matrix, we obtain :

$$\begin{vmatrix} dx \\ dy \\ dz \end{vmatrix} = \begin{bmatrix} \cos\varphi\cos\theta & -r\cos\varphi\sin\theta & -r\sin\varphi\cos\theta \\ \cos\varphi\sin\theta & r\cos\varphi\cos\theta & -r\sin\varphi\sin\theta \\ \sin\varphi & 0 & r\cos\varphi \end{bmatrix} \begin{vmatrix} dr \\ d\theta \\ d\varphi \end{vmatrix}$$

If this matrix is called M, we have $M^{-1} = M^t$, where M^t is the transposition of matrix M.

To find the main mathematical operators in spherical coordinates, we start with their expression in cartesian coordinates, then we apply the formula below and replace $\partial r/\partial x$, $\partial\theta/\partial x$, $\partial\varphi/\partial x$, etc. by the above found expressions.

$$\begin{aligned} \frac{\partial f}{\partial x} &= \frac{\partial f}{\partial r}\frac{\partial r}{\partial x} + \frac{\partial f}{\partial \theta}\frac{\partial \theta}{\partial x} + \frac{\partial f}{\partial \varphi}\frac{\partial \varphi}{\partial x} \\ \frac{\partial f}{\partial y} &= \frac{\partial f}{\partial r}\frac{\partial r}{\partial y} + \frac{\partial f}{\partial \theta}\frac{\partial \theta}{\partial y} + \frac{\partial f}{\partial \varphi}\frac{\partial \varphi}{\partial y} \\ \frac{\partial f}{\partial z} &= \frac{\partial f}{\partial r}\frac{\partial r}{\partial z} + \frac{\partial f}{\partial \theta}\frac{\partial \theta}{\partial z} + \frac{\partial f}{\partial \varphi}\frac{\partial \varphi}{\partial z} \end{aligned}$$

Thus, we find these formulae :

Gradient:

$$\vec{\nabla}P = \begin{bmatrix} \frac{\partial P}{\partial r} \\ \frac{1}{r}\frac{\partial P}{\partial \theta} \\ \frac{1}{r\sin\theta}\frac{\partial P}{\partial \varphi} \end{bmatrix}$$

Divergence:

$$\vec{\nabla}.\vec{u} = \frac{1}{r^2}\frac{\partial}{\partial r}(r^2 u_r) + \frac{1}{r\sin\theta}\frac{\partial}{\partial \theta}(\sin\theta.u_\theta) + \frac{1}{r\sin\theta}\frac{\partial}{\partial \varphi}(u_\varphi)$$

Curl:

$$\vec{\nabla}\times\vec{u} = \begin{bmatrix} \left(\frac{1}{r\sin\theta}\frac{\partial}{\partial\theta}(\sin\theta.u_\varphi) - \frac{1}{r\sin\theta}\frac{\partial}{\partial\varphi}(u_\theta)\right) \\ \left(\frac{1}{r\sin\theta}\frac{\partial}{\partial\varphi}(u_r) - \frac{1}{r}\frac{\partial}{\partial r}(r.u_\varphi)\right) \\ \left(\frac{1}{r}\frac{\partial}{\partial r}(r.u_\theta) - \frac{1}{r}\frac{\partial}{\partial\theta}(u_r)\right) \end{bmatrix}$$

Laplacien:

$$\Delta P = \frac{1}{r^2}\frac{\partial}{\partial r}(r^2\frac{\partial P}{\partial r}) + \frac{1}{r^2}\left(\frac{1}{\sin\theta}\frac{\partial}{\partial\theta}(\sin\theta\frac{\partial P}{\partial\theta}) + \frac{1}{\sin^2\theta}\frac{\partial^2 P}{\partial\varphi^2}\right)$$

It is why, the Helmholtz in spherical coordinates is :

$$\boxed{\left[\frac{1}{r^2}\frac{\partial}{\partial r}(r^2\frac{\partial E}{\partial r}) + \frac{1}{r^2}\left(\frac{1}{\sin\theta}\frac{\partial}{\partial\theta}(\sin\theta\frac{\partial E}{\partial\theta}) + \frac{1}{\sin^2\theta}\frac{\partial^2 E}{\partial\varphi^2}\right)\right] + k^2n^2E = 0} \qquad \text{(B.1)}$$

if we search the solution with the form $E(r,\theta,\varphi) = R(r)T(\theta)W(\varphi)$, by dividing the Helmholtz equation by E and multiplying by r^2, we find these three equations where α and β are integration constants :

$$\frac{\partial}{\partial r}(r^2\frac{\partial R(r)}{\partial r}) + (k^2n^2r^2 - \alpha)R(r) = 0 \tag{B.2}$$

$$\frac{1}{\sin\theta}\frac{\partial}{\partial\theta}(\sin\theta\frac{\partial T(\theta)}{\partial\theta}) + \left(\alpha - \frac{\beta(\alpha)}{\sin^2\theta}\right)T(\theta) = 0 \tag{B.3}$$

$$\frac{\partial^2 W(\varphi)}{\partial\varphi^2} + \beta(\alpha)W(\varphi) = 0 \tag{B.4}$$

These three equations are solved in the following sections.

B.2 Bessel functions

equation The equation (B.2) with $\alpha = l(l+1)$ is:

$$\frac{\partial}{\partial r}(r^2\frac{\partial R(r)}{\partial r}) = -(k^2n^2r^2 - l(l+1))R(r) \tag{B.5}$$

We look for the solution as $R(r) = r^{-1/2}h(r)$. $r^{-1/2}$ is necessary because of the energy conservation in far field (in far field the intensity decrease must be in $1/r^2$). Thus, we find:

$$r^{-1/2}\left[r^2\frac{\partial^2 h(r)}{\partial r^2} + r\frac{\partial h}{\partial r} + (k^2n^2r^2 - (l+1/2)^2)R(r)\right] \tag{B.6}$$

$$R(r) = r^{-1/2}\left[a_o J_{l+1/2}(knr) + a_1 Y_{l+1/2}(knr)\right] \tag{B.7}$$

with $J_l(x)$ the Bessel function of the first kind and $Y_l(x)$ the Bessel function of the second kind. Now if we define :

$$j_l(x) = \sqrt{\frac{\pi}{2x}}J_{l+1/2}(x)$$

$$y_l(x) = \sqrt{\frac{\pi}{2x}}Y_{l+1/2}(x)$$

$$h_l^{(1)}(x) = j_l(x) + iy_l(x)$$

$$h_l^{(2)}(x) = j_l(x) - iy_l(x)$$

j_l is the spherical Bessel function of the first kind, y_l is the spherical Bessel function of the second kind and h_l is the spherical Hankel function, $R(r) = j_l(r)$.

$$J_l(x) \simeq \sqrt{\frac{2}{\pi x}}\cos(x - \frac{l\pi}{2} - \frac{\pi}{4}) \text{ if } x \gg 1$$

Bessel functions differentiation

$$\frac{1}{r}\frac{\partial}{\partial r}(rJ_\nu)(mr) = mJ_{\nu-1}(mr) \tag{B.8}$$

what is equivalent to:

$$\frac{\partial}{\partial r}J_\nu(mr) = mJ_{\nu-1}(mr) - \frac{\nu}{r}J_\nu(mr) \tag{B.9}$$

It is why, if we have:

$$j_l(kr) = \sqrt{\frac{\pi}{2kr}}J_{l+1/2}(kr) \tag{B.10}$$

so,

$$\frac{\partial}{\partial kr}j_l(kr) = j_{l-1}(kr) - \frac{l+1}{kr}j_l(kr) \tag{B.11}$$

The formula is also true if we replace $J_{l+1/2}$ by the Hankel function $H_{l+1/2}$

Basics properties

$$e^{ik_o\rho\cos\theta} = \sum_{n=-\infty}^{\infty} i^n J_n(k_o\rho)e^{in\theta}$$

$$J_l(z) \to \delta_{l,0} \text{ when } z \to 0$$

$$J_l(x) \to \sqrt{\frac{2}{\pi x}}\cos(x - \frac{\pi}{4} - l\frac{\pi}{2}) \text{ when } x \to \infty$$

$$Y_l(x) \to \sqrt{\frac{2}{\pi x}}\sin(x - \frac{\pi}{4} - l\frac{\pi}{2}) \text{ when } x \to \infty$$

$$h_l(x) = \sqrt{\frac{\pi}{2x}}H_{l+1/2}(x) = \sqrt{\frac{\pi}{2x}}(J_{l+1/2}(x) + iY_{l+1/2}(x)) \to \frac{e^{i(x-\frac{\pi}{2}-l\frac{\pi}{2})}}{x} \text{ when } x \to \infty$$

B.3 Legendre functions

In some books (for example in the Abramovitz [106]) the formula are written for complex variables z whereas we use only real variables x. Because of the analytical expansion, the complex variables can not be simply replaced by the real variable. The correspondences are (see formulae in [106], [Web7] and analytical expansion theory in [83]):

$$z - 1 \longmapsto (1 - x)e^{\pm i\pi}$$

$$(z^2 - 1) \longmapsto (1 - x^2)e^{\pm i\pi}$$

$$(z + 1) \longmapsto (x + 1)$$

For example $P_l^{(m)}(z) = (z^2-1)^{m/2} d^m P_l(z)/dz^m$ must be written $P_l^{(m)}(x) = (-1)^m (1-x^2)^{m/2} d^m P_l(x)/dx^m$
If the third equation is written with $\beta = m^2$:

$$\frac{\partial^2 W(\varphi)}{\partial \varphi^2} = -m^2 W(\varphi) \tag{B.12}$$

we have :

$$W_m(\varphi) = K_1 e^{-im\varphi} + K_2 e^{im\varphi} \tag{B.13}$$

and the second equation can be written :

$$\frac{1}{\sin\theta}\frac{\partial}{\partial\theta}(\sin\theta\frac{\partial T(\theta)}{\partial\theta}) + \left(l(l+1) - \frac{m^2}{\sin^2\theta}\right) T(\theta) = 0 \tag{B.14}$$

If we use $x = \cos\theta$:

$$(1-x^2)\frac{\partial^2 T(x)}{\partial x^2} - 2x\frac{\partial T(x)}{\partial x} + \left(l(l+1) - \frac{m^2}{1-x^2}\right) T(x) = 0 \tag{B.15}$$

The solutions are the Legendre function $T(x) = P_l^{(m)}(x)$ with l a positive integer and $-l \leq m \leq l$.
In the following $W_m(\varphi)$ will be describe as $a\cos m\varphi + b\sin m\varphi$ with a and b two constants, in this case $0 \leq m \leq l$.
The general solutions of (B.1) are:

$$\boxed{E(\vec{r}) = \sum_{l=1}^{\infty}\sum_{m=0}^{l}\left[A_l^m \cos(m\varphi) P_l^{(m)}(\cos\theta) h_l(knr) + B_l^m \sin(m\varphi) P_l^{(m)}(\cos\theta) h_l(knr)\right]}$$

Legendre functions differentiation

$$P_l^{(m)}(x) = (-1)^m (1-x^2)^{m/2} \frac{\partial^m}{\partial x^m} P_l(x) \tag{B.16}$$

so, with (B.16) we can demonstrate that:

$$\frac{\partial}{\partial x} P_l^{(m)}(x) = -mx(1-x^2)^{-1} P_l^{(m)}(x) - (1-x^2)^{-1/2} P_l^{m+1}(x) \tag{B.17}$$

$$\begin{aligned}\frac{\partial^2}{\partial x^2} P_l^{(m)}(x) &= -\left[m(1-x^2)^{-1} + (2m-m^2)x^2(1-x^2)^{-2}\right] P_l^{(m)}(x) \\ &\quad +2mx(1-x^2)^{-3/2} P_l^{m+1}(x) + (1-x^2)^{-1} P_l^{m+2}(x)\end{aligned} \tag{B.18}$$

Basic properties of Legendre functions

$$P_l^{(-m)}(x) = (-1)^m \frac{(l-m)!}{(l+m)!} P_l^{(m)}(x) \tag{B.19}$$

$$P_l(x) = \frac{1}{2^n n!}\frac{\partial^l}{\partial x^l}(x^2-1)^l \tag{B.20}$$

$$\begin{aligned} P_\lambda^{(m)}(1) &= 1 \text{ if } m = 0 \\ &= 0 \text{ else} \end{aligned} \tag{B.21}$$

$$\begin{aligned} P_\lambda^{(m)}(-1) = (-1)^\lambda \text{ if } m = 0 \\ = 0 \text{ else} \end{aligned} \tag{B.22}$$

B.4 Electromagnetic field in the Rayleigh case

In the Rayleigh case, the scatterer is small compared to the wavelength, only the first eigenmode of the Lorenz-Mie theory is needed: $\vec{E}^s(\vec{r}) = a_1\vec{\Psi}_{l=1,m=1}(\vec{r})$.

$$P_1^{(1)}(\cos\theta) = -\sin\theta$$

$$P_1^{(1)'}(\cos\theta) = \frac{\cos\theta}{\sin\theta}$$

$$P_1^{(1)''}(\cos\theta) = \frac{1}{\sin^{3/2}\theta}$$

$$h_1(kr) = -e^{ikr}(\frac{1}{kr} + \frac{i}{(kr)^2})$$

$$h_1^{'}(kr) = -e^{ikr}\left(-\frac{2}{(kr)^2} + i(\frac{1}{kr} - \frac{2}{(kr)^3})\right)$$

thus for an incident wave (Ex, Hy, kz)

$$\left[\begin{array}{l} \vec{\psi}_{r11} = -\cos\varphi e^{ikr}(\frac{1}{(kr)^2} + \frac{i}{(kr)^3})(\frac{-1}{\sin\theta} + \frac{2\cos^2\theta}{\sin\theta} - \sin^{1/2}\theta) \\ \vec{\psi}_{\theta 11} = \cos\varphi e^{ikr}(\frac{1}{kr} + \frac{i}{(kr)^2}) + \cos\varphi\cos\theta e^{ikr}\left(\frac{-1}{(kr)^2} + i(\frac{1}{kr} - \frac{1}{(kr)^3})\right) \\ \vec{\psi}_{\varphi 11} = -\sin\varphi e^{ikr}\left(\frac{-1}{(kr)^2} + i(\frac{1}{kr} - \frac{1}{(kr)^3})\right) - \sin\varphi\cos\theta e^{ikr}(\frac{1}{kr} + \frac{i}{(kr)^2}) \end{array}\right.$$

which becomes when r is large:

$$\left[\begin{array}{l} \vec{\psi}_{r11} = 0 \\ \vec{\psi}_{\theta 11} = \cos\varphi\frac{1}{kr}(1 + i\cos\theta) \\ \vec{\psi}_{\varphi 11} = -\sin\varphi\frac{1}{kr}(i + \cos\theta) \end{array}\right.$$

Appendix C

Translation matrix

In the T-matrix principle, the field expanded on the basis of Spherical Vectorial Functions (SVF) must be integrated over the surface particles. For one sphere, this integration can be made analytically if the spherical coordinates are centered on the sphere. But when several spheres are considered, these SVF must be translated, that is to be written in a spherical coordinates frame which has been translated compared with the initial one. These translations can be described by matrix, these matrix and their properties are described in this appendix.

C.1 Translation addition theorem

$\vec{\psi}_n$ are the SVF. The translation of the spherical coordinates frame is described in figure C.1. We write $\Re e[A]$ the real part of a matrix A and A^t the transposed matrix of A but transposition without conjugation. $\sigma_{n,n'}$ and $R_{n,n'}$ are the translation matrix:

$$\vec{\psi}_n(\vec{r}+\vec{d}) = \sum_{n,n'} \sigma_{n,n'} \Re e[\vec{\psi}_{n'}(\vec{r})] \; if \; |\vec{d}| > |\vec{r}|$$

$$\Re e[\vec{\psi}_n(\vec{r}+\vec{d})] = \sum_{n,n'} R_{n,n'} \Re e[\vec{\psi}_{n'}(\vec{r})]$$

Basics properties:

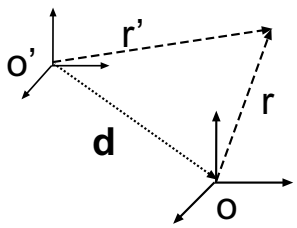

Figure C.1: Translation of the coordinate frame from O' to O. $\vec{d}+\vec{r}=\vec{r'}$.

If $\vec{a}$ is a vector of translation:

$$R(\vec{a}) = \Re e[\sigma(\vec{a})]$$

$$R(-\vec{a}) = R^{-1}(\vec{a}) = R^t(\vec{a})$$
$$\sigma(-\vec{a}) = \sigma^t(\vec{a}) \neq \sigma^{-1}(\vec{a})$$
$$R(\vec{0}) = 1$$
$$R(\vec{a}+\vec{b}) = R(\vec{a})R(\vec{b})$$
$$\sigma(\vec{a}+\vec{b}) = \sigma(\vec{a})\sigma(\vec{b}) \text{ ssi } \vec{a} > \vec{b}$$
$$R(\vec{a})\sigma(\vec{b}) = \sigma(\vec{b})R(\vec{a}) \text{ if } \vec{a} < \vec{b}$$
$$R(N\vec{a}) = R(\vec{a})^N$$

Because of the truncation of the R to have a finite matrix, this last formula is not accurate if N is too large and must not be used for the σ matrix.

C.2 Wigner 3-J symbol

The Wigner 3-J symbol or Clebsch-Gordan symbol are functions used in the computing of translation matrix of spherical vectorial functions [109, 110]. Their main properties can be found in [Web7](http://functions.wolfram.com/HypergeometricFunctions/ThreeSymbol/) and some of them can be computed in [Web8]. Their definition and properties are present in this part.

Basics properties:

$$\begin{pmatrix} j_1 & j_2 & j_3 \\ 0 & 0 & 0 \end{pmatrix} \neq 0 \text{ ssi } j_1+j_2+j_3 \text{ odd} \tag{C.1}$$

$$\text{if } m_1+m_2+m_3 \neq 0 \text{ thus } \begin{pmatrix} j_1 & j_2 & j_3 \\ m_1 & m_2 & m_3 \end{pmatrix} = 0 \tag{C.2}$$

$$\begin{pmatrix} j_1 & j_2 & j_3 \\ m_1 & m_2 & m_3 \end{pmatrix} = (-1)^{j_1+j_2+j_3} \begin{pmatrix} j_2 & j_1 & j_3 \\ m_2 & m_1 & m_3 \end{pmatrix} \tag{C.3}$$

Iterative calculation:
Initialisation:

$$\begin{pmatrix} j_1 & j_2 & j_1-j_2 \\ m_1 & m_2 & -m_1-m_2 \end{pmatrix} = (-1)^{-j_1+2j_2-m_1}$$
$$\frac{\sqrt{(j_1+m_1)!}\sqrt{(j_1-m_1)!}\sqrt{(2j_2)!}\sqrt{(2j_1-2j_2)!}}{\sqrt{(2j_1+1)!}\sqrt{(j_2+m_2)!}\sqrt{(j_2-m_2)!}\sqrt{(j_1-j_2+m_1+m_2)!}\sqrt{(j_1-j_2-m_1-m_2)!}}$$
$$\begin{pmatrix} j_1 & j_2 & j_1-j_2+1 \\ m_1 & m_2 & -m_1-m_2 \end{pmatrix} = (-1)^{-j_1+2j_2-m_1+1} 2(j_1m_2+j_2m_1+m_2)$$
$$\frac{\sqrt{(j_1+m_1)!}\sqrt{(j_1-m_1)!}\sqrt{(2j_2-1)!}\sqrt{(2j_1-2j_2+1)!}}{\sqrt{(2j_1+2)!}\sqrt{(j_2+m_2)!}\sqrt{(j_2-m_2)!}\sqrt{(j_1-j_2+m_1+m_2+1)!}\sqrt{(j_1-j_2-m_1-m_2+1)!}}$$

Recurrence:
if

$$A_1 = \frac{(2j_3-1)(j_3(j_3-1)(m_1-m_2)+m_3j_1(j_1+1)-m_3j_2(j_2+1)}{(j_3-1)\sqrt{j_3-m_3}\sqrt{j_3+m_3}\sqrt{-j_1+j_2+j_3}\sqrt{j_1-j_2+j_3}\sqrt{j_1+j_2-j_3+1}\sqrt{j_1+j_2+j_3+1}}$$

$$A_2 = \frac{(j_3+m_3-1)(j_3-m_3-1)(-j_1+j_2+j_3-1)(j_1-j_2+j_3-1)(j_1+j_2-j_3+2)(j_1+j_2+j_3)}{(j_3-m_3)(j_3+m_3)(-j_1+j_2+j_3)(j_1-j_2+j_3)(j_1+j_2-j_3+1)(j_1+j_2+j_3+1)}$$

we have,

$$\begin{pmatrix} j_1 & j_2 & j_3 \\ m_1 & m_2 & m_3 \end{pmatrix} = A_1 \begin{pmatrix} j_1 & j_2 & j_3-1 \\ m_1 & m_2 & m_3 \end{pmatrix} - \frac{j3}{(j_3-1)}\sqrt{A_2}\begin{pmatrix} j_1 & j_2 & j_3-2 \\ m_1 & m_2 & m_3 \end{pmatrix}$$

C.3 Translation along the z-axis

Change of spherical coordinates after a translation along the z-axis (see figure C.2):

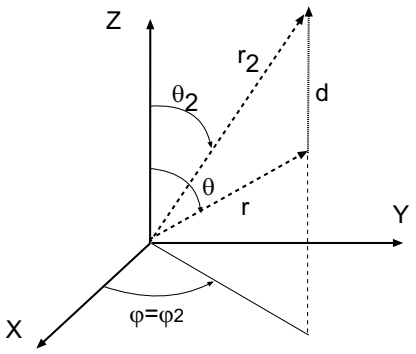

Figure C.2: Change of spherical coordinates after a translation along the z-axis.

$$\begin{cases} r_2 = \sqrt{(r\sin\theta)^2 + (r\cos\theta + d)^2} \\ \theta_2 = \arctan(r\sin\theta/(r\cos\theta + d)) \text{ if } d > 0 \\ \theta_2 = \frac{\pi}{2} - \arctan(r\cos\theta + d/(r\sin\theta)) \text{ if } d < 0 \\ \varphi_2 = \varphi \end{cases}$$

Others translations in direction $(\theta, \varphi) = (\eta, \Psi)$ and distance $r = d$:

translation	η	Ψ	d
$\vec{e_z}$	0	-	d
$\vec{e_y}$	$\frac{\pi}{2}$	$\frac{\pi}{2}$	d
$\vec{e_x}$	$\frac{\pi}{2}$	0	d
$\vec{e_x} + \vec{e_y}$	$\frac{\pi}{2}$	$\frac{\pi}{4}$	d

Translation matrix along the z-axis:

$$R_{ml,m'l'}(d) = \Theta^{\tau\sigma,\tau'\sigma'}_{ml,m'l'}(d, j_\lambda) \tag{C.4}$$

$$\sigma_{ml,m'l'}(d) = \Theta^{\tau\sigma,\tau'\sigma'}_{ml,m'l'}(d, h_\lambda) \tag{C.5}$$

with

$$\begin{aligned}\Theta^{2o,2o}_{ml,m'l'}(d, z_\lambda) &= \frac{(-1)^m}{2}\delta_{m,m'}(1-\delta_{m,0})\sum_{\lambda=|l-l'|}^{l+l'}(-1)^{1/2(l'-l+\lambda)}\left[\frac{(2l+1)(2l'+1)}{l(l+1)l'(l'+1)}\right]^{1/2} \\ &\times (2\lambda+1)[l(l+1)+l'(l'+1)-\lambda(\lambda+1)] \\ &\times \begin{pmatrix} l & l' & \lambda \\ 0 & 0 & 0 \end{pmatrix}\begin{pmatrix} l & l' & \lambda \\ m & -m & 0 \end{pmatrix} z_\lambda(kd)\end{aligned}$$

$$\Theta^{2o,2o}_{ml,m'l'}(d, z_\lambda) = \Theta^{1o,1o}_{ml,m'l'}(d, z_\lambda) = (1-\delta_{m,o})\Theta^{1e,1e}_{ml,m'l'}(d, z_\lambda) = (1-\delta_{m,o})\Theta^{2e,2e}_{ml,m'l'}(d, z_\lambda)$$

$$\begin{aligned}\Theta^{1e,2o}_{ml,m'l'}(d, z_\lambda) &= \frac{(-1)^m}{2}\delta_{m,m'}\sum_{\lambda=|l-l'|+1}^{l+l'}(-1)^{1/2(l'-l+\lambda)+1}\left[\frac{(2l+1)(2l'+1)}{l(l+1)l'(l'+1)}\right]^{1/2} \\ &\times (2\lambda+1)\left[[\lambda^2-(l-l')^2][(l+l'+1)^2-\lambda^2]\right]^{1/2} \\ &\times \begin{pmatrix} l & l' & \lambda-1 \\ 0 & 0 & 0 \end{pmatrix}\begin{pmatrix} l & l' & \lambda \\ m & -m & 0 \end{pmatrix} z_\lambda(kd)\end{aligned}$$

$$\Theta^{1e,2o}_{ml,m'l'}(d, z_\lambda) = \Theta^{2e,1o}_{ml,m'l'}(d, z_\lambda) = -\Theta^{2o,1e}_{ml,m'l'}(d, z_\lambda) = -\Theta^{1o,2e}_{ml,m'l'}(d, z_\lambda)$$

Remarks:
-to calculate $R(-d)$ the formulae are the same than for $R(d)$, you must only add $(-1)^\lambda$ in the sum,
-for an incident plane wave with $\theta_i = 0$ only $m = m' = 1$ are need, $(1-\delta_{m,0}) = 1$.

C.4 General translation matrixes

If the translation vector $\vec{d}$ has the general coordinates $(r, \theta, \varphi) = (d, \eta, \psi)$,($d$ must be positive for the σ functions) the translation matrixes are more complex [20]:

$$R_{ml,m'l'}(d) = \Theta^{\tau\sigma,\tau'\sigma'}_{ml,m'l'}(d, j_\lambda) \tag{C.6}$$

$$\sigma_{ml,m'l'}(d) = \Theta^{\tau\sigma,\tau'\sigma'}_{ml,m'l'}(d, h_\lambda) \tag{C.7}$$

with

$$\begin{aligned}\Theta^{1\sigma,1\sigma}_{ml,m'l'}(d, z_\lambda) &= \frac{(-1)^m}{2}(\epsilon_m.\epsilon_m)^{1/2}\Big[(-1)^{m'}C_{mlm'l'}(\vec{d}, z_\lambda)\cos(m-m')\psi \\ &\quad +(-1)^\sigma C_{ml-m'l'}(\vec{d}, z_\lambda)\cos(m+m')\psi\Big]\end{aligned} \tag{C.8}$$

$$\Theta^{1\sigma,1\sigma'}_{ml,m'l'}(d,z_\lambda) = \frac{(-1)^m}{2}(\epsilon_m.\epsilon_m)^{1/2}\Big[(-1)^{m'+\sigma'}C_{mlm'l'}(\vec{d},z_\lambda)\sin(m-m')\psi + C_{ml-m'l'}(\vec{d},z_\lambda)\sin(m+m')\psi\Big] \quad \text{(C.9)}$$

$$\Theta^{1\sigma,2\sigma}_{ml,m'l'}(d,z_\lambda) = i\frac{(-1)^m}{2}(\epsilon_m.\epsilon_m)^{1/2}\Big[(-1)^{m'+\sigma'}D_{mlm'l'}(\vec{d},z_\lambda)\cos(m-m')\psi - D_{ml-m'l'}(\vec{d},z_\lambda)\cos(m+m')\psi\Big] \quad \text{(C.10)}$$

$$\Theta^{1\sigma',2\sigma}_{ml,m'l'}(d,z_\lambda) = i\frac{(-1)^m}{2}(\epsilon_m.\epsilon_m)^{1/2}\Big[(-1)^{m'}D_{mlm'l'}(\vec{d},z_\lambda)\sin(m-m')\psi + (-1)^{\sigma}D_{ml-m'l'}(\vec{d},z_\lambda)\sin(m+m')\psi\Big] \quad \text{(C.11)}$$

where

$$C_{ml,m'l'}(\vec{d},z_\lambda) = \frac{(-1)^{m'}}{2}\sum_{\lambda=|l-l'|}^{l+l'} i^{(l'-l+\lambda)}\left[\frac{(2l+1)(2l'+1)(\lambda-m+m')!}{l(l+1)l'(l'+1)(\lambda+m-m')!}\right]^{1/2} \times (2\lambda+1)[l(l+1)+l'(l'+1)-\lambda(\lambda+1)] \times \begin{pmatrix} l & l' & \lambda \\ 0 & 0 & 0 \end{pmatrix}\begin{pmatrix} l & l' & \lambda \\ m & -m & -m+m' \end{pmatrix} z_\lambda(kd)P_\lambda^{m-m'}(\cos\eta)$$

$$D_{ml,m'l'}(\vec{d},z_\lambda) = \frac{(-1)^{m'}}{2}\sum_{\lambda=|l-l'|+1}^{l+l'} i^{(l'-l+\lambda)}\left[\frac{(2l+1)(2l'+1)(\lambda-m+m')!}{l(l+1)l'(l'+1)(\lambda+m-m')!}\right]^{1/2} \times (2\lambda+1)[(\lambda^2-(l-l')^2)((l+l'+1)^2-\lambda^2)]^{1/2} \times \begin{pmatrix} l & l' & \lambda-1 \\ 0 & 0 & 0 \end{pmatrix}\begin{pmatrix} l & l' & \lambda \\ m & -m & -m+m' \end{pmatrix} z_\lambda(kd)P_\lambda^{m-m'}(\cos\eta)$$

Appendix D

T-matrix algorithm

In this appendix, several calculations are carried out to compute the coefficients of the incident wave expansion and the T-matrix.

D.1 Incident coefficients

The incident coefficients are the expansion coefficients of the incident plane wave on the basis of spherical vectorial functions. Here we calculate these coefficients in the limit case when $\theta_i = 0$ and $\vec{E}^i(\vec{r}) = \exp(i\vec{k}.\vec{r})\vec{e}_2$ (see in figure 3.3). The i in mathematical formulae is the complex number such as $i^2 = -1$, but i in exponent indicates that the value is linked to the incident wave.
The general formula is:

$$\begin{aligned}(a_{2e})^i_{lm} &= i^{n+1}\left[\frac{4\pi(2l+1)(l-m)!}{l(l+1)(l+m)!}\right]^{1/2}\frac{\sqrt{\epsilon_m}}{\sin\theta_i} \\ &\quad\times\left[(l+1)\cos\theta_i P_l^{(m)}(\cos\theta_i) - (l-m+1)P_{l+1}^{(m)}(\cos\theta_i)\right] \qquad \text{(D.1)}\end{aligned}$$

If $\theta_i = 0$,

$$\begin{aligned}P_l^{(m)}(\cos\theta_i) = P_l^{(m)}(1) &= 1 \text{ if } m = 0 \\ &= 0 \text{ else} \qquad \text{(D.2)}\end{aligned}$$

Thus, if $\theta_i = 0$ and $m = 0$:

$$(a_{2e})^i_{10} = \lim_{\theta_i\to 0} i^{n+1}\left[\frac{4\pi(2l+1)}{l(l+1)}\right]^{1/2}\frac{\sqrt{1}}{\sin\theta_i}\left[(l+1)-(l+1)\right] = 0$$

and if $\theta_i = 0$ and $m = 1$:

$$(a_{2e})^i_{l1} = i^{n+1}\left[\frac{4\pi(2l+1)(l-1)!}{l(l+1)(l+1)!}\right]^{1/2}\sqrt{2}\lim_{\theta_i\to 0}\left[(l+1)\frac{P_l^{(1)}(\cos\theta_i)}{\sin\theta_i} - l\frac{P_{l+1}^{(1)}(\cos\theta_i)}{\sin\theta_i}\right]$$

$$(a_{1o})^i_{lm} = i^n \left[\frac{4\pi(2l+1)(l-m)!}{l(l+1)(l+m)!}\right]^{1/2} \frac{\sqrt{2}m}{\sin\theta_i} P_l^{(m)}(\cos\theta_i)$$

if $m = 0$ $(a_{1o})^i_{lm} = 0$
if $m = 1$ and $\theta_i = 0$:

$$(a_{1o})^i_{lm} = i^n \left[\frac{4\pi(2l+1)}{l^2(l+1)^2}\right]^{1/2} \sqrt{2} \lim_{\theta_i \to 0} \frac{P_l^{(1)}(\cos\theta_i)}{\sin\theta_i}$$

We must now calculate $\lim_{\theta_i \to 0} P_l^{(1)}(\cos\theta_i / \sin\theta_i$
with (B.20) and (B.16) we find:

$$\begin{aligned} P_l^{(1)}(x) &= \frac{-(1-x^2)^{1/2}}{2^l l!} \frac{d^{l+1}(x^2-1)^l}{dx^{l+1}} && \text{(D.3)} \\ &= \frac{-1}{2^l l!}(1-x^2)^{1/2} \frac{d^{l+1}(x^2-1)^l}{dx^{l+1}} && \text{(D.4)} \end{aligned}$$

but

$$\begin{aligned} \frac{d^{l+1}(x^2-1)^l}{dx^{l+1}} &= \frac{d^{l+1}\left((x-1)(x+1)\right)^l}{dx^{l+1}} \\ &= \sum_{k=0}^{l+1} C_{l+1}^k \frac{d^k(x-1)^l}{dx^k} \frac{d^{l+1-k}(x+1)^l}{dx^{l+1-k}} && \text{(D.5)} \end{aligned}$$

therefore

$$\lim_{x\to 1} \frac{d^{l+1}(x^2-1)^l}{dx^{l+1}} = \lim_{x\to 1} C_{l+1}^l l! \frac{d(x+1)^l}{dx} \qquad \text{(D.6)}$$

because

$$\begin{aligned} \lim_{x\to 1} \frac{d^k(x-1)^l}{dx^k} &= 0 \text{ if } k \le l-1 \\ &= n! \text{ if } k = l \\ &= 0 \text{ if } k = l+1 \end{aligned}$$

so,

$$\begin{aligned} \lim_{x\to 1} \frac{d^{l+1}(x^2-1)^l}{dx^{l+1}} &= C_{l+1}^l l! \lim_{x\to 1} l(x+1)^{l-1} \\ &= (l+1)! l 2^{l-1} && \text{(D.7)} \end{aligned}$$

with (D.4) and (D.7) we find

$$\lim_{\theta_i \to 0} \frac{P_l^{(1)}(\cos\theta_i)}{\sin\theta_i} = \lim_{x\to 1} \frac{P_l^{(1)}(x)}{(1-x^2)^{1/2}} = \frac{-(l+1)l}{2} \qquad \text{(D.8)}$$

so,

$$(a_{2e})^i_{l1} = i^{l+1}[2\pi(2l+1)]^{1/2} \qquad \text{(D.9)}$$

$$(a_{1o})^i_{l1} = -i^l[2\pi(2l+1)]^{1/2} = -i(a_{2e})^i_{l1} \qquad \text{(D.10)}$$

There is a mistake in the article of Perterson and Strom [20]: a bad minus sign.

D.2 T-matrix for 2 spheres

The T-matrix for several spheres can be expressed in function of the T-matrix of each sphere. For two spheres, the T-matrix is:

$$\begin{aligned} T_{1+2} &= R(\vec{a_1})\left\{T_1\left[1-\sigma(\vec{a_2}-\vec{a_1})T_2\sigma(\vec{a_1}-\vec{a_2})T_1\right]^{-1}\left[1+\sigma(\vec{a_2}-\vec{a_1})T_2R(\vec{a_1}-\vec{a_2})\right]\right\}R(-\vec{a_1}) \\ &\quad +R(\vec{a_2})\left\{T_2\left[1-\sigma(\vec{a_1}-\vec{a_2})T_1\sigma(\vec{a_2}-\vec{a_1})T_2\right]^{-1}\left[1+\sigma(\vec{a_1}-\vec{a_2})T_1R(\vec{a_2}-\vec{a_1})\right]\right\}R(-\vec{a_2}) \end{aligned}$$

$\vec{a_1}$ is the position of the first sphere and T_1 the T-matrix of this sphere expressed in coordinates centered on the sphere. $\vec{a_2}$ is the position of the second sphere and T_2 its T-matrix.

For more spheres:

$$\begin{aligned} T_{1+2+..+N} &= \sum_{k=1}^{N} R(0,k)T_k\left\{1-\sum_{i=1,i\neq k}^{N} A(k,i)\sigma(i,k)T_k\right\}^{-1} \\ &\quad \times\left\{1+\sum_{i=1,i\neq k}^{N} A(i,k)R(i,k)\right\}R^{-1}(0,k) \end{aligned} \tag{D.11}$$

with

$$A(k,i)=\left[\sigma(k,i)+\sum_{l\neq i\neq k}^{N}\sigma(k,l)T_l\sigma(l,i)\right]\left[1-\sum_{l\neq i\neq k}^{N}T_i\sigma(i,l)T_l\sigma(l,i)\right]^{-1}T_i$$

where $R(k,i)$ and $\sigma(k,i)$ are the translation matrix of SVF from frame k to frame i. In the general case, the size of the T-matrix is $2N(N+1)/2+N)$.

D.3 Study of an indeterminate case

In the computing of the general expression of translation matrix (appendix C.4), there is an indeterminate case. This case is explained in this section and a solution is proposed.

$$A=P_\lambda^{(m-m')}(\cos\eta)\left[\frac{(\lambda-m+m')!}{(\lambda+m-m')!}\right]^{1/2} \tag{D.12}$$

if $m-m'>0$:

$$A=P_\lambda^{(|m-m'|)}(\cos\eta)\left[\frac{(\lambda-|m-m'|)!}{(\lambda+|m-m'|)!}\right]^{1/2}$$

if $m-m'<0$ by applying (B.19):

$$\begin{aligned} A &= (-1)^{-m+m'}P_\lambda^{-m+m'}(\cos\eta)\frac{(\lambda+m-m')!}{(\lambda-m+m')!}\left[\frac{(\lambda-m+m')!}{(\lambda+m-m'!}\right]^{1/2} \\ A &= (-1)^{|m-m'|}P_\lambda^{(|m-m'|)}(\cos\eta)\left[\frac{(\lambda-|m-m'|)!}{(\lambda+|m-m'|!}\right]^{1/2} \end{aligned} \tag{D.13}$$

In these two cases $(\lambda - |m - m'|)!$ can be divergent when $\lambda < |m - m'|$. It can be simplified by $(\lambda - |m - m'|)!$ at the numerator of the Wigner symbol (Appendix C.2) when the recurrence is initiated and in the recurrence formula because at the denominator of these two formulae we find:

$$\sqrt{(\lambda - m + m')!}\sqrt{(\lambda + m - m')!} = \sqrt{(\lambda - |m - m'|)!}\sqrt{(\lambda + |m - m'|)!}$$

D.4 Calculation of the magnetic field

In section 3, we have explained how the electric field can be computed. The calculation of the magnetic field is developed in this appendix.

Definition :

$$\vec{\psi}_{2\tau} = (k^{-1}\vec{\nabla}) \times \vec{\psi}_{1\tau}$$

so,

$$\begin{aligned} \vec{\nabla} \times \vec{\psi}_{2\tau} &= k^{-1}\vec{\nabla} \times \vec{\nabla} \times \vec{\psi}_{1\tau} \\ &= k^{-1}(-\Delta\vec{\psi}_{1\tau} + \mathrm{grad}(\mathrm{div}(\vec{\psi}_{1\tau}))) \\ &= -k^{-1}\Delta\vec{\psi}_{1\tau} \end{aligned}$$

because $\mathrm{div}(\vec{\psi}_{1\tau}) = 0$. But $\Delta\vec{\psi}_{1\tau} + k^2\Delta\vec{\psi}_{1\tau} = 0$, so we have :

$$\vec{\nabla} \times \vec{\psi}_{2\tau} = k\vec{\psi}_{1\tau}$$

If we have :

$$\vec{E} = (a_{2e})\vec{\psi}_{2e}(knr) + (a_{1o})\vec{\psi}_{1o}(knr) + (a_{1e})\vec{\psi}_{1e}(knr) + (a_{2o})\vec{\psi}_{2o}(knr)$$

thus,

$$\vec{\nabla} \times \vec{E} = (a_{2e})kn\vec{\psi}_{1e}(knr) + (a_{1o})kn\vec{\psi}_{2o}(knr) + (a_{1e})kn\vec{\psi}_{2e}(knr) + (a_{2o})kn\vec{\psi}_{1o}(knr)$$

but $\vec{\nabla} \times \vec{E} = ik\vec{H}$, thus

$$\vec{H} = -in\left((a_{2e})\vec{\psi}_{1e}(knr) + (a_{1o})\vec{\psi}_{2o}(knr) + (a_{1e})\vec{\psi}_{2e}(knr) + (a_{2o})\vec{\psi}_{1o}(knr)\right)$$

Appendix E

Matlab Programs

To have a better understanding of the T-matrix algorithm, we have code our own program by using the paper of Peterson and Ström [20]. Our program has been developed with Matlab13 6.5 and can be used with a graphic user interface. This appendix briefly describes our program.

E.1 Notations

All the authors do not use the same notations. In order to help the reader to compare results, the table E.1 summarizes notations of the main references.

The scalar propagation equation has two different solutions which are not described with the same notation in all references. The table E.2 summarizes notations of the main references.

Born & Wolf [8]	Van de Hultz [3]	Peterson & Strom [20]	Thesis
$e^{-i\omega t}$	$e^{+i\omega t}$	$e^{-i\omega t}$	$e^{-i\omega t}$
$k^2 = (2\pi N/\lambda_o)^2 = -k_1 k_2$ $k_2 = i2\pi/\lambda_o$ $k_1 = i2\pi N^2/\lambda_o$	$k = \omega/c$	$k = \omega/c$	$k = \omega/c$
$N^2 = n^2 + i4\pi\sigma/\omega$	$N^2 = n^2 - i4\pi\sigma/\omega$	$\sigma = \infty$	$n_2^2 + i4\pi\sigma_2/\omega$
$\Psi_l(kr) = \sqrt{\frac{\pi kr}{2}}$ $\times J_{l+1/2}(kr)$	$j_l(kr) = \sqrt{\frac{\pi}{2kr}}$ $\times J_{l+1/2}(kr)$	$j_n^{(1)}(kr) = \sqrt{\frac{\pi}{2kr}}$ $\times J_{n+1/2}^{(1)}(kr)$	$j_l(kr) = \sqrt{\frac{\pi}{2kr}}$ $\times J_{l+1/2}(kr)$

Table E.1: Comparison of notations between several references.

Math	Thesis	Born & Wolf	Peterson & Strom
$\sin\varphi$	o	$m\Pi$	$\sigma = o$
$\cos\varphi$	e	$e\Pi$	$\sigma = e$

Table E.2: Comparison of notations between several references.

E.2 Algorithm structure

The algorithm is adapted to optimize computing time according to the studied case. The different possible cases are described here. For each case the possible variation of index l and m but also the possible couplings are described.

1-Wave vector direction
The incident wave vector $\vec{k_i}$ is considered to be in the $(\vec{e_x}, \vec{e_y})$ plane.
• $\theta_i = 0 \implies m = 1$
• $\theta_i \neq 0 \implies 0 \leq m \leq l$
(change the size of matrix, see section 3.6)

2-Incident polarization
The output structure P_i contains the expansion coefficients of the incident wave a^i noted (e1,e2,o1,o2) (see section 3.2). For example $P_i.e1$ is for (a^i_{e1}). In the general case $P_i.e1$ is a matrix depending of l and m index.
For a given incident wave vector $\vec{k_i}$ in the plane $(\vec{e_x}, \vec{e_y})$, two possible polarization states must be distinguished $H_i = H_y$ and $E_i = E_y$. According to the polarization state, some of the variables of P_i will be equal to zero:

if $H_i = H_y$ o1 and e2 are not equal to zero.
if $E_i = E_y$ o2 and e1 are not equal to zero.

Value of the variable *polarisation* in function of the incident field:

Hi=Hy	$\theta_i = 0$	polarisation=1
Hi=Hy	$\theta_i \neq 0$	polarisation=2
Ei=Ey	$\theta_i = 0$	polarisation=3
Ei=Ey	$\theta_i \neq 0$	polarisation=4
Circular	-	polarisation=5

3-Number and position of spheres
According to the number of spheres and to their positions the possible couplings between the incident modes and the scattered modes will not be the same. Above $o1 \rightarrow e2$ means that the (a^i_{o1}) component of the incident wave has an influence on the component (a^s_{e2}) of the scattered wave.

• **For one sphere**: (the sphere is considered to be centered on the coordinate frame)

there is not coupling:

$$\left\{ \begin{array}{l} o1 \rightarrow o1 \\ e2 \rightarrow e2 \end{array} \right. = \left\{ \begin{array}{l} o2 \rightarrow o2 \\ e1 \rightarrow e1 \end{array} \right. \tag{E.1}$$

• **For several spheres on the z-axis**:
there are coupling but not between the two polarized case:

$$\left\{ \begin{array}{l} o1 \rightarrow o1 \\ o1 \rightarrow e2 \\ e2 \rightarrow e2 \\ e2 \rightarrow o1 \end{array} \right. = \left\{ \begin{array}{l} o2 \rightarrow o2 \\ o2 \rightarrow e1 \\ e1 \rightarrow e1 \\ e1 \rightarrow o2 \end{array} \right. \tag{E.2}$$

• **For several spheres (general case)**:
there are coupling between the two polarized case:

$$\left\{ \begin{array}{l} o1 \rightarrow o1 \\ \quad \rightarrow e2 \\ \quad \rightarrow o2 \\ \quad \rightarrow e1 \\ e2 \rightarrow e2 \\ \quad \rightarrow o1 \\ \quad \rightarrow e1 \\ \quad \rightarrow o2 \end{array} \right. = \left\{ \begin{array}{l} o2 \rightarrow o2 \\ \quad \rightarrow e1 \\ \quad \rightarrow e2 \\ \quad \rightarrow o1 \\ e1 \rightarrow e1 \\ \quad \rightarrow o2 \\ \quad \rightarrow e2 \\ \quad \rightarrow o1 \end{array} \right. \tag{E.3}$$

General structure
The programm is separated in three main parts (figure E.1). The first is the running of the algorithm and the descriptions of the aggregate and of the incident wave. This description can be made by a graphic user interface or by using the Matlab command editor. The description can be made by giving each parameter in the interface or by using a description file which is called by the programm. All description variables are grouped in the structure **data**.

The second part of the programm computed the expansion coefficients of the incident field (structure P_i), of the scattered field (structure P_s) and of the field inside the sphere (structure P_o, only of one sphere). In order to carry out calculation, the T-matrix (structure $\mathbf{T}$) must be computed. This part takes into account the user choice in order to optimize the computing time.

The last part carries out the Post-treatment. The field is reconstructed (incident or scattered or total field can be studied) and several physical parameters can be computed:

- the Poynting vector (in spherical or cartesian coordinates),
- the electromagnetic field (in spherical or cartesian coordinates),

- the intensity phase function (scattering diagram) in a plane or in all directions,
- the Stokes parameters in a plane or in all directions,
- the (backscattering, extinction, scattering) cross sections.

The post-treatment choices are described in structure **Post** and the space description is in the structure **space**. The computed field is regrouped in structure **champ** and the other physical parameters in structure **result**.

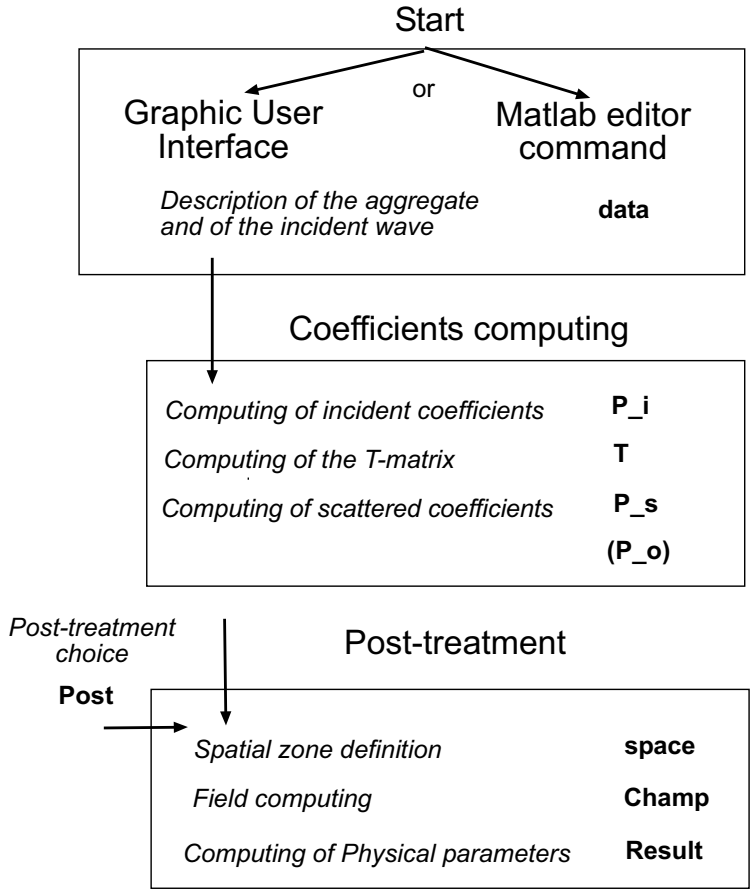

Figure E.1: General structure of the algorithm.

E.3 Input and output of the program

In order to make variables exchange between programs easier, variables have been grouped in structures. For example, the variable *lambda* that contains the wavelength is in the structure *data*, so to call this variable in program we must write: *data.lambda*

Structure *data*
data is a structure that contains variables concerning the description of the incident

wave and the aggregate.

Name	description	format
lambda	wavelength in free space, in nm	number
R	Radius of spheres	vector
n1	real index of the environment	number
n2	real index of spheres	vector
N	complex index of spheres	vector
k	$2\pi/\lambda$	number
ConducInf	perfectly conductive sphere if 1	vector
sigma	conductivity of spheres	vector
Nbspheres	number of spheres in the aggregate	integer
d	distance between spheres for linear regular spheres on z-axis	number
position	radius position of each spheres	vector
eta	θ position of each spheres	vector
psi	φ position of each spheres	vector
angledincidence	incidence angle of the propagation vector	number
polarisation	$(1 \rightarrow 6)$ state of polarization	integer
Lmin	minimum order (1 in general)	integer
Lmax	expansion order $0 \leq l \leq$ Lmax	integer

Structure for the T-matrix:
The T-matrix is described by the structure **T**. This structure contains 16 variables, which are the 16 components of the matrix:

$$\left|\begin{array}{c} e1 \\ e2 \\ o1 \\ o2 \end{array}\right| = \left[\begin{array}{cccc} T11 & T12 & T13 & T14 \\ T21 & T22 & T23 & T24 \\ T31 & T32 & T33 & T34 \\ T41 & T42 & T43 & T44 \end{array}\right] \left|\begin{array}{c} e1 \\ e2 \\ m1 \\ m2 \end{array}\right|$$

Each coefficient of this matrix can be a scalar or a matrix following the case.

Structures for expansion coefficients
The incident field, the scattered field and the field inside a sphere are expanded on the basis of SVF. These structures contain their expansion coefficients.

structure	description
P_i	coefficients of the incident field
P_s	coefficients of the scattered field
P_o	coefficients of field inside the sphere

The variables of these 3 structures are: o1, o2, e1 and e2 (see section 3.2). Each variable, for example $P_i.o1$ can be a vector or a matrix according to the studied case. In the general case they depend on the l and m index.

Structure *space*
space is a structure that contains variables concerning the space area where the electromagnetic field will be studied.

Name	description	
xmin	describes the studied windows in pixels	integer
xmax	describes the studied windows in pixels	integer
ymin	describes the studied windows in pixels	integer
ymax	describes the studied windows in pixels	integer
unit_x	real size of one pixel in horizontal direction	number
unit_y	real size of one pixel in vertical direction	number
X	real horizontal coordinates	matrix
Y	real vertical coordinates	matrix
phi	φ positions of the studied points	number or matrix
theta	θ positions of the studied points	number or matrix
RR	radius of the studied points	number or matrix
Ntheta	number of θ angles	integer
Nphi	number of φ angles	integer
alpha	angle of point in a selected plane	number or matrix
alphamin	minimum value of the alpha angle	number
alphamax	maximum value of the alpha angle	number
taille_i	horizontal size of the coordinates matrix	integer
taille_J	vertical size of the coordinates matrix	integer
lieu	1 where the field must computed 0 elsewhere	matrix
Mx	label of the horizontal axis	vector
My	label of the vertical axis	vector
title	kind of field: incident, scattered or total	string
symetrie	1: the field in the symmetric plane is computed	0/1
sphere	choice to plot the sphere around the aggregate	0/1
inclinaison	angle used to described the studied plane	number

Structure *post*

post is a structure that contains variables concerning the choice of what post treatment must be done.

Name	values	description
composante	(0/1)	plot the 6 components of electromagnetic field
poynting	(0/1)	plot the components of the Poynting vector
stokes2d	(0/1)	plot the Stokes elements in a plane (x, y)
stokes1d	0→4	0/ 1: Stokes elements(α)/ 2:idem (θ, φ) 3: Stokes elements(x, y)/ 4:idem in N points
section_eff	0→2	0/ 1: extinction cross section/ 2: backscattering cross section
axespolar	(0/1)	choice to plot the axis of polarization
diagram	0→2	0/ 1:choice to plot the phase function F(α) 2: idem with F(φ, θ)
coord	0→3	0: no view/ 1: view in spherical coordinates/ 2: view in cartesian coordinates/ 3:view of the absolute value
onde	1→3	studied field 1: scattered/ 2: incident/ 3: total
espace	1→13	kind of studied space area
choixexploitation	(0/1)	choice to execute the post treatment

Post.espace=space.espace can have several values:

space	description
1	half-plane containing Oz axis and defined by φ
2	angular variation in the half-plan containing Oz axis and defined by φ
3	R constant and variation as a function of (θ, φ)
4	N points $(R_N, \theta_N, \varphi_N)$
5	half-plane (X, Y)
6	the studied space is defined out of the programm
7	half-plane containing Oy axis and defined by the angle (Oz, u)
9	angular variation in the plane containing Ox axis and defined by angle (Oz, u)
10	half-plane containing Ox axis and defined by angle (Oz, u)
11	$R = R_o$ and angular variation in the plane containing Oy axis and defined by angle (Oz, u)
12	study in the backward direction
13	study in the forward direction

Structure *champ*

champ is a structure that contains variables concerning the electromagnetic field in space.

Name	format	description
Er	matrix	r component of electric field
Et	matrix	θ component of electric field
Ep	matrix	φ component of electric field
Hr	matrix	r component of magnetic field
Ht	matrix	θ component of magnetic field
Hp	matrix	φ component of magnetic field

Structure *result*

result is a structure that contains variables concerning physical properties of the electromagnetic field in space.

Name	description
poynting_r	r component of the Poynting vector
poynting_t	θ component of the Poynting vector
poynting_p	φ component of the Poynting vector
poynting	Absolute value of the Poynting vector
phase_fct	Phase function
Csca	Scattering cross section
S0, S1, S2, S3	The 4 Stokes elements
degreP	Polarization degree
Ex, Ey, Ez	Component of electric field in cartesian
Hx, Hy, Hz	Component of magnetic field in cartesian
NormeE	Absolute value of the electric field

E.4 Graphic user interface

A graphic user interface has been coded to make the used of the T-matrix algorithm easier. This interface is separated in two parts. The first part allows us to describe the incident field (figure E.2), and the aggregate, the second makes possible to choose what kind of post treatment we want (figure E.3).

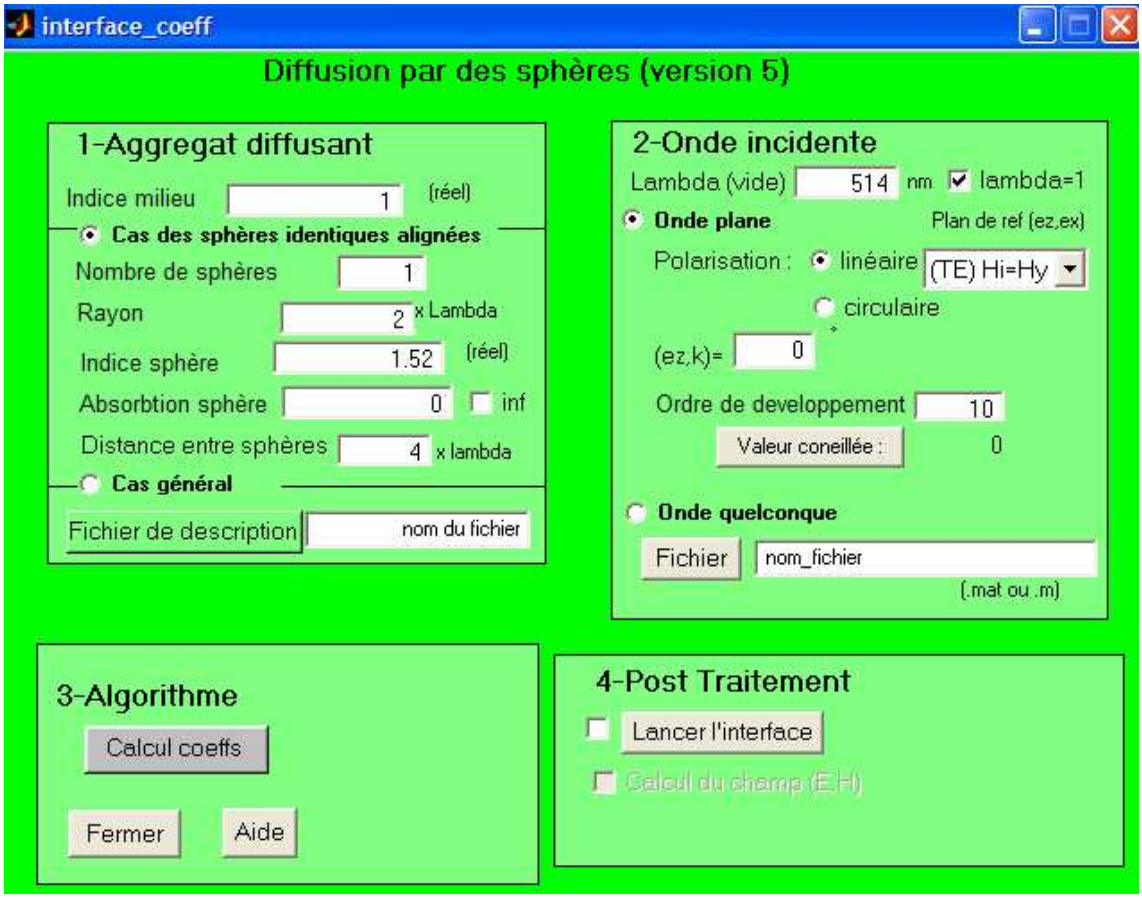

Figure E.2: Interface to describe the incident field and the aggregate.

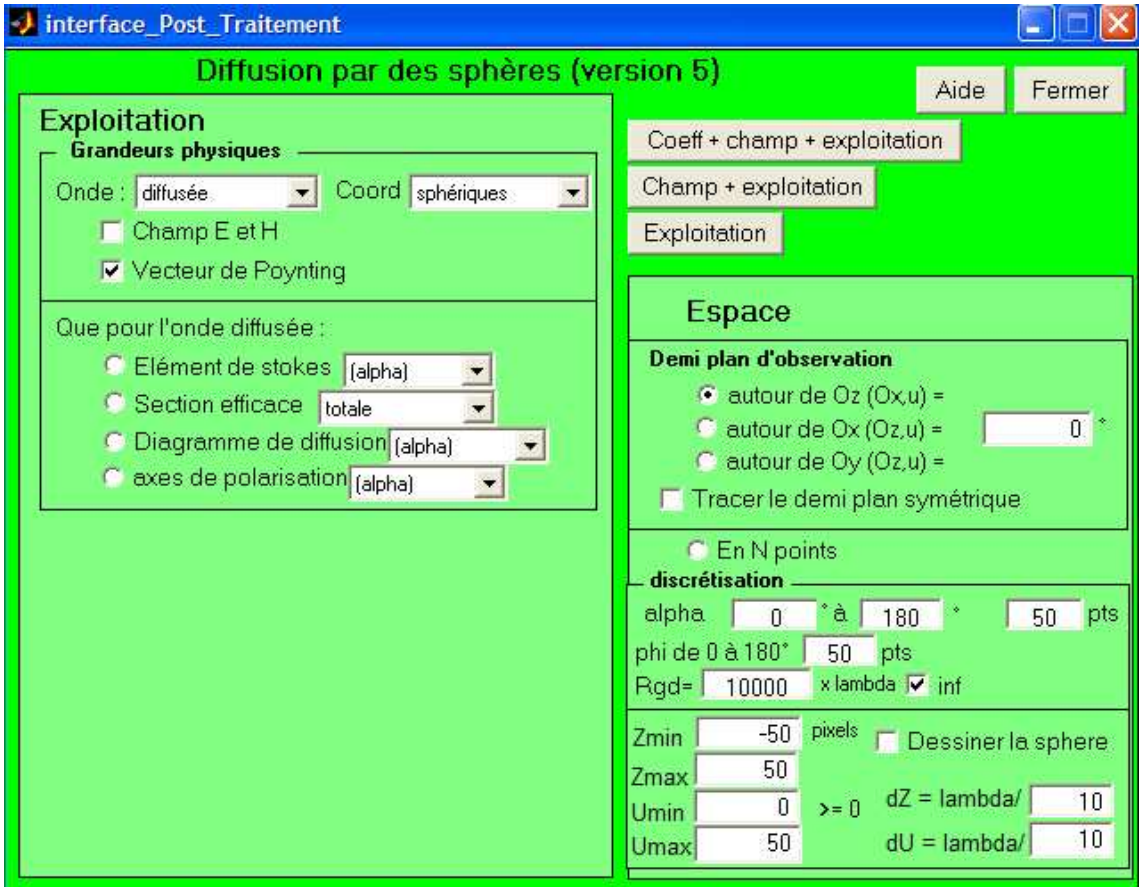

Figure E.3: Interface to choose what kind of post treatment we want.

This interface is made of objects whose description follows:
Button (Push Button): to run an action
Check (Checkbox): to make an independent choice
Radio (Radio Button): to make a choice that is incompatible with others
Edit (Edit Text): area to write number or string
Pop (Popmenu): menu

Object	Value/Name	Description	TAG
Button	simulation	to run simulations	
Button	close	to close the interface	
Edit	514	wavelength (λ)	lamb
Check	1	consider that $\lambda = 1$	LambdaUnit
Button	1	choice of an incident plane wave	plane
Button	0	choice of another incident wave	qcq
Edit		name of the file describing the incident wave	nom_fichier
Radio	0	circular incident polarization	circ
Radio	1	linear incident polarization	lin
Pop	TE/TM	kind of linear polarization	choixlin
Edit	0	incident angle	angledincidence
Edit	5	Radius in λ	RRayon
Edit	1	index of environment	indice1
Edit	1.52	index of spheres	indice2
Edit	0	absorption of spheres	absorption
Check	0	perfectly conducting sphere	conducinf
Radio	1	for similar spheres on a line	CasP
Edit	4	distance between spheres	d
Edit	1	number of spheres	Nbspheres
Radio	0	general case of aggregate	casG
Edit	nom_fichier	name of the file describing the aggregate	NomAggr
Button	6	advised order	
Edit	6	order of expansion	ordre
Check		choice to run post treatment after coef computing	choixexploitation
Button	0	open the post-treatment interface	interface2

Object	Value/Name	Description	TAG
Radio	1	plane containing Oz	planphi
Radio	0	plane containing Ox	planxy ?
Radio	0	plane containing Oy	planincl
Edit	-60	space area to study	xmin
Edit	60	idem	xmax
Edit	-50	idem	ymin
Edit	50	idem	ymax
Edit	4	dicretisation $dx = \lambda/n$	dx
Edit	3	dicretisation $dy = \lambda/n$	dy
Check	0	plot the symmetric plane	symetrie
Check	0	plot the sphere on the map	sphere
Edit	0	minimum angle	aphamin
Edit	180	maximum angle	alphamax
Edit	10	Angular	Ntheta
Edit	10	Angular	Nphi
Edit	10000	Radius of observation	RRR
Check	1	Observation in far field	Rinf
Check	1	if we want to represent the EM field	composantes
Check	0	if we want to represent the Poynting vector	poynting
Pop	scat/inc/total	EM Field to represent	onde
Pop	1	coordinates choice	coord
Radio	0	if we want to calculate a cross section	section
Pop	scat/back/ext	choice of cross section to calculate	SectionChoix
Radio	0	if we want to calculate the Stokes elements	Stokes
Pop	$\alpha/(\theta\phi)$	format of Stokes elements	StokesType
Radio	0	if we want to represent the axis of polarization	axes
Radio	0	if we want to calculate the phase function	diagram
Pop	$\alpha/(\theta\phi)$	format of phase function	DiagType
Button	Coef+champ+expl.	run coefficients and fields computing, and plot	-
Button	Champ+expl.	calculate the field and plot	-
Button	Exploitation	Plot post-treatment	-